The Messenger

ALMA inauguration
NACO vector vortex coronagraph
Forecasting PWV over Paranal and Chajnantor
VVV wide view of the Galactic Bulge

The Inauguration of the Atacama Large Millimeter/submillimeter Array

Leonardo Testi[1]
Jeremy Walsh[1]

[1] ESO

On 13 March 2013 the official inauguration of the Atacama Large Millimeter/submillimeter Array (ALMA) took place at the Operations Support Facility in northern Chile. A report of the event and the preceding press conference is presented and the texts of the speeches by the President of Chile, Sebastián Piñera, and the Director General of ESO, Tim de Zeeuw, are included.

The ALMA project underwent its official opening on 13 March, with a ceremony attended by representatives from all the partner Executives, many who are currently working on the project or were involved in the past, as well as the President of Chile and local representatives from the Atacameño community. Although the array is not yet fully operational, 57 of the 66 antennas were at the ALMA Operations Site (AOS), 5050 metres above sea level on the Chajnantor Plateau in northern Chile, at the time of the inauguration. The inauguration took place at the Operations Support Facility (OSF) at 2900 metres above sea level and was preceded by a press conference on 12 March, also held at the OSF. Dignitaries and attendees also visited the high site on the morning of the 13th and on the 14th. On the evening of the 13th, a private party for ALMA staff was hosted at the OSF by the then ALMA Director, Thijs de Graaw, who also presented everyone with a commemorative canvas depicting the array (Figure 1).

The genesis of the project to construct a large-area millimetre/submillimetre array for astronomy dates back about 30 years to independent initiatives and plans in Europe, the USA and Japan. In the USA the Very Large Array, now called the

Figure 2. Tim de Zeeuw, ESO Director General, the President of Chile, Sebastián Piñera, the Director of the USA's National Science Foundation (NSF) Subra Suresh, the former Director of ALMA, Thijs de Graauw, and the Senior Vice Minister of Japan's MEXT (Ministry of Education, Culture, Sports, Science and Technology) Teru Fukui (shown left to right) aboard one of the ALMA transporters.

Jansky Very Large Array, provided a precedent, but since it operates at radio frequencies, the technology was very different from that needed for a millimetre/submillimetre array. The construction of a large array was endorsed by the US astronomy decadal survey released in 1991. Through the Swedish–ESO submillimetre telescope (SEST) on La Silla, ESO had been participating in millimetre-wave astronomy since the mid-1980s, and then, in 1991, the suggestion to build an array was discussed by the SEST User Group (Madsen, 2012, p. 371ff). At about

the same time, Japan, which already had a single-dish millimetre telescope at Nobeyama and a small interferometer array, was also considering a large millimetre/submillimetre array. The size of the undertaking rather naturally led, after much discussion and negotiation, to the three agreeing on a joint project. In 1996 Chajnantor was selected as indisputably the best millimetre/submillimetre site worldwide. The progress of the project has been regularly reported in *The Messenger* and a chapter is devoted to ALMA in Madsen (2012).

Inaugural ceremony

The inauguration was attended by about 500 people, with large representations from the three Executives — ESO, North America (USA and Canada) and East

Figure 1. On the day of the inauguration, Thijs de Graauw presented the ALMA staff with this print on canvas of the ALMA array. ALMA astronomer Antonio Hales collected the signatures from members of the ALMA science team, array operators, engineers and data analysts on his canvas.

Asia (Japan and Taiwan). It took place in a large tent that had been erected specially for the occasion. The high level of public interest in ALMA was reflected in the large number of press representatives (120) attending, all of whom also visited the AOS on the Chajnantor Plateau. The logistics of transporting all the attendees to the remote OSF at 2900 metres above sea level were considerable.

Following a short reception, the inauguration began at 12:00 noon after the President of Chile Sebastián Piñera had had an opportunity to visit the AOS and the OSF facilities. The ceremony was introduced and chaired by the ALMA Executive Officer Paulina Bocaz. The proceedings could be viewed remotely by live streaming and are archived[1]. Thijs de Graauw, the ALMA Director at the time of the inauguration, launched the official speeches by introducing ALMA as opening up the cold Universe to high sensitivity and high spatial resolution study. Later in 2013 the full contingent of 66 antennas will be in place and the operation of the array will be developed, with longer baselines, polarisation observations, Solar observations, new bands and observing modes. The Director emphasised the technological aspects of the project — the four types of antennas with 7- and 12-metre apertures and their stringent surface and pointing accuracies, the two correlators for 16 and 64 antennas, and the demand for antenna signal synchronisation that is accurate to a fraction of a picosecond. He also emphasised the strong links with the host nation, Chile, in terms of the educational, scientific, technical and cultural aspects, and displayed some paintings by Chilean children of the antennas and the array. He closed by thanking all the visionary scientists and engineers who have worked to realise the project, and all those currently working (a staff complement composed of 20 nationalities, with 80% of staff from Chile). He also thanked the previous Director Massimo Tarenghi. Thijs de Graauw retired from his position as ALMA Director on 31 March 2013 and has been replaced by Pierre Cox.

ALMA's Chief Scientist, Ryohei Kawabe then spoke about some of the recent science results from ALMA. Its high angular resolution and wavelength coverage will

Figure 3. Tim de Zeeuw presenting his speech at the ALMA inauguration.

contribute to a wide range of topics from chemistry and planet formation to cosmology. The ability to detect emission from biotic and pre-biotic molecules contributes to study of the origin of human life. Although ALMA is intrinsically a narrow-field telescope, large areas of sky can be efficiently observed using a mosaicking technique, which was admirably demonstrated by the results of wide-field CO imaging, revealing the distribution of molecular clouds in the bar and spiral arms of M83. A study of molecular and atomic gas in lensed high-redshift galaxies, released on the day of the inauguration, demonstrates that the chemistry at early epochs is now within reach of ALMA observations (see also ESO PR 1313). These and other early observations from Science Verification (SV) and Cycle 0 have demonstrated the potential of ALMA and Ryohei Kawabe concluded that ALMA is a dream come true!

The Director of the US National Science Foundation, Subra Suresh, emphasised the NSF's investment in Chile, over a period of more than 60 years, of which the ALMA project was just one component, although the largest in terms of investment. The broad international aspects of ALMA make it a key example for future collaborations in ground-based astronomy. He concluded by introducing

a live link from the International Space Station orbiting above the Atacama Desert, where astronauts Tom Marshburn and Chris Hadfield greeted the attendees at the ALMA inauguration and sent their best wishes for future discoveries to the new observatory.

The Japanese government representative, Teru Fukui, described how discussions on a large millimetre/submillimetre array had taken place in Japan as early as 1983 and had eventually led to Japan formally joining the ALMA project with the USA and ESO in 2006. The National Astronomical Observatory of Japan (NAOJ) and the National Institute of Natural Sciences had played key roles in securing funding and promoting the project in Japan. Japanese industry has played key roles in the design and construction of the antennas and the correlators. Fukui looked forward to the many fantastic discoveries to come from ALMA.

Tim de Zeeuw, Director General of ESO, stressed what a momentous occasion the inauguration of ALMA was for science and technology (the full text of his speech is printed on p. 5). The inauguration also occurs in the year that marks 50 years of ESO's presence in Chile, underlining ESO's long-term involvement with Chile. He recalled his first trip to the high northern Atacama Desert region, when he travelled on the Calama railway from Calama to La Paz in Bolivia in 1982. Europe's road to ALMA began with

developments in the infrared, which evolved into millimetre/submillimetre telescopes at the Institut de Radioastronomie Millimétrique (IRAM) and SEST at La Silla, which opened in 1987. In the early 2000s, following the choice of Chajnantor as the future ALMA site and the beginning of construction activities, the Atacama Pathfinder Experiment (APEX), a collaboration between the Max Planck Institute for Radio Astronomy (MPIfR, 50 %), the Onsala Space Observatory (OSO, 23 %), and ESO (27 %), was commissioned in 2005. De Zeeuw recalled the prescient plot of the novel by Fred and Geoffrey Hoyle, *The Inferno*, which laid out the case for building a submillimetre telescope as an international collaboration and siting it at high altitude in Chile — all this written 40 years ago. Now that has become a reality, as a result of ESO's collaboration with its partners from North America and East Asia.

Prior to the final speech given by the President of Chile, Sebastián Piñera, a film of the Atacameño ceremony, which asked for blessings from Mother Earth for the ground on which ALMA is built and for the people who live and work nearby, was relayed (see Figure 4). President Piñera referred to this ceremony and pointed out that the choice of the name of the plateau on which ALMA is built was prescient, as Chajnantor means "place of departure, observation point" in the

Figure 4. The Atacameño sacred ceremony, consisting of an offering to ask for blessings and thanks, was performed on Chajnantor at the AOS.

language of the original people. Although the ALMA Observatory is built to satisfy the curiosity of a few, its discoveries will contribute to the knowledge held by all humanity. He expressed his gratitude to all those countries that have invested in astronomical facilities in Chile, and so making it a world astronomy capital. He closed by looking forward to all the discoveries that will come from ALMA. The text of the speech is presented on p. 6.

Finally, a live transmission from the AOS presented by the Chilean ALMA staff astronomer Antonio Hales concluded the official opening ceremony with the ALMA antennas moving to point towards the Galactic Centre (Figure 5).

Following the speeches, lunch was provided for all the attendees, organised by a renowned Chilean chef and featuring regional dishes.

Press conference

The day prior to the inauguration was dedicated to the press, with staff from ALMA and the Executives available to answer questions and tour the laboratories at the OSF. Among the highlights of the day were a press conference at the OSF, a press visit to the AOS and a demonstration of the transporter lifting one of the antennas in the European contractor camp. The press conference, attended in person by 100 journalists from around the world and many more by teleconference, was introduced by the then ALMA Director, Thijs de Graauw. He described the ALMA project: of the 66 ALMA antennas which will constitute the full array, the final nine are in an advanced state and the final antenna is expected to

Figure 5. The President of Chile, Sebastián Piñera, and Thijs de Graauw, the recently retired ALMA Director, closing the ALMA inauguration ceremony with a background projection of the ALMA antennas observing the Galactic Centre.

be delivered by August 2013. Most of the hardware and software is in place and the second year of observations, actually named Early Science Cycle 1, has begun, after the successful Cycle 0 in 2011–2012.

Al Wootten, the ALMA Project Scientist for North America, then spoke about the history of the project. He stressed the large amount of research and development that had to be done to construct the high performance antennas, fitted to the high altitude conditions, the state-of-the art receivers with seven of the ten proposed bands furnished, and the correlator to combine the signals from all the antennas. This was followed by the incoming ALMA Director, Pierre Cox, who reported on some of the extragalactic science results from the science verification data and Cycle 0 Early Science. He emphasised the power of ALMA for the detection of normal galaxies out to high redshift and for its potential to study the earliest stages of galaxy formation. He described ALMA as a renaissance for millimetre/submillimetre observation after

the discovery of CO emission from a galaxy at $z > 1$ in 1991.

Ewine van Dishoeck from Leiden Observatory, and a former member of the ALMA Board, then described the science that ALMA is beginning to achieve in the area of star and planet formation. ALMA allows us to probe the initial phases of the growth of the rocky cores of planets (see ESO Release eso1248). The complexity of the astro chemistry just beginning to be explored is clear from the vast numbers of unidentified emission lines in the spectra of nearby star-forming regions such as Orion, and is exemplified by the early discovery of glycolaldehyde in a protostellar binary system (see ESO Release eso1234). But ALMA is also making discoveries in the late stages of stellar evolution, as revealed by the spiral CO outflow from the asymptotic giant branch star R Sculptoris (see ESO Release eso1239).

The final speaker at the press conference was Michael Thorburn, the head of ALMA Engineering, who described some of the

engineering and infrastructure that makes ALMA an operational observatory, such as the 192 antenna foundations spread across the Chajnantor Plateau, the two ALMA transporters, named Otto and Lore, and the provision of electrical power to the whole facility. The press conference closed with questions from the members of the press present and online participants.

References

Madsen, C. 2012, *The Jewel on the Mountaintop – The European Southern Observatory through Fifty Years*, (Weinheim: Wiley-VCH)

Links

[1] ALMA inauguration page: http://www.almaobservatory.org/inauguration/

Texts of Speeches

Tim de Zeeuw, ESO Director General

President Piñera, Doña Cecilia Morel, Excellencies, Minister Fukui, Director Suresh, Ambassadors, former, present and future ALMA Directors, other luminaries, colleagues and friends,

In 1982, Ewine van Dishoeck and I visited Chile for the first time, for an observing trip to the La Silla Observatory. Afterwards we travelled north, and took the legendary narrow-gauge train from Calama to La Paz. We were stunned by the beauty of the terrain, and remember particularly well the magnificent sunset near Ollague on the border between Chile and Bolivia. Little did we realise that 30 years later we would both be attending the inauguration of the world's most powerful radio telescope, so nearby on the similarly stunning Chajnantor Plateau.

It is therefore a great pleasure and a privilege to speak at this momentous occasion for science in general, and astronomy in particular. I represent the European Organisation for Astronomical Research in the Southern Hemisphere, commonly known as the European Southern Observatory. ESO is an intergovernmental organisation with fourteen European Member States and Brazil poised to join as soon as the Accession Agreement has been ratified by the Brazilian Parliament.

ESO was founded in 1962, and came to Chile in 1963, where it built the La Silla Observatory, followed by the Paranal Observatory with the Very Large Telescope, which will be joined in about a decade by the Extremely Large Telescope on nearby Cerro Armazones. All these facilities observe the Universe at visible and near-infrared wavelengths. So why did ESO join ALMA?

The development of infrared detectors made it possible to peer deeper into the dusty and cold regions of the Universe, where stars form, and to study objects at higher redshift, i.e., in the early Universe. The community which was engaged in this research in Europe realised it could do even better by capitalising on the development of submillimetre detector technology, with Thijs de Graauw as one of its pioneers. This led to the creation of Institut de Radioastronomie Millimétrique (IRAM) and the James Clerk Maxwell Telescope (JCMT), and to ESO entering the short-wavelength radio domain with the 15-metre Swedish–ESO Submillimetre Telescope (SEST) on La Silla, a copy of one of the IRAM dishes and operational between 1987 and 2003. SEST was followed by the 12-metre Atacama Pathfinder Experiment (APEX) on Chajnantor in 2005, operated by ESO in partnership with the Max Planck Institute for Radio Astronomy in Bonn and the Onsala Space Observatory. As a result, the European optical and millimetre communities integrated naturally.

The logical next step was to increase resolution and sensitivity by going from a single dish to an interferometer on a really high site, with the best high-frequency receivers that could be built. The power of a radio interferometer goes up with the square of the number of antennas, so by joining the worldwide ALMA partnership it was possible to build a much more powerful facility at an affordable price. Building the array in Chile with the strong support of the Chilean government, was of course also natural for ESO.

ESO's model of operation is to work very closely with institutes and industries in its Member States, for the construction of observatories, telescopes and instruments, all with the goal of enabling scientific discoveries. ESO's contributions to the ALMA project are similarly drawn from all over Europe, in industry (for example, the antennas provided by the AEM consortium and the transporter built by Scheuerle), and in institutes (for example, the high-frequency receivers built by IRAM and the Netherlands Research School for Astronomy [NOVA]). This same distributed model underlies ESO's approach to the science support: this is done in a network of nodes (the ALMA Regional Centres) in the Member States. That this model works is clear: the pressure on observing time for ALMA is highest in the ESO Member States.

This same spirit of collaboration between multiple partners and multiple institutions is now working

at the global level and can serve as an example for other large research infrastructures.

When preparing for today's event I could not help but recall an amusing science fiction book written by Fred Hoyle and his son Geoffrey in 1973, entitled *The Inferno*. Fred Hoyle was the genius who contributed to working out how stars can make carbon through nuclear fusion of lighter elements. One strand of the story concerns the protagonist, a fictional Scottish physicist who was the Director General of the European Organization for Nuclear Research (CERN), working together with the Director of the US National Radio Astronomy Observatory (NRAO) to review plans for a new radio telescope in

Australia to be built in partnership with the United Kingdom. At stake were different antenna designs, new solid-state techniques to detect the radiation, selecting the best wavelength range and finding the ideal location. The protagonist comes out strongly in favour of shorter wavelengths to study the gas and molecules in the Universe, allowing smaller antennas and enabling the most promising new science. He furthermore suggests putting the telescope, not in Australia, but in Chile, and to ignore those who do not think this is radio astronomy. All of this sounds extremely familiar! But the remarkable aspect is that this was written forty years ago as part of a novel, at a time when only a few interstellar molecules had been found. Amazing!

Since then the field of submillimetre astronomy has indeed gone from very humble beginnings (which featured a small telescope on top of a building at Columbia University in New York) to the transformational ground-based facility we are inaugurating today in the 50th year of ESO's presence in Chile. The first scientific results that have been obtained with a partial array are already stunning, and I look forward to much more.

Thank you very very much to all who have helped create ALMA!

Sebastián Piñera, President of Chile

Friends of science, astronomy, research, progress and the Universe:

The truth is that mankind, since our origins, has always felt an irresistible drive to learn about, discover, and understand what is beyond the horizon, to expand the frontiers of knowledge.

Newton told us that to achieve that goal, he stood upon the shoulders of giants.

And that's why this afternoon, here in this desert, the driest in the world, the Atacama Desert, it is a great privilege to inaugurate this observatory, a true giant of astronomy and observation.

It is undoubtedly the most powerful radio telescope in the world, and it will enable us to expand the frontiers of knowledge, to go further than our predecessors and probably find out the secrets of the origin of the Universe, as well as its destiny, the origins of life, and the origins of the Galaxy. Because this observatory is not here just to satisfy the curiosity of a few, but will contribute significantly to the knowledge of all of humanity, by enabling us to learn more about the world in which we live, the Universe in which we live, and it may even enable us to find life beyond planet Earth.

It is true, Tim, that 40 years ago a novel called *The Inferno* was published, which in a certain way anticipated this project. For more than 30 years, men and women in Europe, the United States and Japan, not only dreamed about, but planned and worked to make it a reality today. But there were others who knew that this would happen even before then. The Atacameño people always knew that this great observatory would be here, in this land, because the name of this plateau, home to these 66 antennas, is not a coincidence. Chajnantor, in the language of the original people of this land, means "place of departure, observation point".

And so perhaps they knew that it was an exceptional place to look at the stars, the Universe, and through observing, to get to know ourselves better.

The name of this telescope, ALMA, Atacama Large Millimeter/submillimeter Array, is a technical one, but it has a very profound meaning in the Spanish language, which is "soul".

And therefore, we recall from the Book of Genesis that "God created man from dust", but finally, with one breath he introduced life, the soul, and transcendence along with that.

This project, this adventure, this ALMA initiative, is not merely technological, but also has a profound mystical, metaphysical meaning, related to the expansion of our knowledge of ourselves, where we come from, and where we're going.

That's why astronomy has always played an exceptional role in the history of humanity. Since antiquity, astronomers have always been renowned and admired, including Copernicus and Galileo. Because in the end, as so many have said for so long, we are not alone in the Universe. We don't know if there is life as we understand it out there, but we do know that we are part of a Universe that is vastly larger and more extensive than we believed for a long time.

And it is very likely that this remarkable observatory will allow us to learn more about the scope, the nature, the extension of this great Universe in which we live.

And it will enable us to learn about stars that perhaps don't exist today, and to penetrate, with an eye that is much more powerful than the human eye, because the human eye is only capable of perceiving certain colours. But the Universe has many more colours, and it will enable us to look into that cold area of the Universe that requires specialised technologies, not only to see and observe, but also to interpret.

Therefore, I would like to express my sincere gratitude to all who have been part of this major effort. Of course, I am grateful for the efforts made by countries in Europe and North America, and Japan as well, the efforts made by scientists, astronomers, the engineers who have worked on this project, the ALMA array, for so long. I would also like to thank the Chilean workers who built this observatory and made this day possible.

I would like to say to the scientists, to the Chilean astronomers who have joined this project with so much enthusiasm, that Chile is a small country, but when it comes to astronomy, with your support, we hope to become a true giant.

So for Chile it is a great privilege that thanks to your contributions, today Chile has practically become

the astronomy capital of the world. And probably, with the projects that are on the way, in addition to existing ones such as La Silla, Tololo, Paranal and ALMA, plus all those to come, Chile will be home to 60 % of mankind's capacity to observe the Universe.

And in that endeavour, I want you to know, all who have that curiosity, that commitment, that interest in investigating, discovering, you will always be able to count on the steady, clear, decisive and enthusiastic support of the Government of Chile.

I would like to conclude by saying that for Chile this is a great privilege. We want Chile to become a world astronomy capital. We also want to take advantage of astronomy to create a real astronomical tourism industry, because every day there are more men and women in the world who want to know more about the stars, the Universe, that perhaps infinite world that surrounds us.

So our commitment is not only to develop astronomical tourism, but also to take advantage of the opportunity to play an exceptional role in the world of astronomy, to make Chile a country in which innovation, science and technology are an essential part of the society we want to build.

That's why this is the year of innovation, because we understand that for a country to be developed, it is not enough to increase *per capita* income. We also have to be a country capable of becoming a full member of this new and modern society, the knowledge society, the information society. And for that, no doubt, projects such as ALMA will be a tremendous stimulus and support.

Finally, I would like to hope that good things come out of this great adventure of mankind that today we are inaugurating at ALMA. Hopefully all that we discover here will not only help us know more, but also help us be better. And I believe that no one should be afraid of knowledge, no one should be afraid of that spirit of awakening, inquisitiveness and curiosity that has moved the world since its origins, and which today is manifested fully in a project with the scope, magnitude and transcendence of ALMA.

Two aerial views of the ALMA Array Operations Site (AOS) on the Chajnantor Plateau taken in December 2012. Upper image shows the centre of the array with (lower right) the ALMA Compact Array; lower image (looking north-west) shows the AOS technical building to the right of the array and APEX in the distance. The prominent mountain peak is Licancabur volcano.

High Contrast Imaging with the New Vortex Coronagraph on NACO

Dimitri Mawet[1]
Olivier Absil[2]
Julien H. Girard[1]
Julien Milli[1,3]
Jared O'Neal[1]
Christian Delacroix[2]
Pierre Baudoz[4]
Anthony Boccaletti[4]
Pierre Bourget[1]
Valentin Christiaens[2]
Pontus Forsberg[5]
Frederic Gonté[1]
Serge Habraken[1]
Charles Hanot[2]
Mikael Karlsson[5]
Markus Kasper[1]
Anne-Marie Lagrange[3]
Jean-Louis Lizon[1]
Koraljka Muzic[1]
Eduardo Peña[1]
Richard Olivier[6]
Nicolas Slusarenko[1]
Lowell E. Tacconi-Garman[1]
Jean Surdej[2]

[1] ESO
[2] Département d'Astrophysique, Géophysique et Océanographie, Université de Liège, Belgium
[3] Institut de Planétologie et d'Astrophysique de Grenoble (IPAG), Université Joseph Fourier, Grenoble, France
[4] LESIA, Observatoire de Paris, Meudon, France
[5] Department of Engineering Sciences, Ångström Laboratory, Uppsala University, Sweden
[6] GDTech s.a., Liège Science Park, Belgium

The installation and successful commissioning of an *L'*-band annular groove phase mask (AGPM) coronagraph on VLT/NACO is presented. The AGPM is a vector vortex coronagraph made from diamond sub-wavelength gratings tuned to the *L'*-band. The vector vortex coronagraph enables high-contrast imaging at very small inner working angles (here 0.09 arcseconds, the diffraction limit of the VLT at *L'*), potentially opening up a new parameter space in high-resolution imaging. During technical and science verification runs, we discovered a late-type companion at two beamwidths from an F0V star, and imaged the inner regions of β Pictoris

down to the previously unexplored projected radius of 1.75 astronomical units. The circumstellar disc of β Pic was also resolved from 1 to 5 arcseconds. These results showcase the potential of the NACO *L'*-band AGPM over a wide range of spatial scales.

Introduction

High contrast imaging is an attractive technique to search for exoplanets as it provides a straightforward means to characterise them and their host systems through, e.g., orbital motion, spectrophotometry of the planetary atmospheres or planet–disc interactions. For these reasons, it constitutes one of the main science drivers of today's ground-based near-infrared adaptive optics instruments. One in two proposals to use NACO, VLT's adaptive optics workhorse instrument, is related to extrasolar system science. The same ratio is observed in the number of publications (see Figure 1).

In terms of the detection of new objects, the current capabilities of NACO have almost been exhausted, a situation faced by most first generation adaptive optics imagers and even the Hubble Space Telescope. This does not mean that new discoveries will come to a halt, but we seem to have reached a plateau simply because the current parameter space has been combed through pretty thoroughly (although it should be emphasised

that the early surveys were not optimal and could be productively repeated). Recently, only a few objects have been discovered, and many non-detections reported and statistically interpreted (e.g., Chauvin et al., 2010; Vigan et al., 2012). The field is now in need of a technological breakthrough. It is expected that opening the parameter space to fainter/smaller planets closer to their parent stars will indeed bring many new objects (Crepp & Johnson, 2011). This intermediate parameter space will be opened by the second generation coronagraphic instruments that have started to arrive at all major observatories: SPHERE at the VLT (Beuzit et al., 2010); the Gemini Planet Imager (Macintosh et al., 2012); P3k-P1640 at Palomar (Oppenheimer et al., 2012); and SCExAO at Subaru (Martinache et al., 2012).

These new instruments have all been designed around coronagraphs fed by extreme adaptive optics systems, a configuration which is expected to break through the current contrast and inner working angle (IWA) floor. However, first generation instruments, such as NACO, still possess untapped potential that, only after ten years of operations and understanding, allow us to fully exploit it (Girard et al., 2012), especially in the mid-infrared (*L'*-band, from 3.5 to 4.2 μm). This wavelength range offers significant advantages compared to shorter wavelengths (Kasper et al., 2007): (i) the *L'*-band contrast of planetary-mass companions with
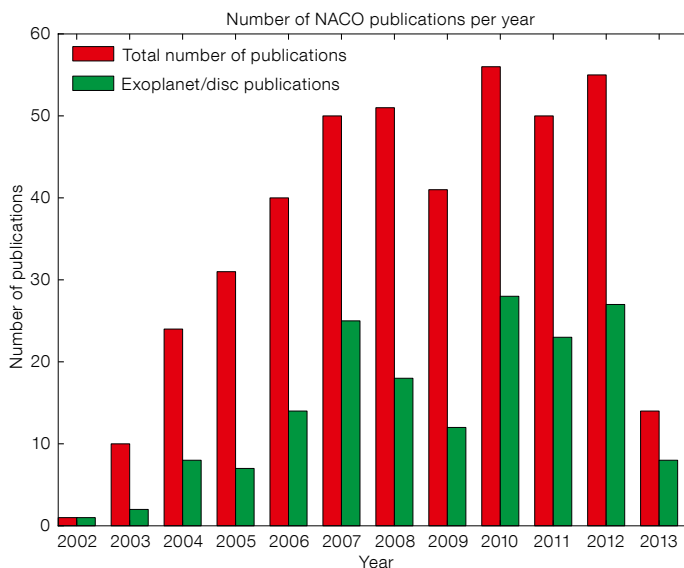

Figure 1. Total number of NACO refereed publications per year (red) and the number of articles related to extrasolar planetary system imaging and characterisation (green). Source: telbib[1].

respect to their host stars is predicted to be more favourable than in the *H*-band (e.g., Spiegel & Burrows, 2012) so that lower-mass, older objects can be addressed; and (ii) the *L'*-band provides better and more stable image quality, with Strehl ratios well above 70%, and sometimes as high as 90%, thus reducing speckle noise. These advantages certainly compensate for the increased sky background in the thermal infrared and the loss in resolution, especially if small IWA phase-mask coronagraphs are available.

The annular groove phase mask vector vortex coronagraph

While working on the four-quadrant phase-mask (FQPM) coronagraph achromatisation for the future VLT-Planet Finder (SPHERE) more than ten years ago (work later published in Mawet et al. [2006]), the idea of making the FQPM circularly symmetric occurred (Mawet et al., 2005). It was quickly noticed that the FQPM is indeed nothing more than an overly discrete optical vortex. Optical vortices occur when the phase structure of light is affected by a helical ramp around the optical axis, given by $e^{il\theta}$, where θ is the focal plane azimuthal coordinate and l is the vortex "topological charge", i.e., the number of times the phase accumulates 2π along a closed path surrounding the phase singularity; i denotes $\sqrt{-1}$. The phase dislocation forces the amplitude to zero at its centre, which is a singularity. Nature prevents the phase from having an infinite number of values at a single point in space, which is non-physical, by simply nulling the light locally. In Mawet et al. (2005), we demonstrated for the first time that, when centred on the diffraction pattern of a star seen by a telescope, optical vortices have the remarkable property of affecting the subsequent propagation to the downstream Lyot stop by redirecting the on-axis starlight outside the pupil, where it is simply blocked.

On account of this property, and from the fact that it is a pure phase mask, the advantages of the vortex coronagraph over classical Lyot coronagraphs or phase/amplitude apodisers are: (i) small IWA, down to 0.9 λ/D, where λ is the wave-

length of light and D the telescope diameter, e.g., 0.09 arcseconds in the *L'*-band at the VLT, thus slightly smaller than the diffraction limit; (ii) clear 360° off-axis field of view/discovery space; (iii) outer working angle set only by the instrument and/or mechanical/optical constraints; (iv) achromatic over the entire working waveband (here *L'*-band); (v) high throughput (here ~ 88%); and (vi) optical/operational simplicity.

Developed with colleagues and collaborators from the Université de Liege and the Observatoire de Paris-Meudon, we had no idea at the time that this concept would be potentially revolutionary and so difficult to realise. It took seven years to manufacture the first "vector vortex coronagraph" made from liquid crystal polymers at NASA-JPL (Mawet et al., 2009), and another three years to manufacture a fully functioning annular groove phase mask (AGPM) from diamond subwavelength gratings. The AGPM is one possible realisation of the vortex coronagraph, especially adapted to longer wavelengths (the first AGPM was actually optimised for the *N*-band, and installed in VISIR). It took two generations of PhD theses, the craftsmanship and the super high-tech capabilities of the Swedish foundry at Uppsala University to attain the stunning results presented here. The AGPM has now reached a sufficient read-

iness level for telescope implementation (Delacroix et al., 2013).

The AGPM selected for NACO was the third in a series of four realisations (AGPM-L3). Its theoretical raw null depth, limited by its intrinsic chromatism, was estimated (assuming a trapezoidal profile, see Figure 2) and measured to be around 5×10^{-3} (corresponding to a raw contrast of 2.5×10^{-5} at 2λ/D), which is more than needed for on-sky operations, where the limit is set by the residual wavefront aberrations.

The AGPM was installed inside NACO as part of a planned overhaul in November 2012. The AGPM was mounted on the entrance slit wheel by means of a dedicated aluminium mount, designed by GDTech s.a.. The mount was designed to sustain the differential contraction/dilatation of the aluminium relative to diamond, between room temperature and CONICA's working temperature of 60 K at the level of the slit/mask wheel, while providing enough thermal conduction capabilities. The assembly of the mount and AGPM was done on site at Paranal Observatory in a cleanroom environment (see Figure 3). Prior to on-sky tests and operations, a CONICA internal image of the mask was made (see Figure 4), revealing significant dust contamination, marginally affecting the background
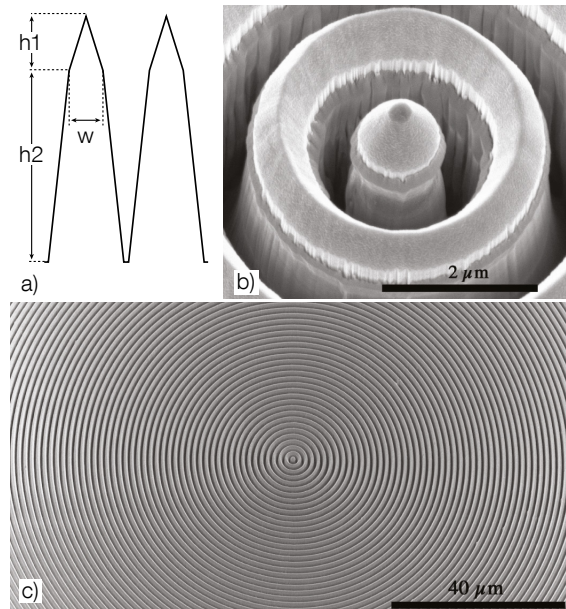
Figure 2. Scanning electron microscope images of the NACO AGPM made from diamond sub-wavelength gratings. a) The structure profile schematic, with h2 = 5 ± 0.1 μm, h1 = 1 ± 0.1 μm, and w = 0.65 ± 0.03 μm (the grating pitch is 1.42 μm). b) A zoom on the centre of the diamond AGPM. c) An overview of the structure showing the uniformity and original cleanliness of this particular device.
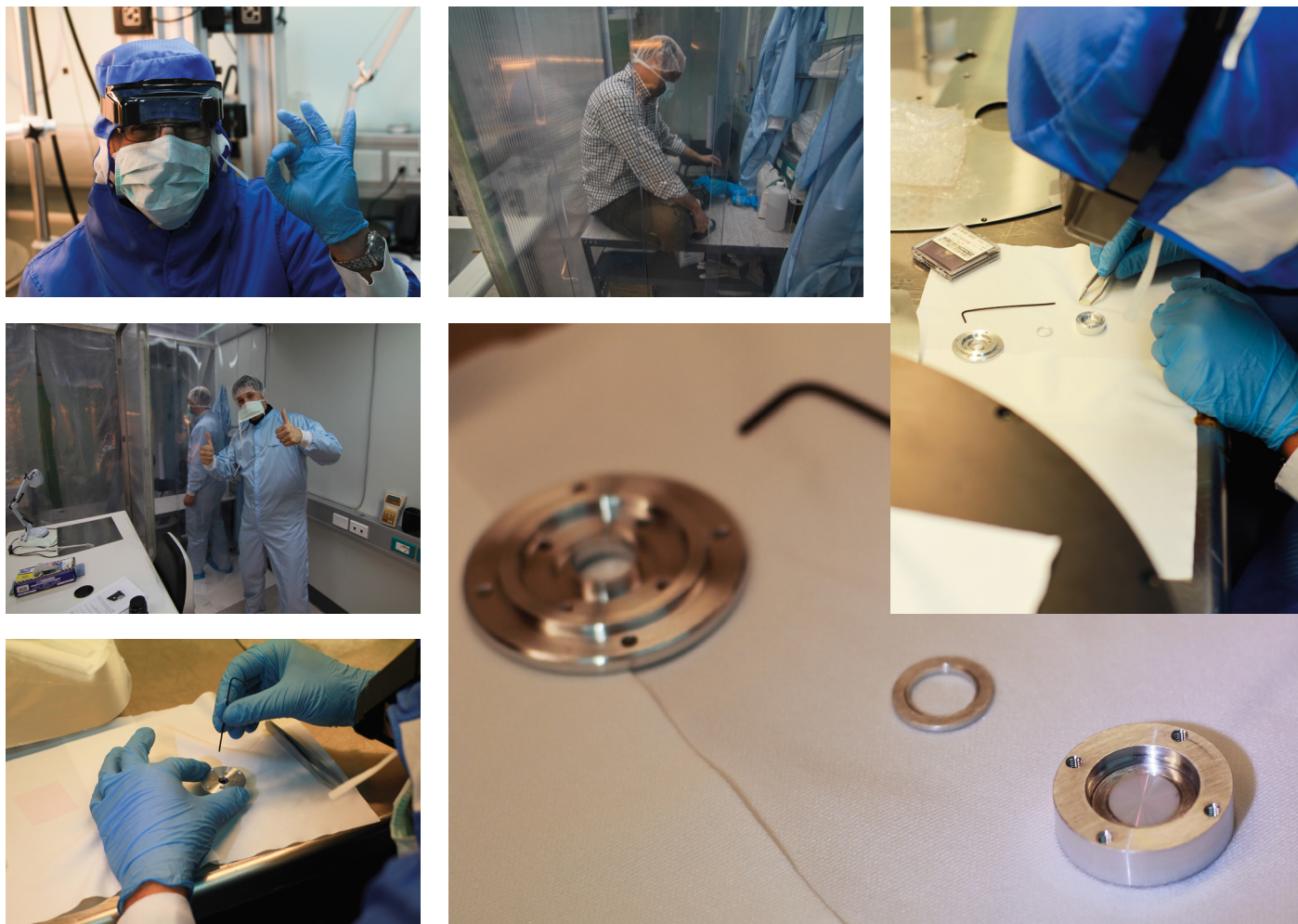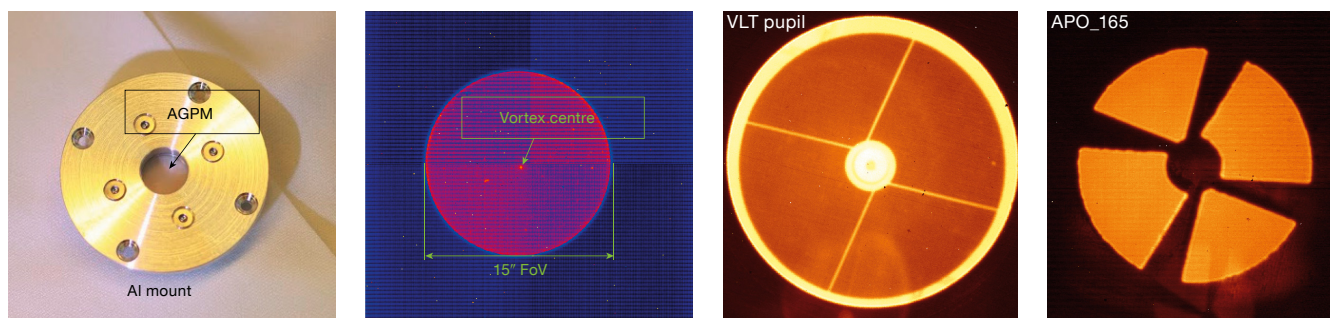
Figure 3 (above). Mounting of the AGPM in the Paranal cleanroom. The component, which looks like a tiny compact disc (10 mm diameter and 0.3 mm thickness), was handled with care and inserted into a dedicated mount (designed in Belgium by GDTech s.a. to support a cooldown from room temperature to a few tens of K). The assembly was then mounted onto the slit/mask wheel (focal plane) of CONICA. A great amount of synergy between Paranal Science Operations (Julien Girard and Dimitri Mawet, the Instrument Scientists) and Instrumentation (Jared O'Neal, the Instrument Responsible) was necessary for this whole process to succeed.

Figure 4 (below). From left to right: (i) The fully assembled aluminium mount with a 9 mm clear aperture containing the AGPM. (ii) View from inside CONICA, showing the 9 mm clear aperture corresponding to a 15-arcsecond field of view (diameter), fully contained within the 27-arcsecond field of view of CONICA's L27 objective. (iii) Full oversized stop of CONICA, showing the VLT pupil (including the central obscuration and struts). (iv) APO_165 pupil mask (diameter = $0.87 \times D_{pupil}$) available inside CONICA, aligned to cover the diffraction and thermal background from the central obscuration and struts.
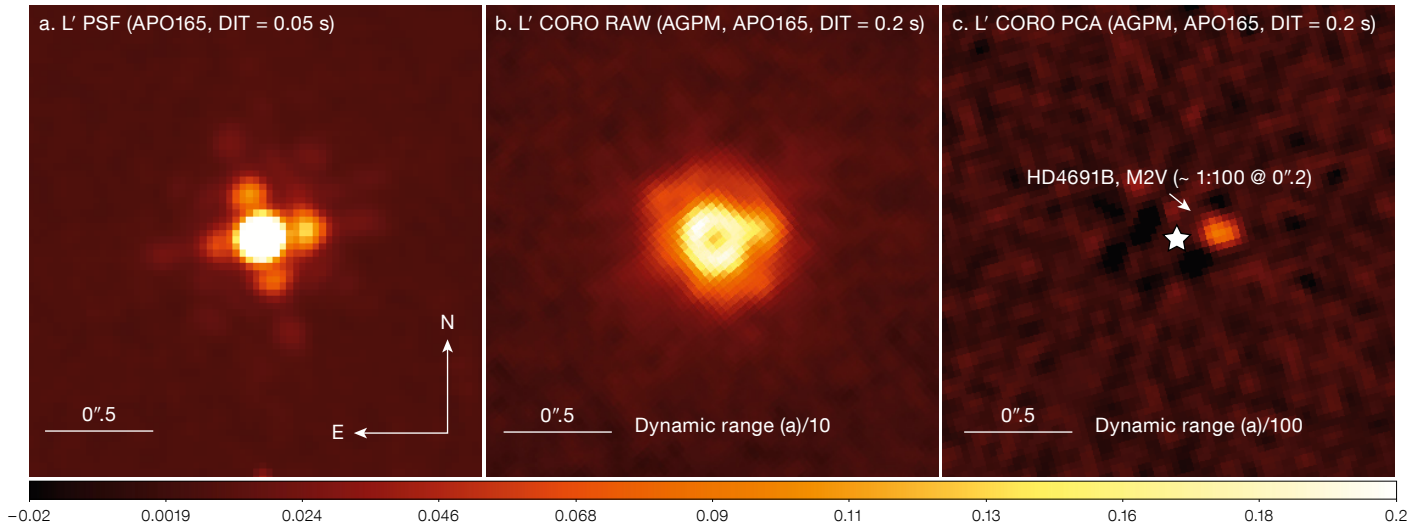
a. L' PSF (APO165, DIT = 0.05 s)

b. L' CORO RAW (AGPM, APO165, DIT = 0.2 s)

c. L' CORO PCA (AGPM, APO165, DIT = 0.2 s)

N

E

0".5

0".5   Dynamic range (a)/10

0".5   Dynamic range (a)/100

HD4691B, M2V (~ 1:100 @ 0".2)

−0.02   0.0019   0.024   0.046   0.068   0.09   0.11   0.13   0.16   0.18   0.2

Figure 5. a) *L'*-band NACO PSF with the APO165 pupil mask in the beam. b) *L'*-band NACO coronagraphic image with the star centred on the AGPM (the dynamic range and corresponding colour bar scale are a factor of ten smaller than in image a). c) Result of our PCA-ADI data reduction pipeline, revealing a putative faint off-axis M2V companion at a separation of only ~ 0.19 arcseconds (the dynamic range and corresponding colour bar scale are a factor of 100 smaller than in image a). The scale is linear on all images (and scaled down by a factor of 10 and 100 for b and c, respectively), illustrating in sequence the benefits of coronagraphy and optimised data reduction technique. The bottom colour bar refers to Figure 5a.

noise. The slit wheel was set so that the centre of the AGPM falls close to, but slightly away from, CONICA's detector quadrant intersection. The AGPM field of view is ~ 15 arcseconds, corresponding to an outer working angle (OWA) of 7.5 arcseconds. The OWA is only limited by the size of the device (10 millimetres in diameter) and its mount. The mask transmittance at *L'*-band was measured on the sky to be 85 % ± 5 %, which is consistent with the theoretical value and laboratory measurements, both ~ 88 %, limited by imperfect antireflective treatments and mild absorption features around 4 μm (Delacroix et al., 2013).

In order to stabilise speckles, we used the pupil-tracking mode enabling angular differential imaging (ADI), which is perfectly adapted to the circular symmetry and 360° field of view of the AGPM. The CONICA camera is equipped with a pupil mask (APO_165) which blocks the telescope's central obscuration and spiders. Once correctly aligned with the pupil

(in *x*, *y* and *θ*), this mask is optimal for use with the AGPM in pupil-tracking mode (see Figure 4). The measured throughput of the APO_165 mask used here is ~ 60 %. In terms of sensitivity, it is worth noting that the throughput loss is almost entirely compensated for by the improved thermal background. Indeed, the pupil obscuration is responsible for more than 25 % of the thermal emissivity of the telescope, even though its area only covers ~ 5 %. Blocking it with the APO_165 mask is therefore very efficient at reducing background noise, limiting the increase in background noise to 10 % with respect to non-coronagraphic imaging (Mawet et al., 2013).

First light: A discovery and breakthrough contrast capabilities

On 9 December 2012, a representative observing sequence was performed on the 1.9-Gyr-old main sequence standard star HD4691, under ~ 1.2 arcsecond visual seeing conditions. This star was chosen to maximise brightness and field rotation during the short time allocated for this technical test. A ~ 30-minute ADI sequence was obtained with a parallactic angle (PA) range of 30° and for a total exposure time of 200 seconds on source; the efficiency was mediocre for technical reasons. After acquiring an off-axis point spread function (PSF) star for photometric reference, we measured an instantaneous contrast of ~ 50 peak-to-peak (despite the average-to-bad conditions).

The attenuation is about five times higher than measured with NACO's four-quadrant phase-mask coronagraph at *Ks* (Boccaletti et al., 2004). The coronagraph diffraction control yields two instantaneous benefits compared to classical imaging: (i) the peak saturation limit is decreased by a factor ~ 50; and (ii) the level of quasi-static speckles pinned to the PSF and the stellar photon noise limit are potentially decreased by a factor ~ 7, both within the AO control radius of 7λ/D. All in all, the *L'*-band AGPM coronagraph allows the background limit to be reached much closer in to the source.

After applying basic cosmetic treatment to our sequence of 100 frames (background subtraction, flat fielding and bad pixel/cosmic ray correction), we decided to use the quality and stability of the *L'*-band PSF provided by NACO to perform a sophisticated speckle subtraction. We used the very efficient principal component analysis (PCA) algorithm presented in Soummer et al. (2012). The result, using the whole image and retaining three main components, is presented in Figure 5. By pure chance, the object has a ~ 1 : 100 (or Δ*L'* ~ 5 mag) off-axis companion located at ~ 0.19 arcseconds (< 2λ/D), making this our first unexpected scientific result. The companion flux and astrometry were obtained by using the fake negative companion technique (Marois et al., 2010). At an absolute *L'*-band magnitude of 6.65, and age 1.9 Gyr for the system, the putative companion would most likely be an M2V star

at projected separation of 11.8 ± 0.4 astronomical units (AU), and 354.5 ± 0.6 degrees position angle (see Mawet et al. [2013] for more details).

Since the presence of the companion affects the contrast, we took another similar representative ADI sequence on a different standard star (HD123888). This technical test was performed under better conditions (seeing ~ 0.85 arcseconds), and benefited from our improved mastering of the new mode (efficiency was four times better than during the first light). A similar instantaneous attenuation was confirmed. To calibrate our detection limits against flux losses induced by PCA, we injected fake companions (at 15σ) prior to PCA and measured their throughput after PCA. We used the derived throughput map to renormalise the initial contrast curve *a posteriori* (Figure 6). This shows excellent detection capabilities down to the IWA of the AGPM. The final calibrated contrast presented here (green dash-dot curve), is limited by the small PA range, especially at small angles. The floor reached beyond an offset of 1-arcsecond is due to the background at *L'*, and will be lower for brighter targets and/ or longer integrations.

The β Pictoris disc and planet at *L'*-band: a teaser

During the science verification run on 31 January 2013, we imaged the inner regions of β Pictoris down to the previously unexplored projected radius of 1.75 AU with unprecedented point source sensitivity. The ~ 8 Jupiter-mass planet (see Lagrange & Chauvin [2012], and references therein) was imaged with excellent signal-to-noise ratio (see Figure 7), which, combined with the 5-millarcsecond-level astrometric precision enabled by the phase mask (contrary to Lyot coronagraphs, the star is always visible as a residual doughnut), allowed us to derive excellent photometric and astrometric data points (details to appear in a forthcoming paper, Absil et al. [2013], in preparation). The disc was also clearly resolved down to its inner truncation radius (Milli et al. [2013], in preparation).

It is truly a challenge to directly image such a faint debris disc at 3.8 μm, for

which both scattered starlight and dust thermal emission are weak. The relatively bright blobs that are visible away from the plane of the disc are remnants of the highly variable background modulated by the adaptive optics system. They are on similar spatial scales to those of the disc and we are currently studying new methods to isolate the astrophysical signal (disc only, including complex shape and warps) from the background residuals.

Outlook

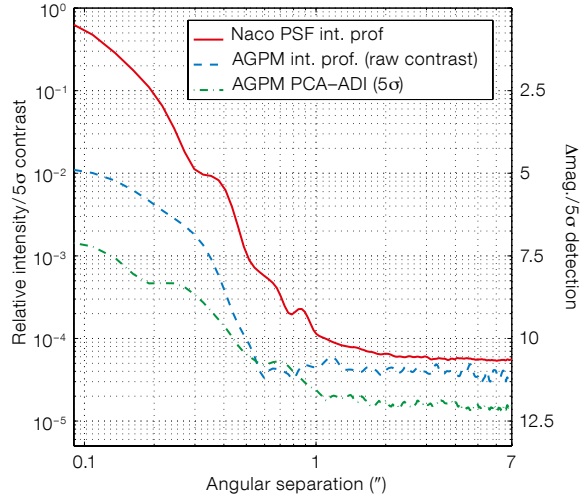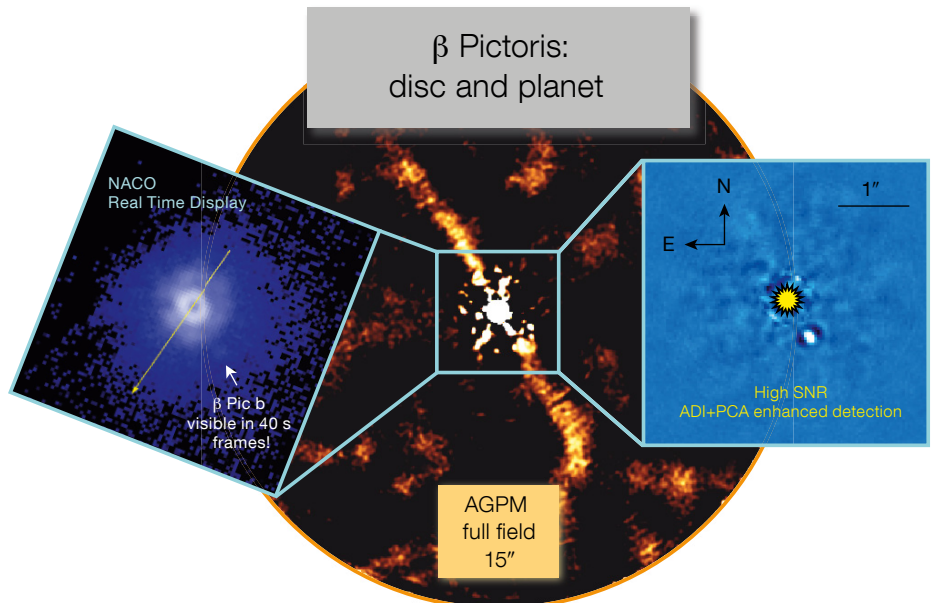The AGPM was designed to provide exquisite IWA (and OWA) capabilities,

Figure 6. Normalised azimuthally averaged relative intensity profiles and contrast curve on a log–log scale. The plain red curve shows the intensity profile of a typical saturated NACO *L'* PSF (similar brightness and exposure time). The blue dashed curve shows the AGPM intensity profile before PCA, demonstrating the instantaneous contrast gain provided by the coronagraph at all spatial frequencies within the adaptive optics control radius (~ 0.7 arcseconds). The green dash-dot curve presents the reduced PCA–ADI 5σ detectability limits (40 frames, 800 s, ΔPA ≈ 30°), taking both the coronagraph off-axis transmission and the PCA–ADI flux losses into account.

Figure 7. β Pictoris NACO+AGPM *L'*-band observations. This figure showcases the potential of the AGPM over a wide range of spatial scales: the central image represents the full field of view (15 arcseconds) of the AGPM with, at the centre, the masked star surrounded by both the planet (within 0.5 arcseconds) and the faint disc, several arcseconds away. On both sides, the central 4-arcsecond box is zoomed. The left image is a screen capture of the NACO real-time display (in log scale) which shows the star attenuated by the AGPM and the planet visible on single 40-second raw frames (DIT = 0.2 s, NDIT = 100). The right image shows the high signal-to-noise ratio detection of β Pictoris b applying modern post-processing techniques: angular differential imaging (ADI) and principal component analysis. North is up, east to the left.

down to 0.9λ/D (0.09 arcseconds at *L′*). The disadvantage of the AGPM's small IWA is its sensitivity to the Strehl ratio (as all coronagraphs) and to pointing errors. The apodising phase plate (APP) is another advanced coronagraph offered at *L′* (see, e.g., Kenworthy et al., 2013). The only, but significant, benefit of this pupil-plane phase apodiser over the AGPM is its intrinsic immunity to tip-tilt errors. This advantage, which has to be traded off against the significantly limited field of view provided by the APP, is decisive when tip-tilt is an issue, as was the case with NACO prior to November 2011 (Girard et al., 2012). However, it is less obvious when the instrument provides nominal PSF stability. In a single technical run, the *L′*-band AGPM has proved to be a reliable coronagraphic solution, and one of the best high-contrast imaging modes of NACO (and most likely world-wide). Combined with ADI, we have demonstrated that high contrast of the order of Δ*L′* > 7.5 mag can be reached from the IWA of 0.09 arcseconds outwards, even with very modest on-source integra-

tion time, PA variation and average conditions. The field of view is a clear 360° discovery space 15 arcseconds in diameter. The coronagraph is optimised for pupil tracking and is easy to use, thanks to the stability of the NACO *L′*-band PSF.

The vortex coronagraph is now the most advanced new generation coronagraph brought to operational level (it is offered at Palomar at *H* and *K*, at *L′* on NACO and at *N* on VISIR). Moreover, it has recently demonstrated 10^{-9} raw contrast capabilities in the visible at NASA's Jet Propulsion Laboratory's high contrast imaging testbed (Mawet et al., 2012). This coronagraphic solution, which is simple, reliable and now quite affordable, is foreseen for future coronagraphic space-based missions dedicated to exoplanet imaging. Last, but not least, it is considered as a potential baseline for the European Extremely Large Telescope high-contrast imagers, at near-infrared (EPICS-PCS), and/or mid-infrared wavelengths (METIS).

References

Beuzit, J.-L. et al. 2010, in *Pathways Towards Habitable Planets*, eds. Coudé du Foresto V., Gelino D. M. & Ribas. I., ASP Conf. Series, 430, 231
Boccaletti, A. et al. 2004, PASP, 116, 1061
Chauvin, G. et al. 2010, A&A, 509, A52
Crepp, J. R. & Johnson, J. A. 2011, ApJ, 733, 126
Delacroix, C. et al. 2013, accepted by A&A
Girard, J. H. V. et al. 2012, Proc. SPIE, 8447
Kasper, M. et al. 2007, A&A, 472, 321
Kenworthy, M. A. et al. 2013, ApJ, 764, 7
Lagrange, A.-M. & Chauvin, G. 2012, The Messenger, 150, 39
Macintosh, B. A. et al. 2012, Proc. SPIE, 8446
Marois, C. et al. 2008, ApJ, 673, 647
Marois, C., Macintosh, B. & Veran, J.-P. 2010, Proc. SPIE, 7736, 52
Martinache, F. et al. 2012, Proc. SPIE, 8447
Mawet, D. et al. 2005, ApJ, 633, 1191
Mawet, D. et al. 2006, A&A, 448, 801
Mawet, D. et al. 2009, Optics Express, 17, 1902
Mawet, D. et al. 2012, Proc. SPIE, 8442
Mawet, D. et al. 2013, A&A, 552, 13
Oppenheimer, B. R. et al. 2013, ApJ, 768, 24
Soummer, R., Pueyo, L. & Larkin, J. 2012, ApJ, 755, L28
Spiegel, D. S. & Burrows, A. 2012, ApJ, 745, 174
Vigan, A. et al. 2012, A&A, 544, A9

Links

[1] telbib: http://www.telbib.eso.org

FORS1 image of the young star-forming region IC 2944, which was released to mark the 15th anniversary of the first light of VLT UT1 on 25 May 1998. The colour image is formed from exposures in three broadband (*BVR*) and two narrowband filters (centred on the emission lines [O III] 5007Å and Hα). The extended emission across the whole image is ionised by hot early-type stars in the cluster and some prominent dust globules are silhouetted against the background H II region. Further details can be found in Release eso1322.

Automatic Removal of Fringes from EFOSC Images

Colin Snodgrass[1]
Benoît Carry[2]

[1] Max Planck Institute for Solar System
 Research, Katlenburg-Lindau, Germany
[2] Institut de Mécanique Céleste et
 de Calcul des Éphémérides (IMCCE),
 Observatoire de Paris, France

EFOSC, in common with many instruments with older CCDs, shows a fringe pattern in images taken at red wavelengths. These fringes are difficult to remove without significant manual adjustment for each individual frame, which is a time-consuming exercise, but necessary for reliable photometry of faint objects across the whole field of view. We present a simple technique to automatically remove fringes from CCD images, and provide scripts (available on the ESO website) to apply this to EFOSC data, or to any other images.

Fringing in CCD images

Astronomical charge-coupled device (CCD) images are often affected by fringe patterns (Figure 1a). These fringes are created by the interference of monochromatic light within the CCD. Narrowband filters are typically affected, as well as broadband filters containing strong sky emission lines. Lines due to atmospheric OH affect bandpasses at the red end of the CCD wavelength range ($\lambda > 700$ nm), i.e., R-, I- and Z-bands. The problem is discussed in more detail in the broad introductions to CCD data reduction by Gullixson (1992) and Howell (2006), and in the recent paper by Howell (2012). While the latest generation of CCDs does not suffer from this problem, there are many instruments still in active use (such as EFOSC2 at the New Technology Telescope [NTT]; Buzzoni et al., 1984) that employ older CCDs. Given the increasing popularity of ESO's archival data in publications, removal of fringes from images remains a necessary reduction step for many users.

Fringes are a cosmetic problem — obvious to the human eye when a typical "z-scale" algorithm is used to display astronomical images — but add only a
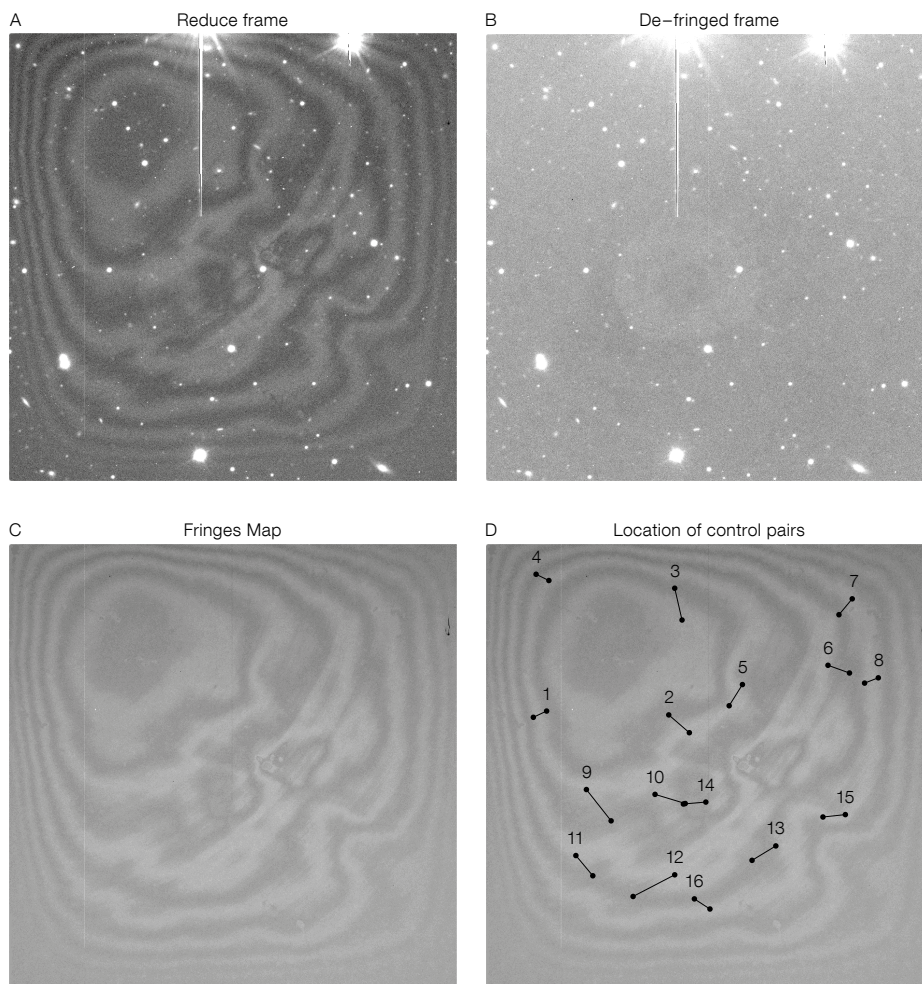
Figure 1. a) R-band EFOSC2 frame presenting a strong fringe pattern (following standard reduction steps: bias subtraction and flat fielding); b) same as a), but after application of the defringing method presented here; c) the fringe map used in the correction; d) location of the control pairs used to scale the fringe map (see text).

small additional flux to the image. For shorter exposure images they are hardly noticeable and attempts to remove them can be more trouble than they are worth (even a good fringe map has some associated noise, and it is worth remembering that all reduction steps add noise to the image; Newberry [1991]). However, for longer exposures, and especially when dealing with photometry of multiple or extended objects, or of moving targets, it can be critical to remove the fringes to provide properly uniform photometry across the field. As calibrations (biases, flats) are taken during the day, or during twilight, they do not show the faint night

sky-emission fringes and cannot be used for correcting the fringe patterns. Therefore, fringes are not removed by the standard data-processing techniques (bias subtraction, bad pixel masking, and flat-fielding). Fringe removal requires an extra step, where a description of the fringe pattern is scaled and subtracted from each image. This has traditionally been a rather labour-intensive step, typically requiring careful manual adjustments for each science image, as the intensity of the fringes is highly variable, depending on atmospheric conditions.

Properties of the fringes

The location of the fringes in the images is determined by changes in the thickness of the CCD. Hence, the pattern of the fringes on the detector is globally stable with time. The intensity of the fringes

depends on the amount of incoming monochromatic light, either from the sky emission lines or selected by a narrow-band filter. The fringes can therefore present large intensity variations from image to image, even during a single night of observation, reaching up to several percent of the noise level from the sky background. This variability presents the largest challenge in correcting for fringing, as care has to be taken to scale the fringe pattern to the correct intensity for each image individually before subtraction.

The stability of the fringe pattern means that a single high signal-to-noise (S/N) fringe map can be used to describe the pattern. These are generally created through a combination of frames taken of the night sky (under moonless conditions, as a bright sky background can mask the faint fringes). When data are taken of a given target with a significant jitter pattern — i.e., movement of the telescope in a random fashion between each image, so that sources do not fall on the same pixels in multiple images — then the data frames themselves can be median-combined to leave only the fringe pattern. Alternatively, images of a deliberately selected "empty" field can be used, but this uses a significant amount of good observing time for calibration. Howell (2012) describes a new method of constructing a fringe map using neon lamp illumination during daytime calibrations, which has the advantage that very high S/N can be achieved without wasting any time during the night. For EFOSC, a pre-prepared fringe map is available for download[1]. Fringe maps for EFOSC have been measured through different filters and at different times (including before and after moving the instrument from the 3.6-metre telescope to the NTT — see Snodgrass et al. [2008]), and demonstrate the stability of the fringe pattern and the fact that it is almost identical in different passbands.

Once a fringe map is obtained by any of the above methods it has to be scaled to the intensity of the fringe pattern in each science frame, and then subtracted from the data. Note that the fringe pattern is additional flux, so it is subtracted from the data, unlike flat-field variations, which are corrected by division. Here lies the difficulty in the operation, as the intensity

of the fringe pattern is highly variable on short timescales. In general it increases with increasing exposure time (longer exposures are more significantly affected), so to first order the pattern can be scaled by the length of each exposure. This is the approach used by the fringe removal option within the widely used *ccdproc* task in IRAF (part of the core *ccdred* package; Valdes [1988]), but this method can considerably over- or under-correct due to the intrinsic variations of the night sky-emission lines, which are not correlated to exposure time. The *ccdproc* task also gives the option of specifying additional scaling factors via image headers, but this requires considerable manual iteration to get a satisfactory result. It is worth noting that the same IRAF package also includes the *mkfringecor* task, which is used to combine frames to construct a good fringe map.

A second approach implemented within IRAF is to scale the fringe map to globally minimise the difference between the map and object frames, which is used by the *rmfringe* and *irmfringe* tasks in the *mscred* package (Valdes, 1998). This approach works better, but requires careful masking of sources, bad pixels and cosmic rays to avoid these affecting the minimisation. It therefore needs some preparatory work, and can be time consuming when dealing with many frames (especially where these are of different fields).

Automatic de-fringing method

Here we describe a method that allows frames to be processed simply and automatically, with minimal preparation beyond the construction of the fringe map. We take advantage of the stability of the shape of the fringe pattern to clean it from the scientific frames, by using knowledge of the pattern to define areas of each image to perform automatic scaling. We describe the fringe pattern in terms of "dark" and "bright" areas, corresponding to the background sky and the fringes themselves (see Figure 1c). The precise choice of areas is not important, providing they sample the variation in the fringe pattern well (in practice, any sufficiently large number of random points will work).

To estimate the amplitude of the fringe pattern, we measure the flux difference between bright and dark areas. Practically, we use a series of "control pairs", each consisting of a couple of reference locations, taken in and out of the fringe pattern (Figure 1d). For each pair *i*, we measure the flux difference on the frame between the bright and dark area, $\delta F_i = F_{bright} - F_{dark}$, and, at the same position on the fringe map, the flux difference between the bright and dark areas, δM_i. The scale factor to be applied to the fringe map is then taken as the median of all the ratios, $\delta F_i / \delta M_i$. Theoretically, a single control pair would be enough to scale the fringe map. However, the presence of any astronomical source (star, galaxy, nebulosity, etc.) close to one of the ends of the control pair would bias the scale factor. Therefore we select several control pairs (typically 5 to 20) spread across the full field. Experimentation with the number and position of the pairs has shown that the quality of the subtraction is hardly affected by these factors.

The list of control pairs is based on the constant fringe pattern, so it can be fixed for a given instrument, and does not need to be modified for different datasets — with a sufficient number of pairs the occasional overlap of a pair with a source doesn't affect the scaling. This allows highly automated de-fringing — once a fringe map and a suitable set of pairs are defined for a given instrument, the de-fringing operation does not require further human intervention. As the measurement of each pair is a simple operation, a large number can be used without any concerns about computing time. The scripting of this operation is relatively straightforward — we provide implementations in two popular systems used for astronomical data reduction, IDL and IRAF. A table of control points for EFOSC is provided with the code[1].

The same approach has been applied as part of the Elixir pipeline for data from the MegaCam instrument at the Canada-France-Hawaii Telescope (Magnier & Cuillandre, 2004; Regnault et al., 2009). The scripts we provide implement a more general solution, designed to work with EFOSC, but applicable to all imaging data with no modification.

Example: photometry of trans-Neptunian objects

As an example of the method presented here, we present an image taken from a photometric survey of faint trans-Neptunian objects; members of a dynamical family related to the dwarf planet (136108) Haumea (Snodgrass et al., 2010; Carry et al., 2012). We measured visible colours (in *BVRi*-bands) and rotational light curves (*R*-band) of 30 targets with *V* magnitudes between approximately 20 and 24, using EFOSC. All the targets were moving relative to the comparison field stars, alternatively coming in and out of the fringe pattern (Figure 1a), and were therefore affected by it at a level that could have a significant influence on the photometry, especially for the faintest targets. We removed the fringe pattern using the method described here, and present the cleaned version of an example frame in Figure 1b. In this particular example, a faint circle is visible near the centre of the image, which is not part of the fringe pattern but a ghost reflection due to the bright star just off of the top of the frame. Such a faint structure is nearly impossible to identify in the original frame due to the fringes. Jitter patterns were employed to allow new fringe frames to be created, and with many moving targets observed over three multi-night runs, a large number of different fields were observed, including some relatively dense star fields. All were automatically processed via this method with no manual adjustments required. Our method has also been successfully applied to EFOSC images of extended sources (active comets) by Lacerda (2013).

References

Buzzoni, B. et al. 1984, The Messenger, 38, 9
Carry, B. et al. 2012, A&A, 544, A137
Gullixson, C. A. 1992, in ASP Conference Series, Vol. 23, *Astronomical CCD Observing and Reduction Techniques*, ed. S. B. Howell, 130
Howell, S. B. 2006, Cambridge observing handbooks for research astronomers, Vol. 5, *Handbook of CCD Astronomy*, eds. R. Ellis, J. Huchra, S. Kahn, G. Rieke & P. B. Stetson, (Cambridge: Cambridge University Press)
Howell, S. B. 2012, PASP, 124, 263
Lacerda, P. 2013, MNRAS, 428, 1818
Magnier, E. A. & Cuillandre, J.-C. 2004, PASP, 116, 449
Newberry, M. V. 1991, PASP, 103, 122
Regnault, N. et al. 2009, A&A, 506, 999
Snodgrass, C. et al. 2010, A&A, 511, A72
Snodgrass, C. et al. 2008, The Messenger, 132, 18
Valdes, F. 1988, in *Instrumentation for Ground-Based Optical Astronomy*, ed. L. B. Robinson, 417
Valdes, F. G. 1998, in ASPacific Conference Series, Vol. 145, *Astronomical Data Analysis Software and Systems VII*, eds. R. Albrecht, R. N. Hook, & H. A. Bushouse, 53

Links

[1] Pre-prepared EFOSC fringe image and de-fringing scripts from: http://www.eso.org/sci/facilities/lasilla/instruments/efosc/inst/fringing.html

Colour-composite image of the large planetary nebula IC 5148 taken with EFOSC2 on the New Technology Telescope at La Silla (image size 4.2 by 4.2 arcminutes) formed from exposures in *B*, Hβ, *V*, *R* and Hα filters. The nebula morphology consists of two distinct shells but the bright ansae indicate more complex substructure. The emission nebula is of high ionisation and the very hot central star is obvious. See Picture of the Week 15 October 2012 for more information.

Precipitable Water Vapour at the ESO Observatories: The Skill of the Forecasts

Marc Sarazin[1]
Florian Kerber[1]
Carlos De Breuck[1]

[1] ESO

Atmospheric precipitable water vapour (PWV) above an observatory is a crucial parameter for the success and quality of submillimetre and mid-infrared science observations. High precision water vapour radiometers are deployed at the ESO observatories on Paranal (VLT) and Chajnantor (APEX and ALMA), providing continuous high time-resolution measurements of PWV. These data have been used to compare the actual conditions with the forecast delivered by the publicly available Global Forecast System provided by the National Oceanographic and Atmospheric Administration. The quality of these predictions has now reached a level at which it can contribute to optimising science operations.

Introduction

We are certainly used to the daily weather forecast and for many a plan for the weekend barbecue is based on, say, Thursday's forecast. While, for the Saturday afternoon party, some basic information such as lack of precipitation and temperatures above 22 degrees suffice. The situation is more complex for astronomical observations. ESO's service mode has been popular with European astronomers and its success derives from its ability to perform demanding science observations under the right environmental conditions. While some user-provided constraints, such as lunar phase and distance from the target, can be simply calculated in advance, other important constraints, such as seeing or atmospheric transparency, can only be known close to the time of observation (often called nowcasting). Any useful astro-meteorological forecast has to make quantitative predictions on very specific atmospheric properties above the observatory.

Modern atmospheric models have been successful in providing such forecasts for air travel, severe weather events, agri-

culture and other fields demanding specialised products (e.g., storm tracks) and, partly as a result, the weather for Saturday's barbecue has become more predictable than 20 years ago. PWV, however, is not easy to predict because of its intrinsic variability in time and location within the atmosphere. It is a very relevant question whether current state-of-the-art models are up to the task of providing forecasts for a given atmospheric parameter, such as PWV, that are good enough to help with the scheduling of service mode observations 12, 24 or even 48 hours in advance.

Atmospheric water vapour

Atmospheric water vapour content (Kerber et al., 2012a), usually given as the height of the column of precipitable water vapour (in mm), has a strong impact on the transparency of the atmosphere in the infra-red (IR) and submillimetre domains. This parameter has only recently become important at ESO's observatories with introduction of operations for the Atacama Pathfinder EXplorer (APEX) and the Atacama Large Millimeter/submillimeter Array (ALMA) at Chajnantor and the upgraded VLT Imager and Spectrometer for mid-IR (VISIR) instrument on Paranal. For APEX and ALMA each antenna carries a bore-sight radiometer to determine the amount of water vapour in the line of sight. For ALMA, correcting for the phase delay introduced by the PWV is essential to ensure proper operations of the ALMA antennas as an array. On Paranal a low humidity and temperature profiling microwave radiometer (LHATPRO) was installed in support of VISIR and other IR instrumentation in late 2011 (Kerber et al., 2012b).

While there are several ways to determine the atmospheric PWV (Otarola et al., 2010; Querel et al., 2011), APEX, ALMA and Paranal have, for a number of practical reasons, decided to use microwave radiometers as operational monitors. The ALMA antennas each house a custom-made water vapour radiometer (WVR) built by Omnisys (Emrich et al., 2009) while both APEX and Paranal use a commercial radiometer (LHATPRO; Rose et al., 2005) developed and manufactured by Radiometer Physics GmbH (RPG). All

of these instruments make use of the same technology and observe an intrinsically very strong H_2O emission line at 183 GHz; see the feature in Figure 1. Hence this line can still be observed under extremely dry conditions (Ricaud et al., 2010; Kerber et al., in preparation). The median PWV on Paranal is 2.5 mm while on Chajnantor it is 1.2 mm. The use of this line and the very accurate and precise receiver technology guarantees that for both sites reliable information on PWV is available at the observatory sites under all — even the driest — conditions. This is crucial since the driest conditions offer the best transparency; in particular both ALMA and APEX are equipped to ob-serve at frequencies above 600 GHz, which become accessible only in very dry conditions from the high site at 5000 metres above sea level.

Here we compare the measured PWV data with a publicly available model (the Global Forecast System [GFS] provided by the US National Oceanographic and Atmospheric Administration) in order to determine whether such a model has enough predictive power or forecasting skill to support advance scheduling.

Operational need for forecasting at Chajnantor and Paranal

A major difference between APEX and ALMA (Chajnantor) on the one hand, and VLT (Paranal) on the other, apart from the difference in altitude, is that the former are carrying out science observations 24 hours a day, while Paranal's instruments only observe during the night. Another fundamental difference is that millimetre and submillimetre science is clearly driven by atmospheric transparency and hence PWV is the crucial parameter in terms of scheduling. For the optical and IR instrumentation on Paranal, more than one environmental constraint are usually specified by the users, e.g., good seeing, dark sky and photometric conditions may all have to be satisfied at the same time. A case in point are cirrus clouds. It is an observational fact that, on both Paranal and Chajnantor, PWV can be very low in the presence of high-altitude cirrus clouds that consist of ice crystals. Hence, during their formation some PWV is removed from the

atmosphere and locked up in the ice crystals. While on Chajnantor, APEX and ALMA would therefore enjoy good atmospheric conditions, observations on Paranal would be negatively affected by the non-photometric conditions due to the cirrus cloud. As a result the PWV forecast provided by the GFS may be directly suitable to guide scheduling for APEX and ALMA, while for the VLT other information likely needs to be considered as well.

Operational needs for APEX and ALMA (Chajnantor)

Both APEX and ALMA are operated exclusively in service mode to be able to make optimal use of the very different atmospheric transparency as a function of PWV. Figure 1 shows the impact of the range of PWV conditions observed at Chajnantor on the frequency coverage of the ALMA and APEX instrumentation. For conditions with PWV > 5 mm, only the windows below 200 GHz open up for observations with the ALMA Band 3 and 4 receivers. While Chajnantor is one of the best sites worldwide, six years of PWV measurements with the APEX radiometer (plotted as the mean annual variation in Figure 2) have shown that there are strong seasonal variations. In fact, conditions with PWV > 5 mm occur for 26 % of the time, as shown by the frequency distribution of PWV values in Figure 3, especially during the altiplanic winter between late December and mid-March. At APEX, no science operations are possible under such conditions, and major technical activities, such as generator maintenance and instrument installations, are planned during this period. Based on the first four years of PWV measurements, this shutdown period was shifted forward by ten days to make better use of the best weather conditions (see Figure 2). During the period of regular science operations, a reliable prediction of such PWV > 5 mm conditions allows the optimal scheduling of maintenance activities that are not time-critical.

If the PWV drops below 5 mm, more atmospheric bands become progressively available (see Figure 1). For APEX, the main difference in operations occurs when the PWV drops below 2 mm, where the bolometer arrays LABOCA (345 GHz;
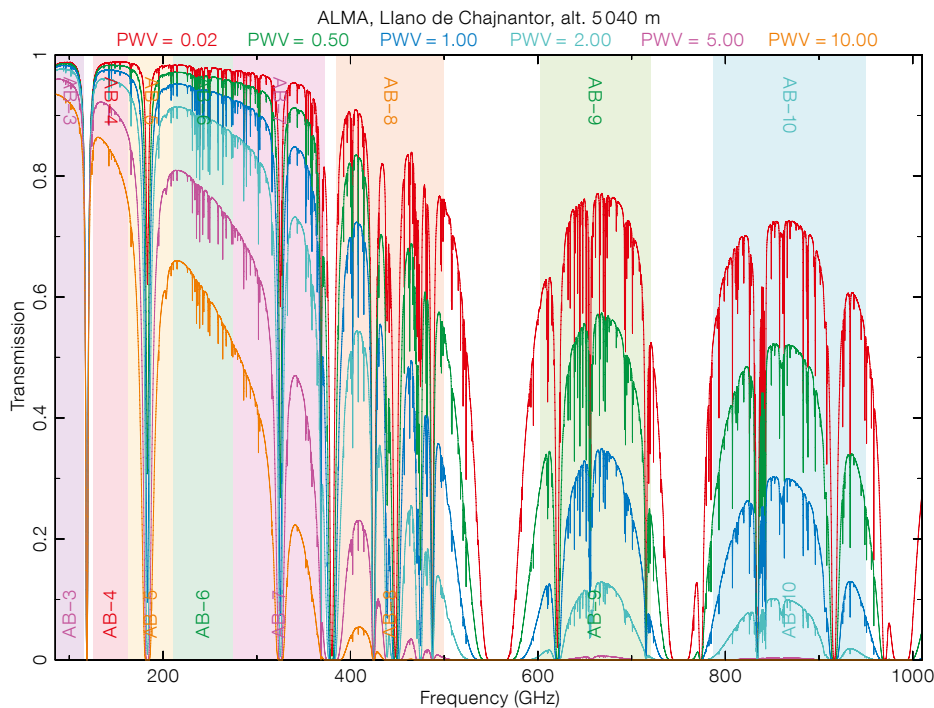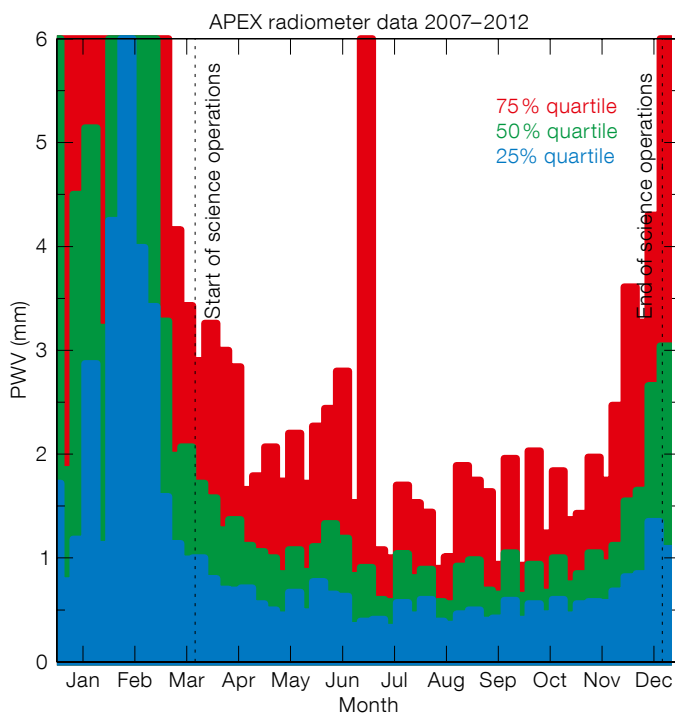

Figure 1 (above). Atmospheric transmission as a function of frequency for six different values of PWV distinguished by coloured lines. Note that at frequencies higher than 600 GHz, the atmosphere only becomes sufficiently transparent when the PWV drops below 1 mm. The coloured regions indicate the ALMA bands. Note that the 183 GHz H_2O line used by the radiometers remains prominent even at minimal PWV.

Figure 2 (below). Annual variation of the PWV at Chajnantor as measured by the APEX radiometer. Months suitable for science operations deliberately avoid the altiplanic winter conditions from late December until early March. Based on the information from this plot, the timing of the shutdown period was shifted forward by ten days to make better use of the best weather conditions.
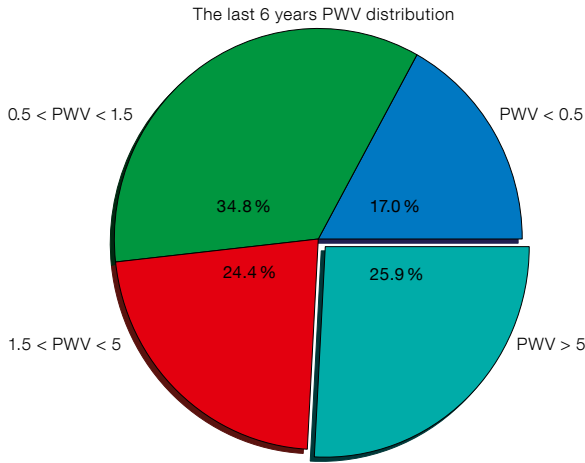
The last 6 years PWV distribution

0.5 < PWV < 1.5

PWV < 0.5

34.8 %

17.0 %

24.4 %

25.9 %

1.5 < PWV < 5

PWV > 5

Figure 3. Pie chart of the distribution of the PWV values at Chajnantor as measured by the APEX radiometer.

Siringo et al., 2007) and SABOCA (850 GHz; Siringo et al., 2010) can observe. Both instruments are cooled with liquid helium, which requires a daily refill and recycling procedure at the telescope to allow the observations. If the PWV forecast predicts that such conditions will not occur during the next 24-hour period, the cryocooler in these instruments does not need to be recycled, allowing savings to be made on expensive helium consumption. As both LABOCA and SABOCA are installed in the Cassegrain cabin of APEX and the cryostats need to be within ~ 15° from vertical during the condensation phase, there are also restrictions on the elevation of the observations during recycling. If the PWV forecast indicates that a recycling is not needed, these restrictions do not have to be taken into account in the observing plan, allowing the observing time to be used more efficiently.

For the very best weather conditions with PWV < 0.15 mm, even the three THz-frequency windows open for ground-based observations. Such conditions are very rare, occurring only 1.4 % of the time. Currently, only APEX has instruments available to observe at these high frequencies, but feasibility studies have been started to build ALMA Band 11 filters for these wavelengths (Yassin et al., 2013). In order to make optimal use of these best-weather conditions, it is essential to have a reliable PWV prediction to adapt the science observations schedule. In particular, as such instruments are used only rarely, there are fewer calibration plan observations, and it is advantageous to start early within an excellent weather slot to allow sufficient time for the science target observations. The current GFS PWV predictions provide not only a warning several days in advance (Figure 4) that such conditions

are likely to occur, but also an indication of the length of time that these THz windows will remain open.

Operational needs for the VLT (Paranal)

Less than half of the observations at the VLT are performed on site by the astronomers who submitted the proposal, assisted by Paranal staff. The remainder are used for service mode observations, which are executed by ESO staff on behalf of the scientific users. In this case all observations are fully prepared (Phase 2) by the astronomer at his/her home institute using ESO-provided software. The observations are organised into self-contained units, known as observation blocks (OBs), of maximum duration one hour. These are checked for consistency and observing strategy by ESO's User Support Department in Garching, and, once released, are ready for execution at the VLT. As part of the preparation of these OBs the astronomer can impose constraints on the environmental conditions under which each OB will be executed. One such constraint parameter is lunar phase, which can be limited to ensure that very faint targets are only observed during dark time. Similarly, PWV is now being used as constraint for several IR instruments, such as VISIR and CRIRES.

Since OBs are relatively short, several OBs from different programmes can be executed during a given night, e.g., OBs requiring dark time can be executed
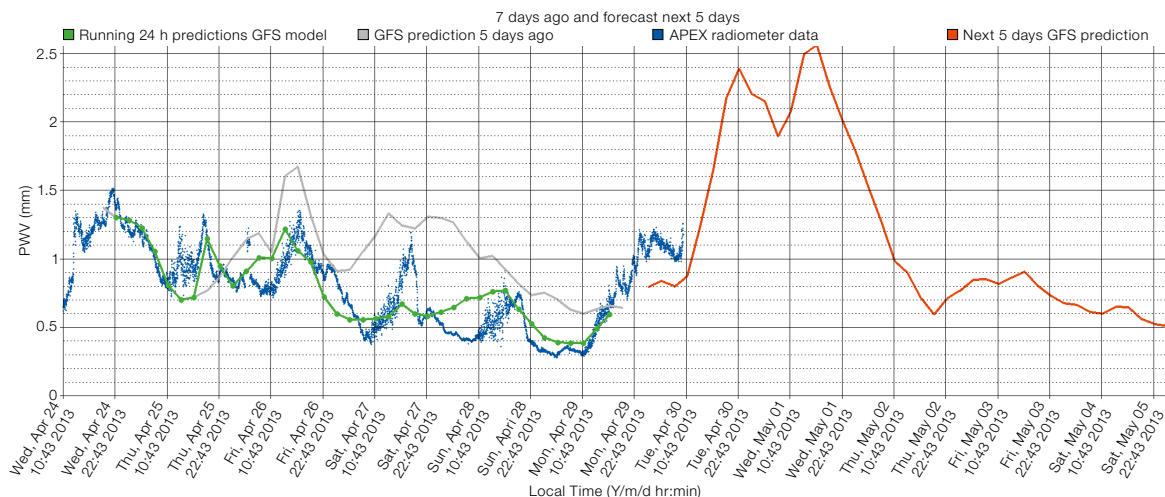

Figure 4. GFS PWV predictions for Chajnantor for the following five days (red line). This plot is continuously updated and available[2]. It is used by both APEX and ALMA to plan observations. To judge the reliability of the forecast, the 24-hour and five-day predictions of the last week (green and grey lines respectively) are compared with the APEX radiometer observations (blue dots).
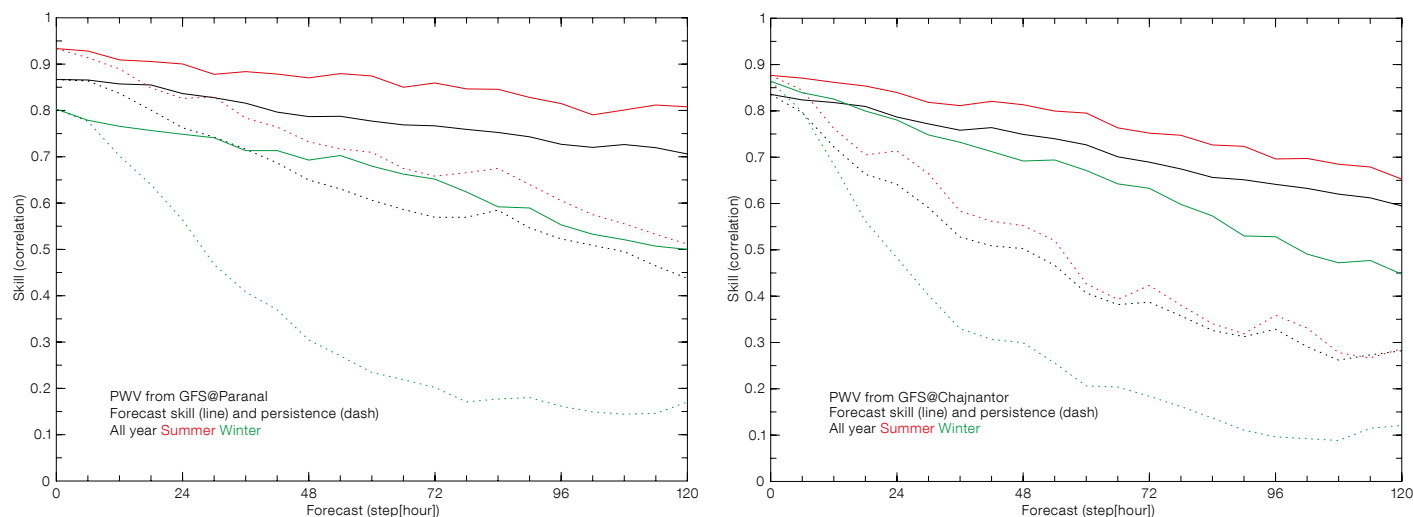
Figure 5. GFS PWV forecast skill (as given by the Pearson correlation coefficient) at Paranal (left) and Chajnantor (right) as a function of forecast step up to five days, compared to persistence (dashed lines) for the whole year (in black), summer (red) and winter (green).

before the Moon rises, or after it sets. As the VLT can switch between instruments within about 15 minutes, the flexibility at the telescope is high and the support astronomer can react to changing environmental conditions. Currently, the ESO support astronomer has to select the OBs for execution in real time assisted by scheduling tools which take into account the scientific priority assigned by the Observing Programmes Committee, as well as the probability that the requested conditions such as PWV or seeing are realised. While this works relatively well, it would be highly advantageous if our ability to forecast atmospheric conditions some hours ahead were good enough to prepare a full night of observations in advance. This would enable the use of much more sophisticated scheduling algorithms that could further optimise the scientific output of all telescopes on Paranal. In the context of PWV, a forecast that would reliably predict conditions with an accuracy of about 1.0 mm would permit a general pre-selection of OBs, while an accuracy of 0.25 mm would allow for highly detailed planning. As observations are only done during the night, such a forecast would have to cover a period of eight hours to a maximum of 14 hours with 24 hours advance notice.

GFS model and output products

The Global Forecast System (GFS) is a global numerical weather prediction system run by the US National Oceanographic and Atmospheric Administration[1]. The GFS model is run four times per day at 0, 6, 12 and 18 UTC. The GFS output is fully public and a web page[2] was designed for ESO in autumn 2010 by the University of Valparaiso to support APEX operation at Chajnantor, displaying up to five days of GFS forecasts of PWV above the Chajnantor Plateau (see Figure 4).

The accuracy of global weather models is improving constantly, but is also very variable, depending on the parameter concerned and the location for which the prediction is made (populated areas are better modelled because more initialisation data is available). It is thus a requirement, before trusting such a product, to compare it to local measurements during a time span long enough to be representative of the weather conditions in the area. This was done at Chajnantor using the APEX radiometer database[3] and the results were convincing enough to extend the service to the Paranal Observatory. Only after enough data had been collected there by the new Paranal PWV monitor could we compare the forecast skill at both observatories, which is the purpose of this article. For this comparison we have used two years of APEX radiometer data at Chajnantor (2011–2012) and one year at Paranal (2012). In Figure 5, the Pearson correlation coefficient of the forecast with the ground-

based data is compared to the persistence (i.e., in the absence of a forecast, simply assuming that the current situation persists without change). It is clear on both sites that forecasting winter conditions is more difficult due to higher variability (the correlation of persistence drops below 50% in less than 24 hours). However in all cases the GFS forecasts provide a clear improvement of the extrapolated knowledge of observing conditions on both sites.

One limitation of the model is the spatial resolution of about 40 kilometres per grid point. Hence local effects cannot be expected to be reflected by the model. When local radiometer data is available in real time, it is possible to correct for local biases by applying a Kalman filter trained on, say, the past 14 days of the GFS forecast. Figure 6 shows that Kalman filtering is able to remove the offsets between GFS forecasts and local measurements on both sites. Evidently, the use of the Kalman filter results in excellent statistical agreement between the observed and modelled PWV distribution.

The confidence in the model results can be expressed in terms of hit rate, i.e., the fraction of time that the prediction falls in the same class (distinguished as best, average or worst conditions defined by 33% and 66% of the distribution) as the measured value. The hit rate for the 24-hour forecasts is reported for Chajnantor and Paranal in Tables 1 and 2, respectively, showing that the best conditions are successfully forecast by
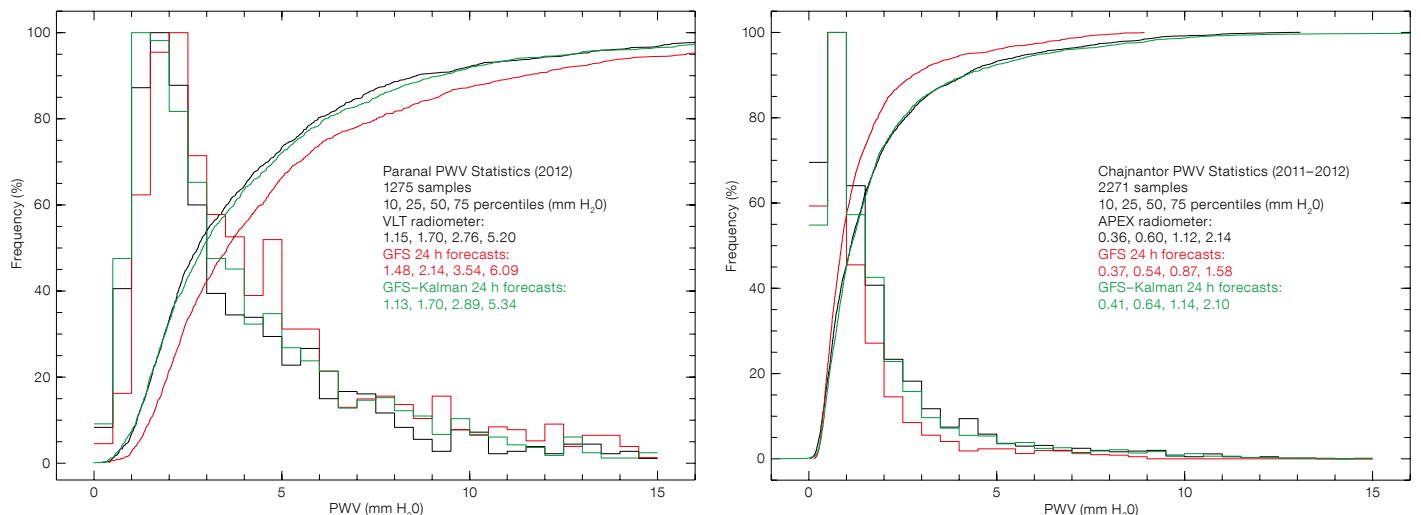
Figure 6. Comparison of the GFS 24-hour PWV forecast, before (red) and after (green) Kalman filtering, to the local radiometer statistics (black) at Paranal (left) and Chajnantor (right) show as normalised histograms and cumulative distributions. The value of the PWV for the 10, 25, 50 and 75 percentiles of the respective database is given in the three cases.

Table 1. 24-hour PWV forecast performance at Chajnantor. Columns refer to the radiometer measurements, while rows refer to the forecasts. The percentage of forecasts falling in each measurement class (Best: PWV < 0.7 mm; Average: 0.7 < PWV < 1.7 mm; and worst: > 1.7 mm) are listed. Percentages in parentheses are obtained after Kalman filtering.

GFS (Kalman) PWV	Radiometer PWV		
	Best	Average	Worst
Best	86(67)	13(29)	1(4)
Average	27(18)	66(62)	7(20)
Worst	5(2)	35(23)	60(75)

Table 2. 24-hour PWV forecast performance at Paranal. Columns refer to the radiometer measurements, while rows refer to the forecasts. The percentage of forecasts falling in each measurement class (Best: PWV < 2.0 mm; Average 2.0 < PWV < 4.2 mm; and Worst: PWV > 4.2 mm) are listed. Percentages in parentheses are obtained after Kalman filtering.

GFS (Kalman) PWV	Radiometer PWV		
	Best	Average	Worst
Best	56(70)	36(25)	8(5)
Average	9(26)	62(53)	29(21)
Worst	1(2)	9(19)	90(79)

GFS 86% of the time at Chajnantor, with a negligible risk of being misled. When using Kalman filtering, the hit rate reaches 70% for the best conditions at Paranal. Note that the Kalman filter can add non-physical noise which may reduce the hit rate, e.g., in presence of strong diurnal trends. An optimisation study is underway.

Outlook for ESO

We have *post facto* compared the values of PWV observed at Chajnantor (two years) and Paranal (one year) with the forecasts provided by a standard atmospheric model (GFS). Agreement is very reasonable and by use of a two-week Kalman filter, excellent statistical agreement can be achieved. A comparison with the persistence assumption shows that the GFS model has significant predictive power. The GFS forecast is particularly useful for ALMA and APEX since their science performance is mostly driven by atmospheric transparency and hence PWV. In addition such a forecast helps to optimise the cooling cycles of instruments, with a direct impact on operational costs.

For Paranal and the VLT instruments, PWV is of course only one aspect of the relevant properties of the atmosphere and more than one constraint needs to be met for optimal science performance. For this more sophisticated application, (meso-scale) models will be required. Such work is also in progress at ESO.

The GFS-based model has demonstrated its value for science operation at ESO observatories. PWV forecasts are now available for Chajnantor[4] and Paranal[5]. We expect that forecasts of specific atmospheric properties will become routine in the era of extremely large telescopes, helping to optimise their scientific performance.

References

Emrich, A. et al. 2009, 20th International Symposium on Space Terahertz Technology, 174
Kerber, F. et al. 2012a, Proceedings of the SPIE, 8448, 84463N
Kerber, F. et al. 2012b, The Messenger, 148, 9
Otarola, A. et al. 2010, PASP, 122, 470
Querel, R. R., Naylor, D. A. & Kerber, F. 2011, PASP, 123, 222
Ricaud, P. et al. 2010, IEEE Transactions Geoscience and Remote Sensing, 48, 1365
Rose, T. et al. 2005, Atmospheric Research, 75, 183
Siringo, G. et al. 2007, A&A, 497, 954
Siringo, G. et al. 2010, The Messenger, 139, 20
Yassin, G. et al. 2013, 23rd International Symposium on Space Terahertz Technology, Tokyo, in press

Links

[1] Global Forecast System (GFS): http://www.ncdc.noaa.gov/model-data/global-forecast-system-gfs
[2] GFS PWV prediction plot for Chajnantor: http://www.apex-telescope.org/weather/RadioMeter/index.php
[3] APEX radiometer database: http://archive.eso.org/eso/meteo_apex.html
[4] Chajnantor PWV forecast: http://www.eso.org/astclim/forecast/gfs/APEX/index.php
[5] Paranal PWV forecast: http://www.eso.org/astclim/forecast/gfs/VLT/index.php

This image of the centre of the Carina Nebula Complex (NGC 3372) was released to mark the inauguration of the VLT Survey Telescope (VST) on 6 December 2012. NGC 3372, at a distance of about 2.3 kpc, is the closest giant star-forming region, with more than 60 early-type stars, several young clusters and active star formation sites. The picture was taken with the help of Sebastián Piñera, President of Chile, during his visit to Paranal on 5 June 2012; see Release eso1250 for more information.

The Wide View of the Galactic Bulge as seen by the VVV ESO Public Survey

Oscar A. Gonzalez[1,7]
Dante Minniti[2,7,8]
Philip Lucas[3]
Marina Rejkuba[1]
Manuela Zoccali[2,7]
Elena Valenti[1]
Roberto Saito[2,4,7,9]
Jim Emerson[5]
Marcio Catelan[2,7]
Ignacio Toledo[6]
Maren Hempel[2,7]
Rodrigo Tobar[1]

[1] ESO
[2] Departamento Astronomía y Astrofísica, Pontificia Universidad Catolica de Chile, Santiago, Chile
[3] Centre for Astrophysics Research, University of Hertfordshire, Hatfield, United Kingdom
[4] Departamento de Física y Astronomía, Universidad de Valparaiso, Chile
[5] School of Physics & Astronomy, Queen Mary University of London, United Kingdom
[6] ALMA Operations Support Facility, San Pedro de Atacama, Chile
[7] The Milky Way Millennium Nucleus, Santiago, Chile
[8] Vatican Observatory, Vatican City State, Italy
[9] Universidade Federal de Sergipe, Departamento de Física, São Cristóvão, SE, Brazil

The first year of observations of the Galactic Bulge in the Vista Variables in the *Via Lactea* (VVV), one of ESO's public surveys with the VISTA telescope, have yielded a deep, near-infrared, multi-colour (*Z,Y,J,H,Ks*) photometric coverage of over 320 square degrees. Results based on this impressive dataset are presented, showing the global properties of the Bulge. Extinction has been mapped using the magnitude and colour of the red clump, revealing a large amount of small-scale structure. This extinction map has been used to de-redden the VVV stellar photometry to study the Bulge morphology from the absolute magnitude of the red clump and to derive photometric metallicities from the colour of red giant branch stars. The VVV survey continues to obtain multi-epoch data to investigate the variable stars in the Bulge.

The Galactic Bulge: An obscured past

The study of the central components of disc galaxies is a key step towards understanding the formation and evolution of spiral galaxies. The shape of the bulges embedded in galactic discs provides an important constraint on the different processes driving the history of galaxy assembly. The correlation between the structural properties of bulges and the properties of their stellar populations — namely the age and chemical abundances of bulge stars — has become an important factor in characterising the past history of the host galaxies, and is a basic ingredient for modern galaxy evolution models.

The main complication of such studies in external galaxies is the impossibility of resolving individual stars in the dense inner bulge regions. The Bulge of the Galaxy on the other hand, located at nearly 8 kpc, allows individual stars to be resolved and the detailed properties of the Bulge stars to be obtained. However, this possibility comes at a high price: we need to overcome the strong interstellar extinction due to the dust and gas across the intervening Disc of the Galaxy, so that we can cover homogeneously, and with a high spatial resolution, an enormous area on the sky. We also need to disentangle the stars in the Bulge from those distributed in the Disc along the line of sight towards the Bulge.

Until recently, spectroscopic and photometric studies had to base their efforts on investigating particular regions towards the Bulge that were not strongly affected by extinction, for example, the well-known Baade's Window. Studies in these regions provided important clues about the age, chemical abundances and morphology of the Bulge and they shared one common conclusion: the Bulge is much more complicated than previously thought, and thus the need for a global, deep and homogeneous study is undeniable.

Our group of investigators, led by Dante Minniti and Phil Lucas, accepted the challenge and using VISTA, the world's most powerful infrared survey telescope, started the Vista Variables in the *Via Lactea* ESO public survey.

The VVV survey

The VVV survey observations are carried out using the 4-metre VISTA telescope located on Cerro Paranal (Emerson et al., 2004), which, coupled with the high-sensitivity infrared camera VIRCAM, has the capacity to overcome the heavy extinction of the Galactic Plane in order to reach Bulge stars up to a limiting magnitude of *Ks* ~ 18 mag, with a median seeing of ~ 0.9 arcseconds. Furthermore, the high efficiency of VISTA allowed us to complete a set of single-epoch, multi-band observations of the entire Bulge region of ~ 320 square degrees using *Z, Y, J, H* and *Ks* filters within less than two Bulge observing seasons. Figure 1 shows the distribution of tile images across the Bulge area covered. Each tile is the result of six exposures (known as pawprints) used to cover a field of 1.48 by 1.18 degrees in size (Arnaboldi et al., 2007). The Bulge survey area consists of 196 of these tiles distributed as shown in Figure 1. Descriptions of the observing strategy, survey goals and first results are available from Minniti et al. (2010) and Saito et al. (2010). The first data release article, DR1 (Saito et al., 2012), describes the survey products in detail.

The final catalogue of the Bulge, as seen by the VVV survey, has a total of more than 84 million sources (Saito et al., 2012) and yielded a magnificent composite image of the Bulge area (ESO Release eso1242). Based on this dataset, we were able to study the global properties of the Galactic Bulge for the first time. An illustrative example is the VVV Bulge colour–magnitude diagram (CMD) shown in Figure 2, which, together with the VVV Disc CMD, are the largest CMDs to date. The CMDs yield important information about the Galaxy, showing the fingerprint of its structure and content.

The solution to the reddening problem

Towards the Bulge of the Galaxy, interstellar extinction effects are not only very strong, but also highly variable on small scales. As a result, sequences in colour–magnitude diagrams (see Figure 2) become very hard to identify and the properties of the Bulge stellar populations cannot be accurately characterised.
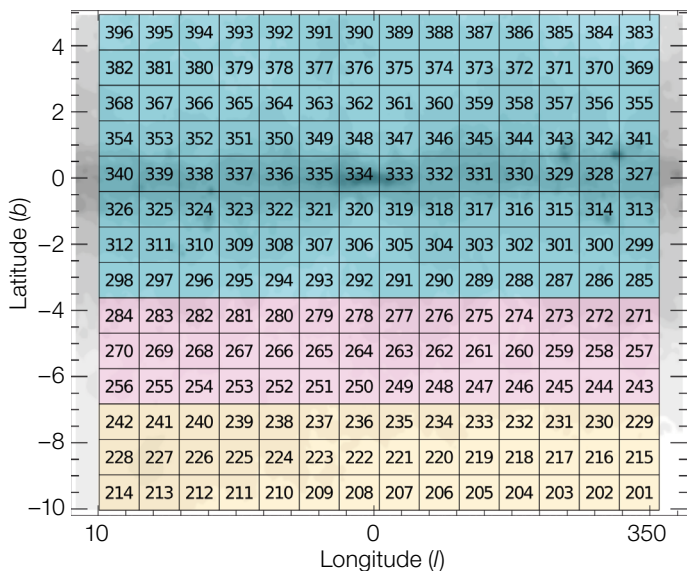
Figure 1. The distribution of tiles across the Bulge area between $-10° < l < +10°$ and $-10° < b < +5°$. Different background colours are used to emphasise the different resolution of our reddening map: 2 arcminutes for $-4° < b < +4°$ (cyan), 4 arcminutes for $-7° < b < -4°$ (pink), and 6 arcminutes for $b < -7°$ (yellow).

Extinction maps with enough resolution to successfully correct observations for reddening have so far been restricted to only a handful of Bulge regions. The only available extinction maps with enough coverage were those from Schlegel et al. (1998). However, these maps are only reliable in regions further from the plane of the Galaxy, meaning that no global studies could be carried out that included Galactic latitudes $|b| < 4°$.

In order to trace the effect of Galactic extinction, the main requirement is to identify a standard candle in the field, which is homogeneously distributed across the Bulge, with a high enough density to construct a high-resolution reddening map. When metal-rich giant stars ignite helium in their cores they concentrate at a relatively fixed position in the CMD known as the red clump (RC). Their average magnitude and colour are well known and have only a small and quite well understood dependence on internal population factors, such as age and metallicity, therefore becoming the ideal tracer for an external factor such as reddening.

In the Bulge, the RC is located at an apparent magnitude of $Ks \sim 14$ in low extinction regions, but it can reach up to $Ks \sim 17$ mag in the highly reddened innermost Bulge areas. The VVV survey is the first survey that provides photometry deep enough to reach the RC magnitude across all the Bulge regions. In Gonzalez et al. (2012) we measured the $(J–Ks)$ colour of RC stars using a Gaussian fit to the colour distribution in a grid of varying spatial resolution dependent on the density of RC stars. The mean colour of RC stars was related to the intrinsic colour of Bulge RC stars in order to derive $E(J–Ks)$ reddening values for each resolution element and to finally construct the high-resolution reddening map of the Bulge. We chose the grid size to maximise the resolution of the map, while having at least 200 stars in each resolution element necessary for an accurate mean colour estimate. The final resolution of our reddening map is 2 by 2 arcminutes for $-4° < b < +4°$, 4 by 4 arcminutes for $-7° < b < -4°$ and 6 by 6 arcminutes for $b < -7°$.

The complete map is shown in Figure 3, where both the general extinction patterns and the small-scale features are clearly traced. A web-based tool, the BEAM calculator, has been made available to the community[1], from which the reddening values of our map can be retrieved. The map has already been used not only for studies of the Bulge stellar populations, but also for studies on the extinction law, Bulge globular clusters and X-ray sources. We have used it to produce a complete set of reddening-corrected VVV catalogues, which can be used to study the Bulge stellar populations in great detail and with the wide coverage provided by the survey.
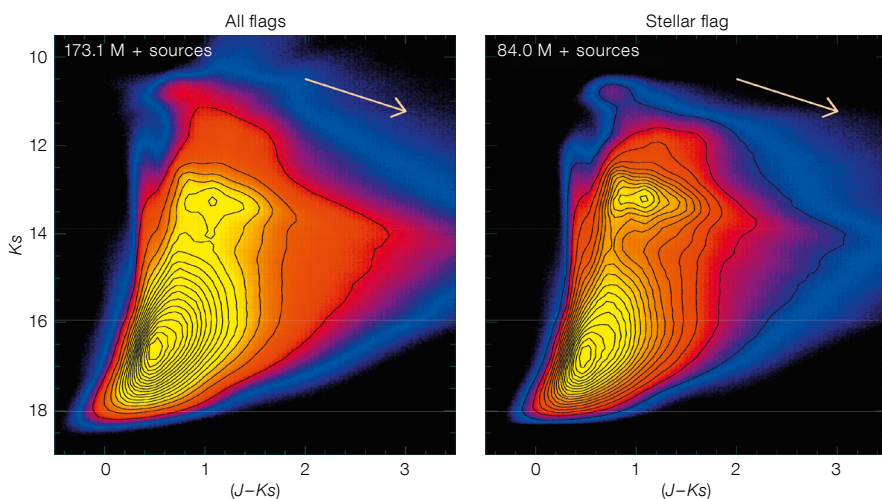

Figure 2. Ks vs. $(J–Ks)$ colour–magnitude diagram for the VVV Bulge area. The left-hand panel shows the CMD for all point sources found with J, H and Ks photometry, a total of 173 150 467 sources. The right-hand panel shows only stellar sources found in the three bands, a total of 84 095 284 sources. The white arrow shows the reddening vector, which strongly affects the shape of the observed Bulge CMD.
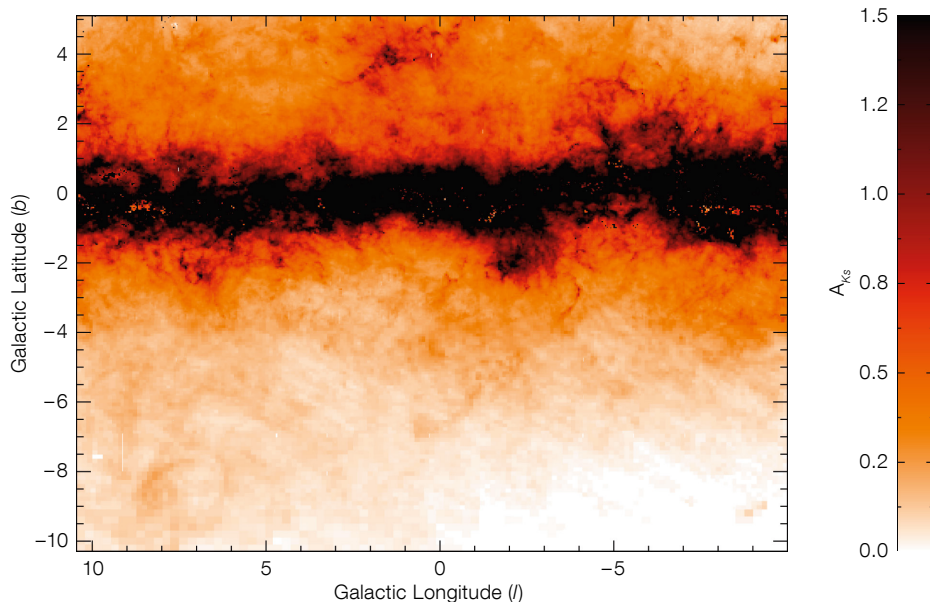
Figure 3. The complete high-resolution map of the Galactic Bulge. A_{Ks} values saturate the colour scale at A_{Ks} = 1.5 mag in this visualisation, in order to show better the extinction variations across the whole area. The central regions of the Bulge have A_{Ks} values extending to ~ 3.5 mag (corresponding to A_V ~ 30 mag).

Solving the mystery of the Bulge metallicity gradients

If there is one property of the Bulge that has been very well established by observations, it is the presence of a metallicity gradient along its minor axis (Zoccali et al., 2008; Johnson et al., 2011). The cylindrical rotation and morphology of the Bulge (Shen et al., 2010), the chemical similarity between Bulge and thick Disc stars (Gonzalez et al., 2011) and the suggested population of intermediate-age stars found in the Bulge (Bensby et al., 2013), have strongly pointed towards a secular evolution origin for the Bulge. However this conclusion is challenged by the presence of the metallicity gradient along the Bulge minor axis, which has always been considered to be a property of merger-built systems.

The need for a more general view of these gradients has increased but, unfortunately, a complete spectroscopic coverage of the Bulge, with the required resolution for such a study, remains infeasible. However, the colour of red giant branch stars in reddening-corrected CMDs, constructed using absolute mag-

The Bulge morphology

One of the most common techniques used for studying the morphology of the Bulge has been the red clump method (Stanek et al., 1997). In this technique, the observed mean RC magnitude, corrected for extinction, is compared to the known intrinsic mean magnitude of the RC stars ($M_{Ks} = -1.55$ mag for the Bulge population) in order to derive the distance to the observed population. With our new high-resolution reddening map, we were able to apply this method at very low latitudes in the innermost regions of the Bulge, where it was not possible to measure it before, and to compare it to the outer Bulge regions.

Figure 4 shows the mean distance to the Bulge population, as traced by the RC stars, as a function of Galactic longitude at two different latitudes $b = -1°$ and $b = -5°$ (respectively 150 and 700 pc below the Galactic Plane). The distribution of Bulge stars clearly follows a downward trend with distance to the Sun for increasing Galactic longitude, tracing the position angle of the Galactic bar. Significant differences are observed between the distribution of stars at both latitudes, and in particular the inner Bulge shows a flattening of the slope between longitudes $l = -4°$ and $l = +4°$.

These results advanced our understanding of the Bulge; the Galactic models were put to the test shortly afterwards in order to reproduce these observations. Gerhard & Martinez-Valpuesta (2012) compared their model to our results, finding that an axisymmetric concentration of stars in the inner Bulge is the cause for the different profiles that trace the bar position angle at low and high latitudes in Figure 4. Most importantly, the overall profiles shown in Figure 4 are fully consistent with a model of a boxy bulge formed as a result of buckling instabilities of the originally thin Galactic bar.
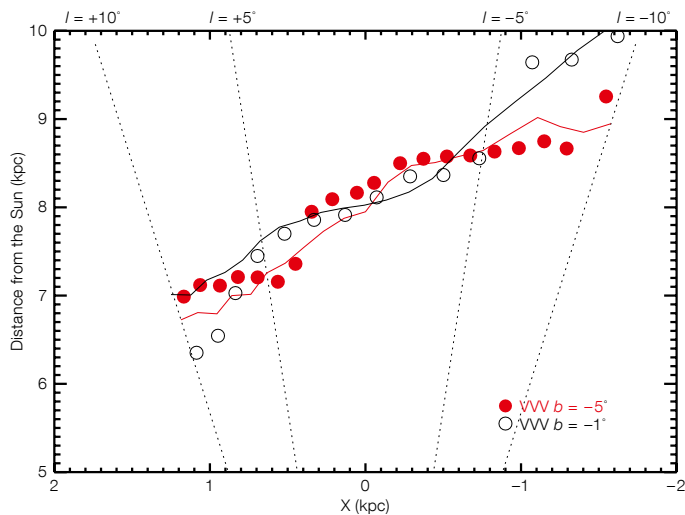

Figure 4. Distances derived using the RC method as a function of Galactic longitude at two fixed latitudes. Values for latitude $b = -1°$ are shown as black open circles, and as red filled circles for $b = -5°$. Models for the corresponding latitudes are shown as thick lines in the respective colours.
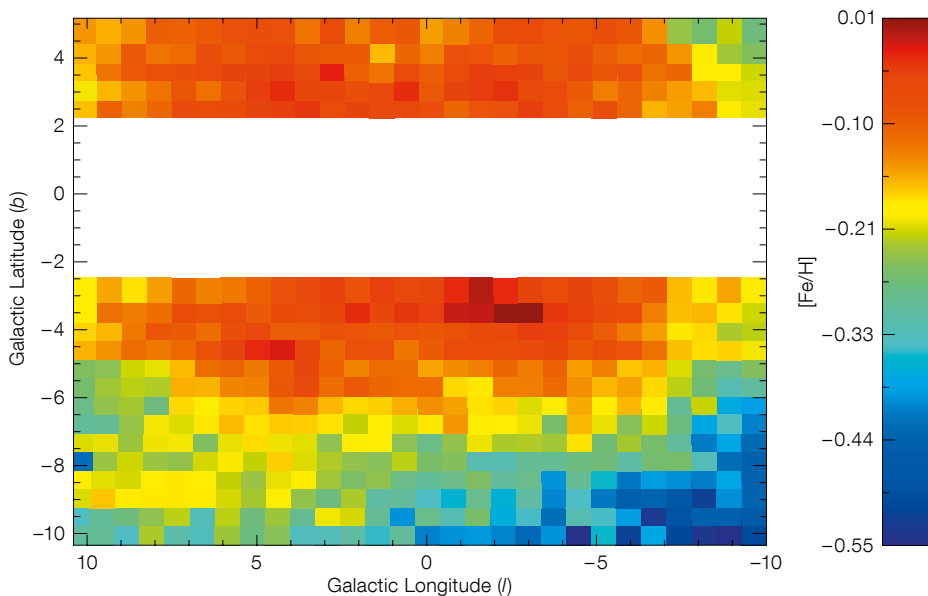
Figure 5. The complete metallicity map of the Galactic Bulge produced using the interpolation of $(J–Ks)_0$ colours of RGB stars between globular cluster ridge lines, with a resolution of 30 by 40 arcminutes.

nitudes, can be used to derive a photometric metallicity value by interpolation between globular cluster ridge lines of known metallicities. Although the photometric metallicities for individual stars are expected to have relatively large uncertainties, the average metallicity distribution for a sample of stars in a given field is a reliable proxy for the mean metal content, and it resembles strongly the mean metallicity derived spectroscopically (e.g., Valenti et al. 2007; Johnson et al. 2011).

Therefore, in Gonzalez et al. (2013) we used our reddening-free VVV catalogues to measure distances towards different Bulge lines of sight and produce a set of CMDs in the absolute plane from which we derived mean photometric metallicities. The end product was the first complete metallicity map of the Bulge, shown in Figure 5. We observe a radial metallicity gradient of ~ 0.28 dex/kpc and the clear domination of Solar metallicity stars in the inner Bulge. The observed metallicity map was recently also reproduced by a boxy-bulge formation model showing that, although other components

might still be present, the general properties of the Bulge are fully consistent with a formation scenario where the Bulge is formed from the buckling instabilities of the Galactic bar (Martinez-Valpuesta & Gerhard, 2013).

Outlook

Great advances have now been made in our understanding of the Bulge properties, thanks to the general view provided by the multi-band products obtained during the first year of VVV observations. However, the revolution does not stop here. The VVV survey keeps accumulating data — it is now in the middle of its variability campaign. The multi-epoch observations in *Ks*-band, will allow us to further characterise the Bulge to a unique level of detail by, for example, studying the 3D morphology of the Bulge using RR-Lyrae variables and using proper motions for the bulge-disc decontamination required to derive stellar ages from the Bulge turn-off magnitude measured in decontaminated CMDs.

References

Arnaboldi, M. et al. 2007, The Messenger, 127, 28
Bensby, T. et al. 2013, A&A, 549, A147
Emerson, J. P. et al. 2004, The Messenger, 117, 27
Gerhard, O. & Martinez-Valpuesta, I. 2012, ApJ, 744, L8
Gonzalez, O. A. et al. 2011, A&A, 530, A54
Gonzalez, O. A. et al. 2012, A&A, 543, A13
Gonzalez, O. A. et al. 2013, A&A, 552, A110
Johnson, C. I. et al. 2011, ApJ, 732, 108
Martinez-Valpuesta, I. & Gerhard, O. 2013, ApJ, 766, L3
Minniti, D. et al. 2010, New Astron., 15, 433
Saito, R. K. et al. 2012, A&A, 537, A107
Saito, R. K. et al. 2010, The Messenger, 141, 24
Saito, R. K. et al. 2012, A&A, 544, 147
Schlegel, D. J., Finkbeiner, D. P. & Davis, M. 1998, ApJ, 500, 525
Shen, J. et al. 2010, ApJ, 720, L72
Stanek, K. Z. et al. 1997, ApJ, 477, 163
Valenti, E., Ferraro, F. R. & Origlia, L. 2007, AJ, 133, 1287
Zoccali, M. et al. 2008, A&A, 486, 177

Links

[1] BEAM calculator: http://mill.astro.puc.cl/BEAM/calculator.php

Investigating High N/O Blue Compact Galaxies with VLT-IFUs

Bethan James[1]
Yiannis Tsamis[2]
Jeremy Walsh[2]
Mike Barlow[3]
Mark Westmoquette[2]

[1] Institute of Astronomy, University of Cambridge, United Kingdom
[2] ESO
[3] Department of Physics and Astronomy, University College London, United Kingdom

A series of publications concerning the spatially resolved chemical abundance analyses of a sample of blue compact galaxies, using VLT–FLAMES and VLT–VIMOS integral field observations, is summarised. Four out of the five galaxies observed were previously labelled as having enhanced nitrogen-to-oxygen (N/O) ratios for their metallicities. However, our analyses reveal regions of enhanced N/O in only three of these galaxies. The integral field unit observations provide maps of the physical and chemical conditions within each system, along with maps of stellar population age, star-forming rate and emission from Wolf–Rayet stars. By combining this plethora of information, we have attempted to disentangle the relationship between N-enrichment and WR stars in blue compact galaxies, and reveal that it is far from being one to one.

High N/O ratio blue compact galaxies

Blue compact galaxies (BCGs) in the nearby Universe provide a means of studying chemical evolution and star formation processes in chemically unevolved environments. They typically have low masses and low metallicities ($1/50$–$1/3$ $Z_\odot$), making them attractive analogues to the young building-block galaxies thought to exist in the high-z primordial Universe (see Kunth & Ostlin [2000] for a review). Having experienced only low levels of star formation in the past, their present-day bursts of star formation occur in relatively pristine environments, and, as such, investigating their chemical evolution can impact our understanding of primordial galaxies and galaxy evolution in general.

One particularly puzzling aspect of galaxy chemical evolution is the nitrogen-to-oxygen ratio. Although most elements have a linear relationship with galaxy metallicity (here oxygen abundance is taken to represent metallicity in the absence of available stellar abundance indicators), nitrogen shows a more complex dependence (Izotov & Thuan, 1999; Izotov et al., 2006; and references therein). At low metallicities, nitrogen behaves as a primary-production element and at high metallicities it behaves as a secondary-production element. At intermediate metallicities, however, there is a large scatter, with a subset of galaxies showing N/O ratios up to three times higher than expected for their metallicity. The most popular explanation for this nitrogen overabundance is chemical pollution from the nitrogen-rich winds of Wolf–Rayet (WR) stars, a theory based primarily on the simultaneous detection of WR emission and high N/O ratios from long-slit spectroscopic observations (Pustilnik et al., 2004; Brinchmann et al., 2008). Whilst this was certainly found to be the case in NGC 5253 (Monreal-Ibero et al., 2012; and references therein), spatially resolved abundance studies are showing that this relationship is not as clear cut as once thought.

With the aim of understanding this scatter, we have used integral field unit (IFU) spectroscopy to observe a sample of BCGs for which previous studies reported anomalously high N/O ratios. We also observed one control object within our sample (UM462), which had a reported normal N/O ratio for its metallicity. IFU data afforded us the spatial information needed to relate the chemical properties to the physical, kinematical and stellar properties of each galaxy. The sample consisted of Mrk996 (James et al., 2009), UM462 and UM420 (James et al., 2010), UM448 (James et al., 2012) and Haro11 (James et al., 2013). Images of Mrk996, UM448 and Haro11 are shown in Figure 1, with the IFU apertures overlaid.

Mapping the complex emission profiles

Two IFUs were used for this sample in order to match the extent of the emission regions to the IFU size: VLT–VIMOS (used to observe Mrk996, UM420 and UM462) and VLT–FLAMES/Argus (used to observe Haro11 and UM448). VIMOS observations were taken using the HRblue and HRorange settings, covering a total wavelength range of 415–740 nm, while FLAMES observations were taken in the LR1–3 and LR6 modes, covering 362–508 nm and 644–718 nm. The observations were designed to cover all of the important emission lines needed to perform a chemical abundance analysis, as detailed below. The data were reduced using standard reduction pipelines, converted into (x, y and wavelength) datacubes and corrected for differential atmospheric refraction.

Upon inspection of the datacubes, it was apparent that the majority of the sample (all except UM420 and UM462) displayed complex emission line profiles at the observed spectral resolution, so that each line was made up of multiple components (see an example in Figure 2 for Haro11). This indicated that along each spatially resolved sightline, there is emission from gas with different physical properties, e.g., velocity, turbulence, temperature and/or density. It was therefore necessary, and indeed useful, to decompose the line profiles and perform a separate chemical abundance analysis on each velocity component, thus undertaking a chemodynamical approach.

We used an automated line-fitting routine to fit the emission components throughout each datacube, aided by a likelihood ratio method (Westmoquette et al. 2001) to rigorously determine the optimum number of Gaussians required to fit each observed profile. Once the emission was deconvolved into its separate components (typically a narrow component; a broad component underlying the narrow one; and sometimes a third, weaker and kinematically offset component), we created flux, velocity and line-width maps for each of the separate components.

Mapping the de-convolved line profiles and creating separate kinematical maps for each component, provided insight into the complex motions of the gas within these irregular systems. Although the kinematics of the narrow-component emitting gas showed signs of ordered, solid-body rotation (in UM448 and
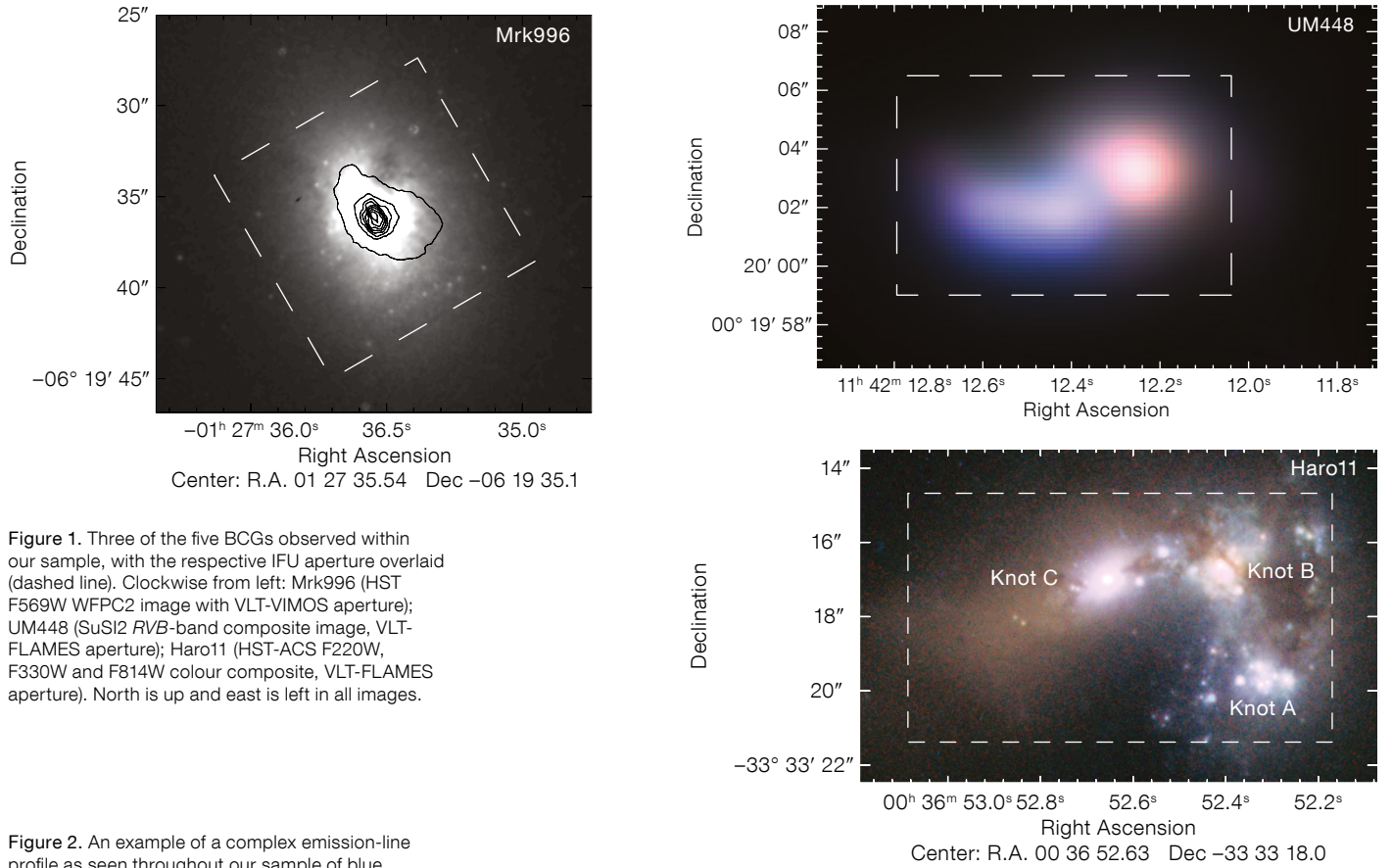
Figure 1. Three of the five BCGs observed within our sample, with the respective IFU aperture overlaid (dashed line). Clockwise from left: Mrk996 (HST F569W WFPC2 image with VLT-VIMOS aperture); UM448 (SuSI2 *RVB*-band composite image, VLT-FLAMES aperture); Haro11 (HST-ACS F220W, F330W and F814W colour composite, VLT-FLAMES aperture). North is up and east is left in all images.

Figure 2. An example of a complex emission-line profile as seen throughout our sample of blue compact galaxies, and the flux maps created by deconvolving its velocity components. The top row shows an example three-component Hα line profile seen in Haro11. The highlighted component (red line) indicates to which component the maps below correspond.
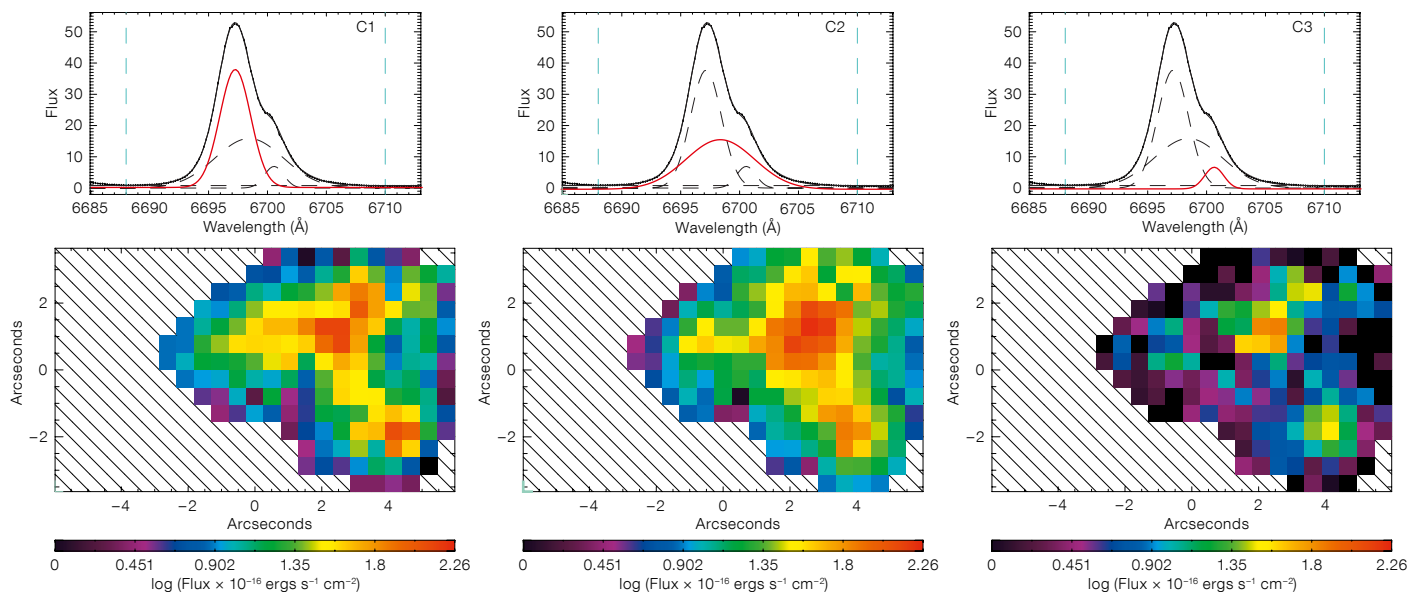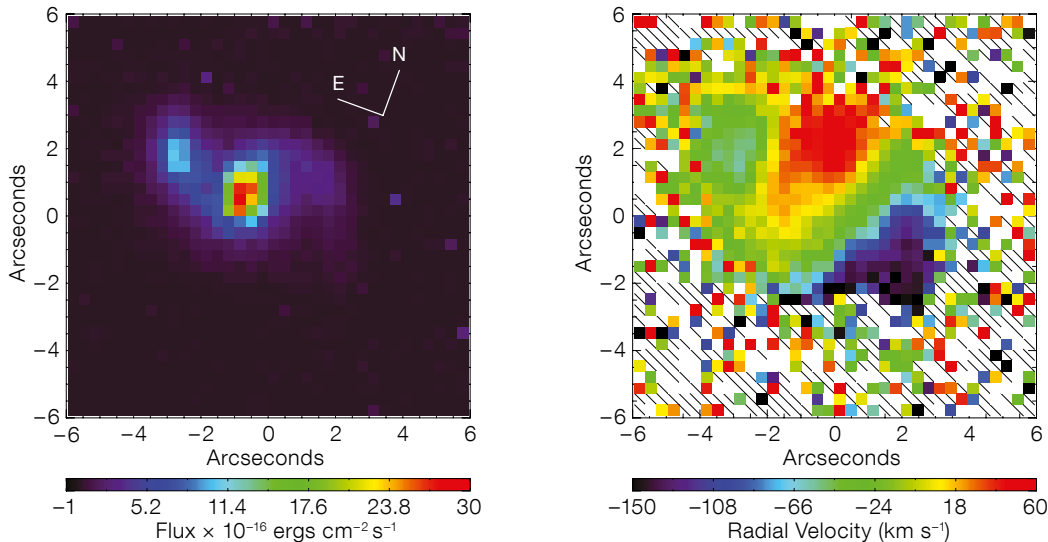
Mrk996), the broad component emission was often offset from this. For example, in Mrk996 we detected the kinematic signature of a turbulent two-arm spiral structure within the nucleus, while in UM420 (Figure 3) and UM448 clear signs of a merger between two distinct kinematical bodies are seen. In Haro11, the gas volume emitting the broad velocity profile is rotating in an orthogonal direction to that of the narrow-component emitting gas — revealing a counter-rotating disc of turbulent gas within the central knot of star formation.

In order to derive accurate chemical abundances, we used the "direct method", which is based on direct measurements of the electron temperature and density of the emitting nebulosity. Abundance maps were derived from reddening-corrected line intensity maps, an electron temperature map (calculated from [O III] (λ5007 + λ4959)/λ4363 line ratios, as shown in Figure 4) and an electron density map (calculated from [S II] λ6716/λ6731 ratios). In this way, each spatial pixel (or spaxel) has its own unique set of measured physical conditions from which to derive the gas chemical composition. Ionic nitrogen, oxygen, sulphur and neon abundances were converted into elemental abundances relative to hydrogen using off-the-shelf ionisation correction factors (ICF; a fairly robust approach in H II region research as the ICFs have been benchmarked against nebular models). Chemical abundances were also calculated using spectra inte-

grated over individual star-forming regions and also the galaxy as a whole.

Several properties were mapped throughout each galaxy, including star formation rate (derived from the Hα flux), the age of the ionising stellar population (from the equivalent width of Hβ), and maps of the WR stellar population. The latter were created from the Wolf–Rayet spectral signature at 465.0 nm (the blue bump). When combined with the chemical abundance maps, the spatial distribution of these properties was used to help disentangle the chemical evolutionary stage and/or chemical feedback processes occurring within each galaxy.

An insight into N-enrichment and its origins

From our IFU sample of four pre-selected high-N/O galaxies, we found that three scenarios were at play:

1) Misdiagnosed high-N/O status: UM420

UM420 was previously thought, based on long-slit studies, to have an N/O ratio 0.5 dex higher than expected for its metallicity. Following the spatially resolved analysis with VIMOS, enhanced N/O was not found to be the case for either of its two main star-forming regions and across the whole galaxy. UM420 shows minimal nitrogen or oxygen abundance variations throughout, implying that this galaxy

has not been caught in the wake of any major chemical self-enrichment episode, and has an oxygen abundance of one-third solar.

In fact, a difference between abundances derived from spectra integrated over the entire galaxy and those derived from regional averages across the abundance maps, was found throughout our studies. Interestingly, abundance ratios relative to hydrogen were found to be inconsistent, whereas those relative to oxygen were in agreement within the uncertainties. This is possibly due to the former having a higher dependency on electron temperature that can be erroneously calculated when using ratios from summed spectra, as they tend to suffer from luminosity weighting. This effect can have significant consequences for abundance measurements based on integrated spectra of high-redshift galaxies.

2) High N/O ratio in the presence of numerous WR stars: Mrk996

The case of Mrk996 was most intriguing. Although the majority of the emission lines showed both broad and narrow component emission (as reported by Thuan, Izotov & Lipovetsky, 1996), certain lines are only detected in their broad-component form — namely the temperature-sensitive lines ([N II] 575.5 nm and [O III] 436.3 nm), which are only emitted from the very core of the galaxy (see Figure 5). A separate analysis of the broad
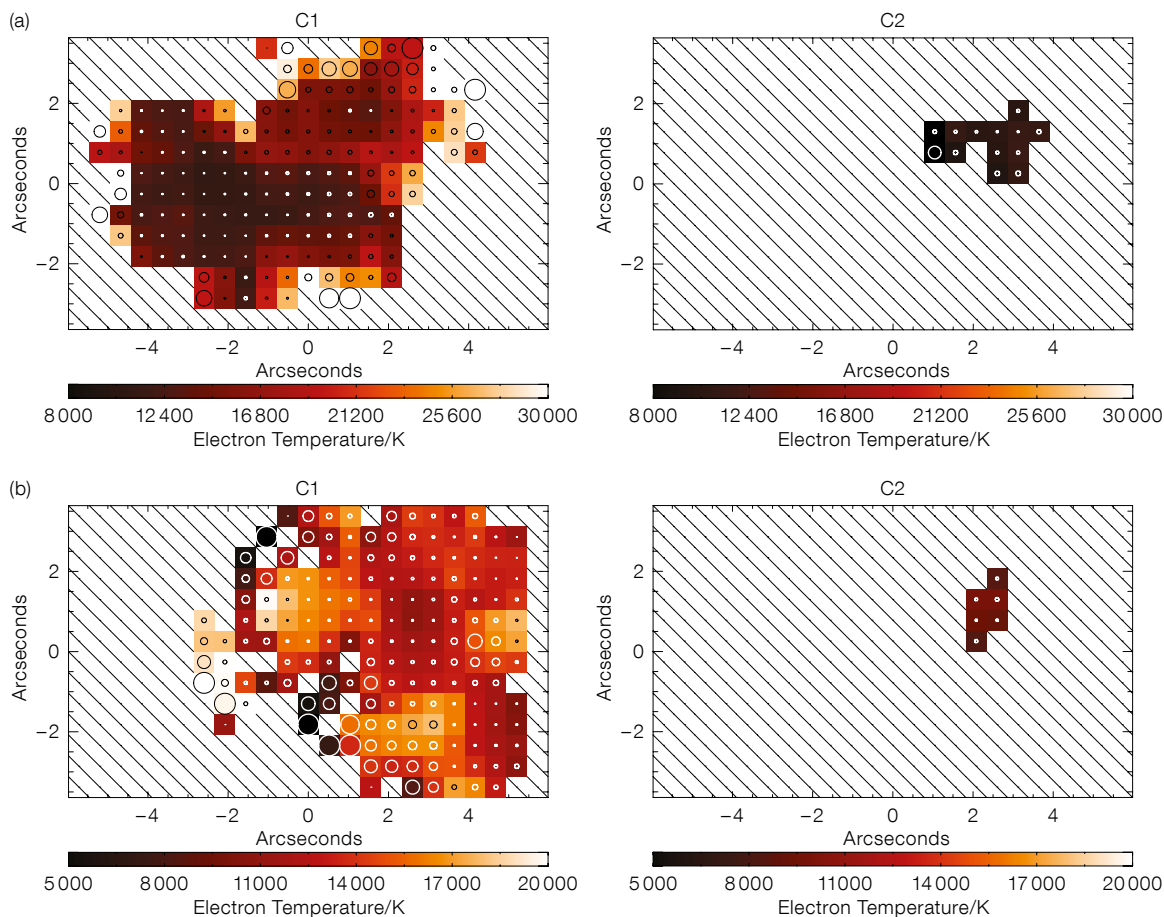
(a)

C1

C2

Electron Temperature/K

(b)

C1

C2

Electron Temperature/K

Figure 4. Electron temperature maps of (a) UM448 and (b) Haro11. The circles overlaid represent the size of the uncertainties within each spaxel's electron temperature. These maps were used in conjunction with electron density maps to derive chemical abundance maps, ensuring that each spaxel in the flux maps had its own set of physical conditions from which to derive its chemical abundance. C1 refers to the narrow, strong, emission component whereas C2 refers to the broad, underlying emission component.

and narrow components detected by VIMOS has helped to isolate the previously reported N-enrichment to the broad-component gas in the galaxy's nucleus. The abundance of nitrogen there is found to be 20 times higher than in the surrounding narrow-line region. No other element shows a pronounced difference in abundance between the two gas components.

The blue WR feature summed over the galaxy indicates the presence of approximately 2600 WNL (late WR-type with enhanced N) stars and 400 WC (WR-type with enhanced C) stars within the turbulent nuclear region (Figure 5). The equivalent width of Hβ indicates a stellar age of 4.5 Myr in this region — an age sufficiently old to have allowed massive stars in the galaxy to evolve to the WR stage. Together, these pieces of information indicate that the overabundance of nitrogen in the broad-component emission can be attributed to the cumulative effect of N-enriched winds of WR stars.

In addition, the N-enhanced material is spatially coincident with a region of extremely high electron density ($\sim 10^7$ cm^{-3}, compared to typical H II region densities of ~ 100 cm^{-3}), which may have impeded and pressurised the WR winds, allowing their metal-rich ejecta to mix with the cooler phases and subsequently become observable.

At present, only one other dwarf starburst galaxy has been reported to display localised N-enrichment, NGC 5253. Deep VLT spectroscopy by Lopez-Sanchez et al. (2007) of this well-studied galaxy showed increased N/O ratio in the two central starburst regions, and within one region the increase was isolated to the broad component only.

3) Perturbed BCGs with or without WR stars: UM448 & Haro11

UM448: The NTT SuSI2 image of UM448 shown in Figure 1 reveals that this galaxy

is made up of two distinct stellar populations; an older, red population in the west and a younger, blue population towards the east. We observed this interacting system with FLAMES/Argus. An analysis of the global kinematics shows solid-body rotation aligned along the intersection of the two distinguished stellar regions, suggesting that they are in the process of merging. Whilst the N/O abundance ratio was found to be rather typical throughout UM448, there was a region of increased N/O located at the intercept of the two regions (Figure 6). Little or no WR-emission was detected throughout the galaxy, in spectra summed regionally or across the galaxy as a whole.

The region of enhanced N/O is, however, spatially coincident with a region of lower O/H. Judging from the kinematical maps, and ages of the stellar populations, we propose that the decrease in oxygen abundance is due to global processes occurring within the galaxy,
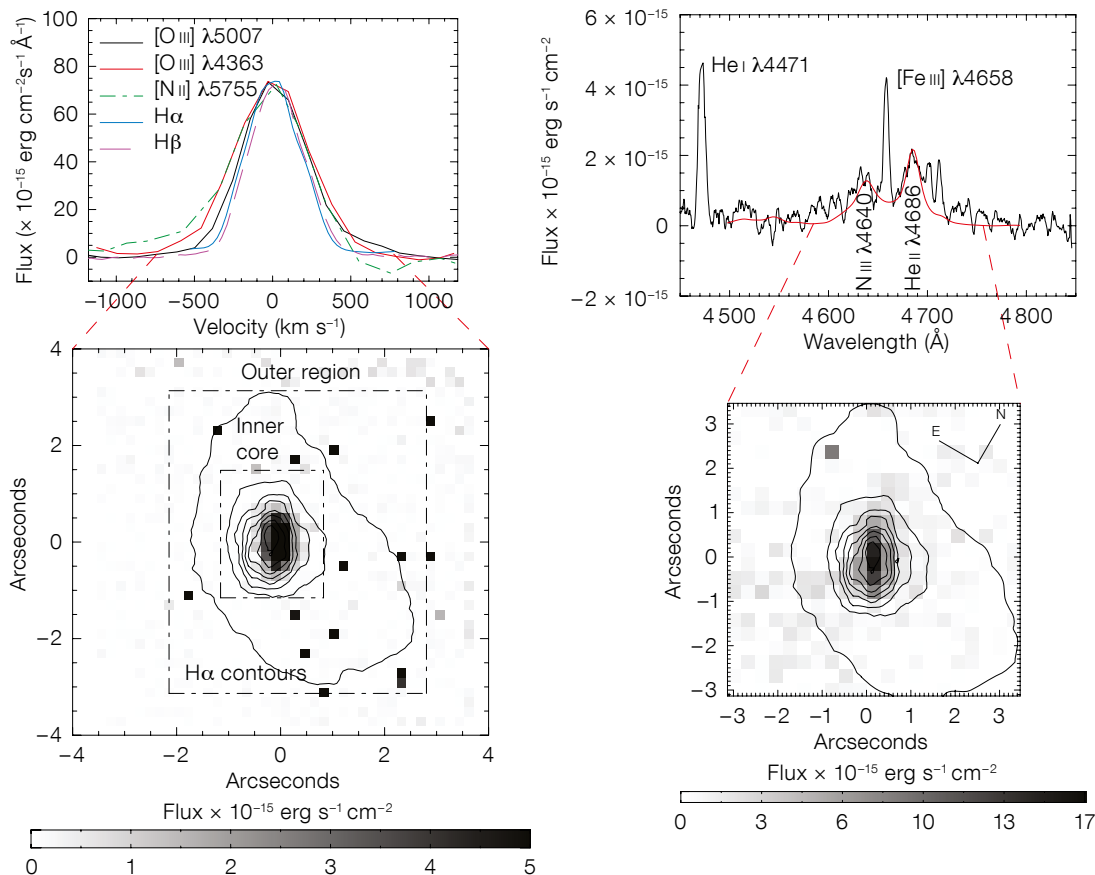
Figure 5. Left panel: Broad component profiles of five emission lines observed within Mrk996. The map shown below is the [O III] λ4363 flux map, displaying emission exclusively within the inner core of the galaxy. A high N/O ratio (5 × solar) was measured exclusively in the broad-component emission. Right panel: The blue bump at 465.0 nm, an emission feature attributable to ~ 2600 N-rich Wolf–Rayet stars and the emission map created from this feature is shown below. Comparing the flux maps, the spatial coincidence of WR-stars and broad-component emission, suggests that N-enrichment could be due to the N-rich winds of WR stars.

namely the likely interaction and/or merger between two bodies as inferred from the SuSI2 images and radial velocity maps, resulting in the accretion of metal-poor gas. This resonates with studies showing that interacting galaxies fall > 0.2 dex below the mass–metallicity relation of normal galaxies due to tidally induced large-scale inflow of metal-poor gas towards the central regions (e.g., Peeples et al., 2009).

Haro11: This galaxy is well known as being a local analogue to the high-redshift Lyman break galaxies. It has been studied in detail from X-ray to infrared wavelengths, being in a rare class of Lyman-α and Lyman-continuum emitters (James et al. [2013] and references therein). As can be seen in Figure 1, Haro11 consists of three distinct knots of emission that are kinematically connected. The galaxy displays complex emission profiles throughout the knots (see Figure 2). The eastern knot (called Knot C) is found to have a higher temperature (by ~ 4000 K) and consequently, an oxygen abundance

that is 0.4 dex lower than the neighbouring regions. A region of enhanced N/O ratio is found specifically in Knot C, confirming previous studies that found an anomalously high N/O ratio in this system (Izotov & Thuan, 1999). However, maps of the WR emission throughout Haro11 reveal large WR populations (~ 900–1500 stars) in Knots A and B only.

Unlike UM448, the properties of Knot C are consistent with the mass–metallicity relationship at low galaxy masses, suggesting that the accretion of metal-poor gas is unlikely. Conversely, there may have been an outflow of oxygen-enriched gas due to supernovae (SNe). Further insight into the source's evolutionary stage was provided by the maps of stellar population age, which show that Knot C is 2–3 Myr older than Knots A and B (~ 4–5 Myr) and so it may indeed have experienced more SNe explosions than the younger knots. Alternatively, its age implies that its WR phase has recently been completed. This suggests that Knot C has had sufficient time to maximise

the injection of nitrogen into the local interstellar medium (ISM) during the WR phase, which may still be relatively undiluted by subsequent mass-loss of lower mass stars. This case is further supported by Knot C having a lower current star formation rate (~ 0.09 $M_\odot$/year) as derived from its integrated Hα flux. Overall, it is clear that Knot C has undergone a separate evolutionary path to the other constituents of the galaxy.

In the younger Knots A and B, on the other hand, we observe the opposite scenario — normal N/O ratios and substantial WR populations (Figure 6). This suggests that we are catching the galaxy at an interesting point in its evolutionary path. We may be observing regions whose stars are in the process of expelling their processed nitrogen (which begins at ~ 5 Myr) and have not had enough time to be diluted by the ambient interstellar medium. If we take into consideration that the cooling and mixing of expelled material can last between 2–8 Myr over regions just 50 pc

in size, and that injection of material can begin as early as 2.5 Myr in the knot's evolution, it is unlikely that just 2 Myr later we would be able to observe the N-rich ejecta from the WR stars within regions as large as Knots A and B (0.4 and 1 kpc^2, respectively).

A complicated relationship

In our quest to understand the high N/O ratios found in a subset of blue compact galaxies, we have discovered that the measured N/O ratio can be sensitive to the type of spectroscopic technique used. Long-slit data can result in flux-weighted, and therefore misleading, line ratios when integrated over large spatial scales. For example, in the case of UM420, previous long-slit spectroscopy found that it had N/O levels 0.5 dex higher than other galaxies of a similar metallicity, whilst our spatially resolved analysis with VIMOS does not find any nitrogen excess.

In support of this result, for both Haro11 and UM448, we find that chemical abundances derived from spectra summed over the entire IFU aperture can differ significantly from those measured on resolved abundance maps. Therefore, although spatially resolved observations have the ability to detect temperature and abundance variations, thus isolating potential sites of enrichment, analyses based on integrated 1D spectra can introduce strong biases if a mixture of regions with different ionisation conditions and metal content are involved. Naturally, such effects could be potentially more severe for unresolved systems such as high redshift galaxies. Moreover, as the case of Mrk996 has clearly shown, accurate deconvolution of the line profiles with sufficiently high spectral resolution is at least as important: completely erroneous physical properties can otherwise be deduced.

Secondly, the spatial profile of the N/O ratio is highly dependent on the evolutionary stage of the galaxy and on environmental effects. In the three cases where spatial variations of the N/O ratio are detected (Mrk996, UM448 and Haro11), the mechanisms responsible are likely different. In Mrk996 we see
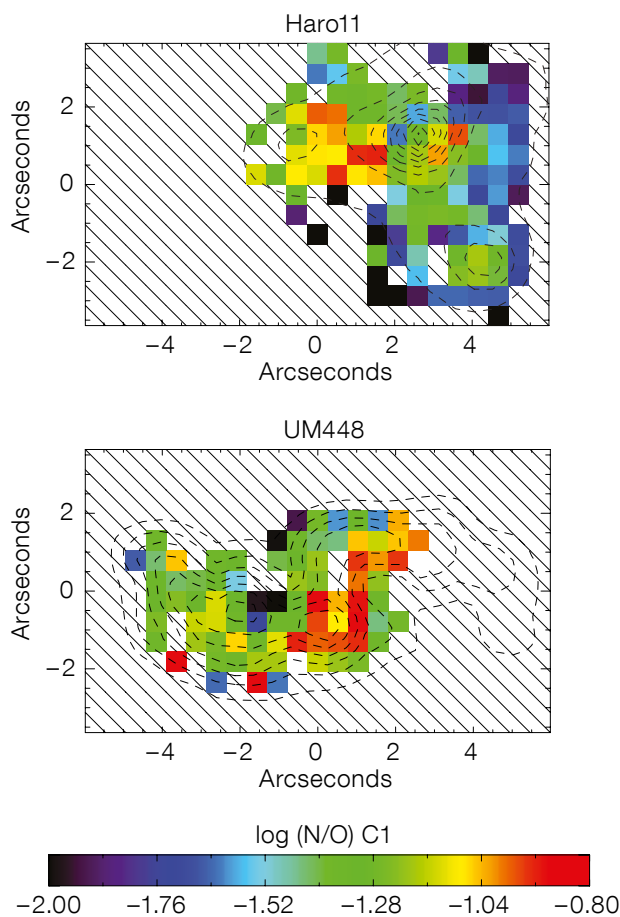

Figure 6. By performing a spatially resolved abundance analysis, we have been able to highlight regions of chemical enrichment. The figure shows maps of log(N/O) for Haro11 (upper panel) and UM448 (lower panel), for their narrow emission line components. A peak in N/O is seen in Haro11 in its most eastern knot, Knot C, whereas UM448 shows an increase in N/O towards the south. These maps, in conjunction with maps of WR emission, stellar population age, radial velocity and star formation rate, were used to investigate the mechanisms responsible for their heightened levels of N/O.

N-enrichment in the broad-component emission, originating in turbulent layers created by N-rich winds of numerous WR stars and confined within a very dense ISM in the centre of the galaxy. In UM448, the region of high N/O appears devoid of WR stars and the measured effect is likely due to accretion of metal-poor gas at the intercept of two merging bodies. Finally, in Haro11, we detect higher values of the N/O ratio in an older region where the WR phase has recently finished, whereas two younger regions that contain WR stars do not show enrichment signatures yet. From these three cases, it is clear that the relationship between localised N-enrichment and the existence of WR stars is far from being one to one. Instead, it is becoming apparent that the simultaneous detection of both WR features and enhanced N/O is a function of starburst age and the properties of the surrounding medium.

The VLT IFU observations that enabled these chemodynamical case studies reveal the complex kinematic and chemical properties of blue compact galaxies. A better understanding of the evolution of these systems can be achieved by IFU-driven analyses combined with chemical evolution models; this is the subject of ongoing work.

References

Brinchmann, J., Kunth, D. & Durret, F. 2008, A&A, 485, 657
Izotov, Y. I. & Thuan, T. X. 1999, ApJ, 511, 639
Kunth, D. & Ostlin, G. 2000, A&AR, 10, 1
Monreal-Ibero, A., Walsh, J. R. & Vílchez, J. M. 2012, A&A, 544, A60
James, B. L. et al. 2009, MNRAS, 398, 2
James, B. L., Tsamis, Y. G. & Barlow, M. J. 2010, MNRAS, 401, 759
James, B. L. et al. 2013, MNRAS, 428, 86
James, B. L. et al. 2013, MNRAS, 430, 2097
Lopez-Sanchez, A. R. et al. 2007, ApJ, 656, 168
Peeples, M. S., Pogge, R. W. & Stanek, K. Z. 2009, ApJ, 695, 259
Pustilnik, S. et al. 2004, A&A, 419, 469
Thuan, T. X., Izotov, Y. I. & Lipovetsky, V. A. 1996, ApJ, 463, 120
Westmoquette, M. S., Smith, L. J., Gallagher, J. S. 2011, MNRAS, 414, 3719

Physical Properties of Strongly Lensed, Low-mass, High-redshift Galaxies Observed with X-shooter

Lise Christensen[1]
Johan Richard[2]
Jens Hjorth[1]
Claudio Grillo[1]

[1] Dark Cosmology Centre, Niels Bohr Institute, University of Copenhagen, Denmark
[2] CRAL, Observatoire de Lyon, Université Lyon 1, France

One of the science drivers for the second generation VLT instrument X-shooter is the exploration of emission-line galaxies at high redshifts. By targeting gravitationally lensed galaxies, we have demonstrated that, with the full spectral coverage and high overall sensitivity at medium spectral resolution for X-shooter, we can explore the physics of galaxies at redshifts between one and four, using the same methods as employed for local galaxies. In particular, we have determined abundances via direct temperature-sensitive methods, and have shown that galaxies at high redshifts also follow a relation between the physical properties of stellar mass, abundance and star formation rate, as seen in the local Universe.

During the past decade, our knowledge of galaxies in the high-redshift Universe has increased tremendously, thanks to the advent of large-aperture telescopes and deep-field surveys. Galaxies selected from Lyman-break dropout techniques have allowed us to efficiently find galaxies up to redshifts of $z \sim 10$. Broadband selection and subsequent fitting of the photometry with template models have enabled us to explore the general characteristics of the galaxies. However, a detailed understanding of their physical properties still requires suitable spectroscopic measurements.

The majority of galaxies at $z > 2$ are faint, and spectroscopic observations are time consuming, considering that the magnitudes of typical Lyman-break galaxies are fainter than $R \sim 24$. Follow-up spectroscopy of individual galaxies at $z > 2$ is limited to the most massive galaxies in a few selected redshift ranges, where strong optical emission lines are redshifted into convenient wavelength ranges that are not absorbed by the Earth's atmosphere.

Measurements of strong emission lines and their line flux ratios are essential to derive the global chemical abundance of galaxies (e.g., Kewley & Ellison, 2008), which is a key ingredient in our understanding of galaxy evolution. Measurements of oxygen abundances of low-redshift galaxies in the Sloan Digital Sky Survey (SDSS) have shown that a relation exists between galaxy mass and metallicity (Tremonti et al., 2004). Further observations have indicated that this relation evolves in such a way that at progressively higher redshifts the abundances are lower for a given stellar mass. While this relation is well-recognised, the still unknown factor is the evolution of low-mass, high-redshift galaxies, because individual galaxies are too faint for conventional follow-up spectroscopy. To date, only a few individual high-redshift galaxies have been targeted for detailed medium to high resolution spectroscopy, generally using tens of hours of telescope time per target.

Before the advent of the E-ELT, the only available method that could increase our knowledge about the physical properties of low-mass, high-redshift galaxies is to take advantage of strong gravitational lensing, which can boost the total flux of a distant galaxy by a factor of 10–100, thereby allowing us to study galaxies that are 2–5 magnitudes fainter than would otherwise be possible. Furthermore, the stretching of some lensed galaxies along tangential giant arcs provides a much higher spatial resolution, thus enabling more detailed analyses to be performed of structures with sizes of around 100 pc in galaxies at $z > 2$.

Currently, a couple of Hubble Space Telescope (HST) multi-cycle programmes are devoted to imaging massive galaxy clusters in multiple filters: the CLASH survey (Postman et al., 2012), and the deeper Frontier Fields cluster survey. These studies are vital for achieving multiple science goals. In the cluster fields, HST images have revealed dozens of spectacular arcs and arclets from multiple background sources. For many of these systems, where several redshifts of lensed galaxies have been spectroscopically confirmed, the mass distribution of the clusters has been modelled and reconstructed very accurately. Given a lens model, it is possible to estimate the factor by which any background source galaxy is magnified. This is a crucial quantity when studying the intrinsic properties of the background sources.

Here we provide a summary of our X-shooter programme for lensed low-mass galaxies, focussing on the study of the detailed physical properties of individual high-redshift galaxies.

The X-shooter survey

The X-shooter instrument has a great advantage in the field of studying strongly lensed galaxies. Firstly, we have no previous information on the redshift of the sources, and, since X-shooter covers the entire wavelength range from 300–2500 nm, any spectral feature, be it the emission or absorption lines that appear in the spectrum, will allow us to constrain the redshift. Secondly, the large wavelength coverage enables us to measure several strong emission lines, which all fall in the near-infrared (NIR) part of the spectrum for galaxies at $z > 1.4$. Thirdly, using the same instrument with no difference in the slit position and instrument setup implies that there are no differential slit losses, apart from the effect of seeing changes, which can safely be ignored in the NIR range. This in turn implies that we can accurately determine emission-line ratios, which are necessary for deriving physical quantities.

The experience from X-shooter science verification (SV) data of lensed galaxies at previously unknown redshifts (Pettini et al., 2010; Christensen et al., 2010; Grillo & Christensen, 2011) demonstrated the strength of X-shooter in deriving physical characteristics of high-redshift galaxies with only a modest investment of telescope time. This advantage is allied to the possibility of deriving accurate lens models that can reproduce the observed geometrical configurations of the background lensed sources.

Subsequent to the SV demonstration, we proceeded with a larger programme using guaranteed time observations (GTO) in the period from 2010–12. The GTO observations were primarily aimed at determining source redshifts for intrinsically faint galaxies magnified by massive galaxy clusters, some of which are part of the CLASH survey. In total we targeted 13 galaxies using one hour of integration time per target. Figure 1 illustrates the lensed galaxies as observed with HST.

Physical characteristics of the galaxies

From the spectra of the lensed galaxies, we have measured the redshifts of 12 of the galaxies to be in the range $0.6 < z < 5$. While the continuum emission of the galaxies, which have apparent magnitudes between 21 and 24 mag, is only detected at low signal-to-noise levels per pixel for the faintest galaxies; binning the spectra to a lower resolution of $R \sim 50$–100 allows us to confidently fit spectral template models and derive stellar ages and masses. Figure 2 shows the H-band 2D spectra of several lensed galaxies. The technique is similar to that used to determine the physical properties of galaxies by fitting their spectral energy distributions from multiband photometric measurements to template models. Targets are selected for their high surface brightness and for being good candidate-lensed objects. For these reasons, some of them have spectral characteristics of star-forming galaxies, while others display much older and more massive stellar populations.

Since the high-redshift galaxies are unresolved in ground-based images, we are typically limited to studying their integrated properties with X-shooter. Although some of the lensed sources are extended along the slit, we only derive integrated quantities. Star formation rates (SFRs) are

inferred from the emission-line (typically Hα and [O II] $\lambda\lambda$3727,3730) luminosities. All the quantities are corrected for lens magnification factors and slit losses. The latter are obtained by measuring, for each target, the fraction of the light falling into the slit relative to the total amount of flux in the broadband HST images. Including these corrections, we measure stellar

Figure 1. 20 × 15 arc-second HST snapshots of the lensed arcs and multiple images in the selected galaxy clusters. The colour-composite images are based on the F606W, F814W, F125W and F160W bands. With our spectroscopic observations we targeted the regions with highest surface brightness, which give the highest chance of detecting bright emission lines.

Figure 2. X-shooter 2D spectra in the NIR (between 1400 and 1800 nm) of three red galaxies that have been magnified by a factor of three by a foreground massive galaxy cluster. The galaxy H-band magnitudes range between 22 and 23. For the galaxy at the top, the detection of an emission line at 1663 nm, identified as [O III] λ5007, has been used to estimate a redshift value of 2.32. For the two lower galaxies, the continuum emission is consistent with a template of a passive galaxy at an approximate redshift of 2.
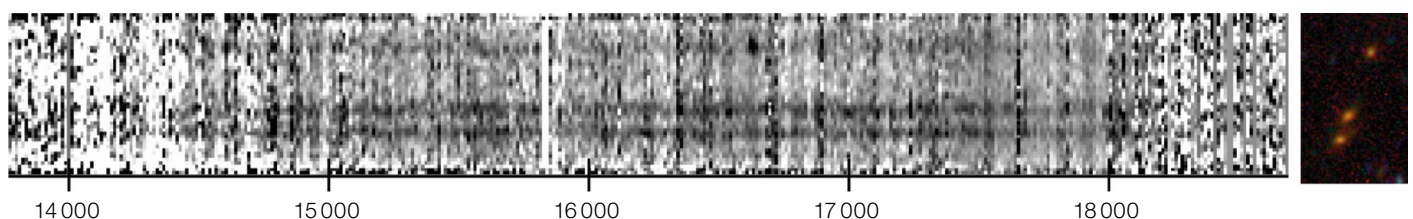
masses spanning four decades from 10^7 to 10^{11} $M_\odot$, relative luminosities between 0.004 and 9 L^*, where L^* corresponds to a characteristic galaxy luminosity at a given redshift, and SFRs from 1–50 $M_\odot$/yr. The range of these quantities is compatible with that of large-scale flux-limited surveys, but, on average, the lensed galaxies probe the low stellar mass end of the distribution.

Since the spectra cover the restframe optical wavelengths of the high-redshift galaxies, we can use conventional strong line abundance diagnostics, such as R_{23} (Pilyugin & Thuan, 2005) to measure their global oxygen abundances. This diagnostic uses ratios of oxygen and hydrogen Hβ emission lines. Unlike the SFRs and stellar masses, the abundance measurements do not depend on the lensing magnification factors, since the abundances are derived from line ratios. The inferred oxygen abundances, 7.6 < 12+log(O/H) < 8.7, corresponding to the range from 10 % to 100 % solar metallicity, are on average smaller than those derived for other high-redshift galaxy flux-limited samples. This finding is in agreement with the trend of how metallicity traces the stellar mass.

Fundamental relation for star-forming galaxies

Figure 3 shows the relation between the SFRs, stellar masses and oxygen abundances for lensed galaxies at 1 < z < 4. The galaxies fall on a simple relation between SFR and M^* known as the "main sequence for star-forming galaxies" (Noeske et al., 2007). Higher redshift galaxies have progressively higher SFRs.

The scatter in the SFR-mass plot is large, but recent analyses have revealed that taking into account the oxygen abundance as a third parameter, a tight sequence, termed "the fundamental metallicity relation" for star-forming galaxies, has been found (Mannucci et al., 2011). As that study is based mainly on low-redshift galaxies, plus a few high-mass high-redshift galaxies, by including lensed galaxies we show that the low-mass high-redshift galaxies also appear to follow the same kind of fundamental relation, albeit with a larger scatter than
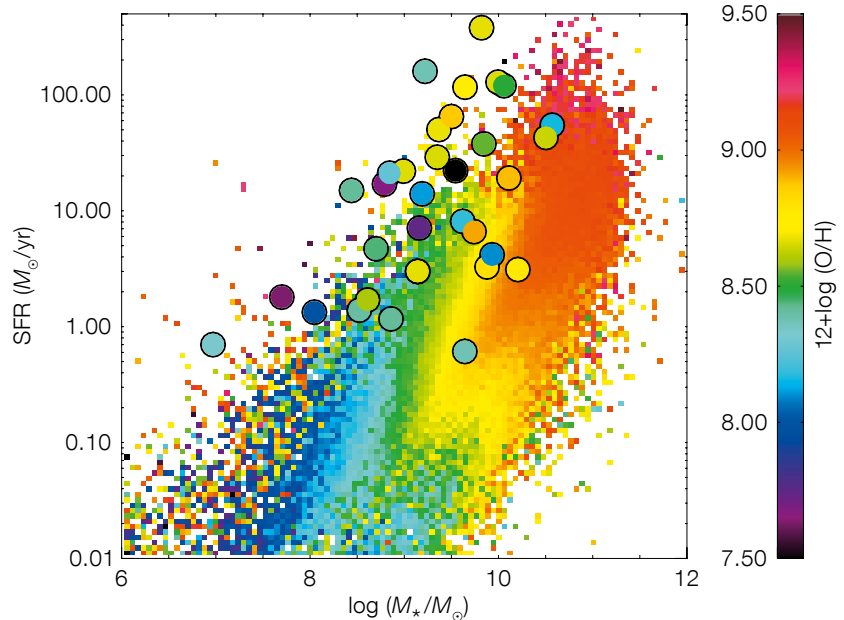

Figure 3. Correlations between integrated galaxy stellar masses and star formation rates. The colour scale represents the oxygen abundances, where the smooth distribution is the average metallicity at a given bin in stellar mass and SFR for ~ 400 000 SDSS galaxies. The three parameters form a tight plane, termed the fundamental relation for star-forming galaxies. The large circles are gravitationally lensed galaxies at 1 < z < 4 (Richard et al., 2011; Wuyts et al., 2012; Christensen et al., 2012a), and they generally lie above the M–SFR relation of lower-redshift galaxies. Typical uncertainties are 0.2 dex for the stellar mass and 0.1 dex for the abundance. For reference, the solar oxygen abundance, 12+log(O/H) = 8.69, is shown in yellow.

seen at low redshift (Christensen et al., 2012a).

Direct abundance measurements of high-redshift galaxies

For faint high-redshift galaxies, spectroscopic studies to derive the physical properties are mainly limited to what can be gained from the strong optical emission lines. The abundance determination depends critically on the temperature in the H II regions. All the strong line abundance diagnostics have been calibrated empirically relative to the direct methods using observations of local H II regions in the Milky Way and in nearby galaxies. To measure the temperatures and abundances with direct methods, detection of auroral lines such as [O III] λ4363, [N II] λ5755 or [O II] λλ7320,7330 is required. These auroral lines are however very faint compared to the strong emission lines from the same atomic species. The [O II] λλ7320,7330 doublet flux is known to contain large random errors, and the line

strength of the [O III] λ4363 line flux increases with decreasing metallicity. Since at high redshifts the galaxies that are typically studied are the most luminous and massive ones, and thus also the most metal-rich, the temperature-sensitive lines are increasingly difficult to detect. Rather than exploring individual galaxies, multiple galaxy spectra are usually stacked in order to detect the faint lines and provide average quantities for a population of galaxies.

Again, the lensing magnification effect allows us to probe deeper into the physical conditions of individual low-mass galaxies, since intrinsically fainter emission lines are boosted by the high magnification factor. Among the sample of galaxies observed with X-shooter, three systems at 2 < z < 3.5 show temperature-sensitive lines (Christensen et al., 2012b). In a similar way to the conventional use of the [O III] λ4363/[O III] λ5007 line ratio, the O III] λ1666/[O III] λ5007 ratio is also sensitive to the electron temperature. We detect the ultraviolet oxygen

lines in two of the objects and use direct methods to calculate their abundances. Finally, we can establish whether using the strong line diagnostics is a valid approach, also at the highest redshifts where such a comparison is currently feasible with ground-based observations. Figure 4 shows the differences between the oxygen abundance derived from direct methods and the strong line methods for the sample observed with X-shooter. The panel also includes all the other $z > 2$ galaxies where direct abundances have been measured, and illustrates that, within the considerable uncertainties, the R_{23} calibration gives results consistent with the direct methods.

Figure 4. The oxygen abundances of six galaxies at $z \geq 2$ measured via the direct method versus those derived from the R_{23} strong line diagnostic. The dotted line is the one-to-one relation. The three lensed galaxies observed in this programme are the annotated red circles, while the yellow squares are two lensed and one unlensed galaxies from the literature.

Next steps

Not only do our observations target the background sources, they also allow us to characterise the mass properties of the main lens galaxies for two systems (Pettini et al., 2010; Grillo & Christensen, 2010) revealing high stellar velocity dispersions between 300 and 500 km/s and dark matter fractions in excess of those typically seen in individual field galaxies. Upcoming X-shooter observations of selected lens galaxies will show if those are indeed the most massive early-type galaxies at intermediate redshifts.

The success of X-shooter observations in finding source redshifts can be extended to lens systems selected by other methods. The Herschel observatory has recently discovered a population of highly luminous submillimetre galaxies, which have been magnified by foreground galaxies at intermediate redshifts. Recent X-shooter observations (March 2013; Christensen et al., in prep.) for 12 systems have revealed the lens galaxies to be very massive, with redshifts at $0.3 < z < 0.8$, but the background sources have much fainter emission lines than seen in the HST sources. Preliminary results show two possible counterparts at $z \sim 2.9$ to the submillimetre galaxies consistent with the average redshift of the population of known submillimetre galaxies. One galaxy has a strong Lyα emission line. The remaining galaxies may be too faint, extremely dusty, or without Lyα emission. The redshift could also be so high that even strong optical emission lines are redshifted out of the NIR region.

References

Christensen, L. et al. 2010, MNRAS, 406, 2616
Christensen, L. et al. 2012a, MNRAS, 427, 1953
Christensen, L. et al. 2012b, MNRAS, 427, 1973
Grillo, C. & Christensen, L. 2011, MNRAS, 418, 929
Kewley, L. & Ellison, S. 2008, ApJ, 681, 1183
Mannucci, F. et al. 2011, MNRAS, 414, 1263
Noeske, K. et al. 2007, ApJ, 660, 43
Pettini, M. et al. 2010, MNRAS, 402, 2335
Pilyugin, L. S. & Thuan, T. X. 2005, ApJ, 631, 231
Postman, M. et al. 2012, ApJS, 199, 25
Richard, J. et al. 2011, MNRAS, 413, 643
Tremonti, C. et al. 2004, ApJ, 613, 898
Wuyts, E. et al. 2012, ApJ, 755, 73

Part of the COMBO-17 extragalactic survey area is shown in this image taken with the MPG/ESO 2.2-metre and Wide Field Imager. The COMBO-17 survey (Classifying Objects by Medium-Band Observations in 17 Filters) was a project dedicated to deep imaging of several small patches of the sky through 17 different filters across the visible spectral range. This image was taken with only three of the 17 filters from the project: *B*, *V* and *R*, but data through an additional near-infrared filter was also used. Further details can be found in the Picture of the Week for 9 January 2012.

ESO/G. Hüdepohl

Above: In the dry Atacama Desert region, electrical storms are quite rare. This one occurred over Cerro Paranal on 7 June 2013; more details under Picture of the Week for 17 June 2013.

Lower: The Federal Minister for Science and Research of Austria, Karlheinz Töchterle (left) and the Portuguese Minister of Education and Science, Nuno Crato (right), visited Paranal Observatory on the same day in March 2013, and are shown flanking the ESO Director General Tim de Zeeuw. See Announcement ann13028 for details.

Report on the ESO Workshop

The Deaths of Stars and the Lives of Galaxies

held at ESO Vitacura, Santiago, Chile, 8–12 April 2013

Henri M. J. Boffin[1]
Dave Jones[1]
Roger Wesson[1]

[1] ESO

This five-day meeting was attended by about 100 astronomers and consisted of 16 invited and 26 contributed talks and more than 40 posters, still leaving ample time for discussions and social activities. A brief overview of the topics is presented, from mass loss in low- and high-mass stars and the ubiquitous importance of binaries, to the influence of this ejected material on galaxy evolution.

AGB and planetary nebulae

The workshop started with a review of the life of solar-like stars by Amanda Karakas, with an emphasis on the asymptotic giant branch (AGB) phase, when stars lose most of their envelope mass in a series of episodic thermal pulses. These thermal pulses (TPs), which each last only a couple of hundred years and are separated by some hundred thousand years, increase the carbon content of the envelope, and only a few TPs are required to make a solar-like star appear as C-rich (C/O > 1). This enrichment in carbon alters the stellar opacity, but this was only very recently taken into account in stellar evolution models, leading to a decrease in the time spent on the AGB and of the possible number of TPs. As the TPs are responsible for the final

amount of chemical elements produced (and expelled into the interstellar medium), knowing how many happen before the AGB star evolves to become a white dwarf (WD) is crucial, but also extremely dependent on the assumed mass-loss rate, whose exact mechanism is still far from being understood.

The situation is yet more complicated, as shown by Falk Herwig in his review on the role that hydrodynamic mixing processes, which are closely related to the convection and nuclear reaction rate uncertainties, play in predictions of the evolution and nucleosynthetic yields of AGB stars. He also talked about the role of rotation in AGB stars, and how it may be best investigated in interacting binaries, such as the post-merger evolution of coalescing He+CO WDs and other sources similar to Sakurai's object. Binaries are also useful to explain the formation of planetary nebulae (PNe), as Orsola de Marco explained. The problem is to understand how the spherical mass-loss on the AGB can produce the collimated outflows seen in many PNe (Figure 2). Magnetic fields alone cannot do the trick — an additional source of angular momentum is needed — so that the most natural explanation is that PNe contain a close or wide binary system. This has now been verified in many cases. The remaining problem is how to go from the known ~ 30 % binary fraction of solar-like stars to the apparent ~ 80 % binary fraction in PNe. This, perhaps, implying that single stars do not form PNe at all! A series of talks by the PN group in ESO Chile (Henri Boffin, Dave Jones, Amy Tyndall) presented further developments

along these lines, including the discovery of PNe in which there was a clear proof of mass transfer between the two components of the system, as well as showing that the jets observed in the PNe always precede the formation of the PN itself.

Novae

Close binaries containing a white dwarf were the topic of the next session, and Claus Tappert reviewed our current knowledge of novae. A nova eruption is a thermonuclear runaway on the surface of the white dwarf component in a close binary system known as a cataclysmic variable (CV). During this event a certain fraction of the previously accreted matter is ejected as a shell, thus enriching the interstellar medium (ISM) with nuclear processed material. Due to the considerable increase in brightness during the eruption, novae are observable in other galaxies, which makes them attractive as distance indicators. The class of novae may not be very homogeneous, however. Nova eruptions are the primary mechanism for mass loss in CVs, and as such they may well prevent the formation of Type Ia supernovae (SNe) via the single-degenerate mechanism since they prevent the white dwarf from reaching the Chandrasekhar mass limit. Olivier Chesneau showed how adaptive optics and optical interferometry can be used to study interacting binaries in detail, while Ken Shen and Ashley Ruiter presented models of the formation of Type Ia SNe,

Figure 1. The participants at the workshop in the grounds of ESO Vitacura.

H. Boffin et al.

Figure 2. The amazing bipolar planetary nebula Fleming 1 was shown by several speakers at the workshop.

either via double detonations or white dwarf mergers.

Nebular abundances

Returning to the topic of PNe, Denise Gonçalves provided an overview of the determination of nebular abundances, and in particular, on the improvements that have been achieved recently. Abundances in PNe are particularly relevant to provide information about low-to-intermediate mass stellar nucleosynthesis, while at the same time, PNe archive progenitor abundances of α elements. To derive nebular abundances, two methods are widely used: the empirical ionisation correction factor (ICF) method and photoionisation model fitting. The former is often the only one used, and despite severe shortcomings, can provide reasonable results, even though it is advisable to extend the wavelength range used as much as possible. The second method uses empirical abundances as the input for photoionisation model fitting, that is, the abundances are varied until the predicted line ratios (and emission line maps if available) match the observations. Unfortunately, abundances are not necessarily better determined from the model-fitting method, but it can provide more accurate ICFs than using the simple formulae in the literature. To apply one of these methods, a wide range of software exists, such as nebular, *ELSA, 2D_Neb, NEAT, PyNeb, CLOUDY* and *MOCASSIN*. ESO Fellow Lizette Guzman-Ramirez used VISIR to observe a sample of PNe that show evidence of mixed chemistry with emission from both silicate dust and polycyclic aromatic hydrocarbons. The mixed-chemistry phenomenon is apparently best explained through hydrocarbon chemistry in an ultraviolet-irradiated, dense torus. This highlights the need to consider carefully the shape of the PNe when determining nebular abundances.

From massive stars … to PNe again

The second day of the meeting dealt with more massive objects, starting with a review of the evolution of massive stars by Georges Meynet. Massive stars form only a very small fraction of all stars produced in a given stellar generation, but nevertheless are of great importance: if only 0.3% of all stars have masses above 8 $M_\odot$, they contain 14% of all the mass, and almost half of that is returned to the host galaxy in the form of processed material with huge amounts of kinetic energy and on very short timescales. Nor can binarity be ignored, as the most recent censuses show that the binary fraction of massive stars is more than 50%, or even 70% in some cases. Apart from mass transfer and drastic evolution, binarity can imply tidal effects that lead to extra mixing inside the stars. It is also likely that binaries produce 50% of all existing Wolf–Rayet (WR) stars.

Massive stars will explode as supernovae and/or gamma-ray bursts, and the study of these explosions can reveal much about stellar evolution. Jose Groh stressed the fact that in some very rare cases, such as SN 2008bk, we are lucky enough to have an image of the progenitor before it exploded, showing that it was an ~ 8 $M_\odot$ star. The case of SN 2009ip is even stranger as this object underwent several outbursts in a few years, before actually exploding in 2012. The progenitor in this case is thought to be a luminous blue variable (i.e. not unlike η Carinae) with a mass of about 50–90 $M_\odot$.

Nathan Smith made the link between massive stars and planetary nebulae, presenting the similarities and dissimilarities in the morphology of these two kinds of objects (Figure 3). Cool hypergiants with large circumstellar envelopes, such as the "Rotten Egg Nebula", are the massive analogues of OH/IR stars (i.e. embedded AGB stars), while rings are seen in both PNe (e.g., the Necklace Nebula) and massive stars (SN 1987A is a fine example), and there are also clear resemblances between some PNe such as Hubble 5 or the Ant Nebula (Mz 3) and some of the most massive stars such as η Carinae. These bipolar outflows may in fact represent evidence of explosive events also taking place in PNe. On the other hand, while PNe often present jets, these are missing from massive stars. All circumstellar shells, around PNe or massive stars, suffer the effects of ionisation, photoevaporation, shocks, winds and explosions. As such, the wind interaction mechanism for explaining PNe might be too naïve in many cases.

Making stars explode

Going further in the evolution of massive stars, Hans-Thomas Janka presented the state of the art in explosion models, highlighting the importance of neutrino heating as the trigger for core-collapse supernovae and the need to use 3D simulations — not only in explosion simulations, but also for the proper initial conditions inside the progenitor. 3D simulations are very time-consuming, however, and require CPU power that is hardly available yet. Nevertheless the few 3D simulations that do exist clearly show different results than in 2D — models exploding in 2D don't necessarily do so in 3D, but at the current state of the art, it is not clear if this is just a resolution issue. This is most relevant as it seems that hydrodynamical instabilities are critical to trigger the final explosion, and
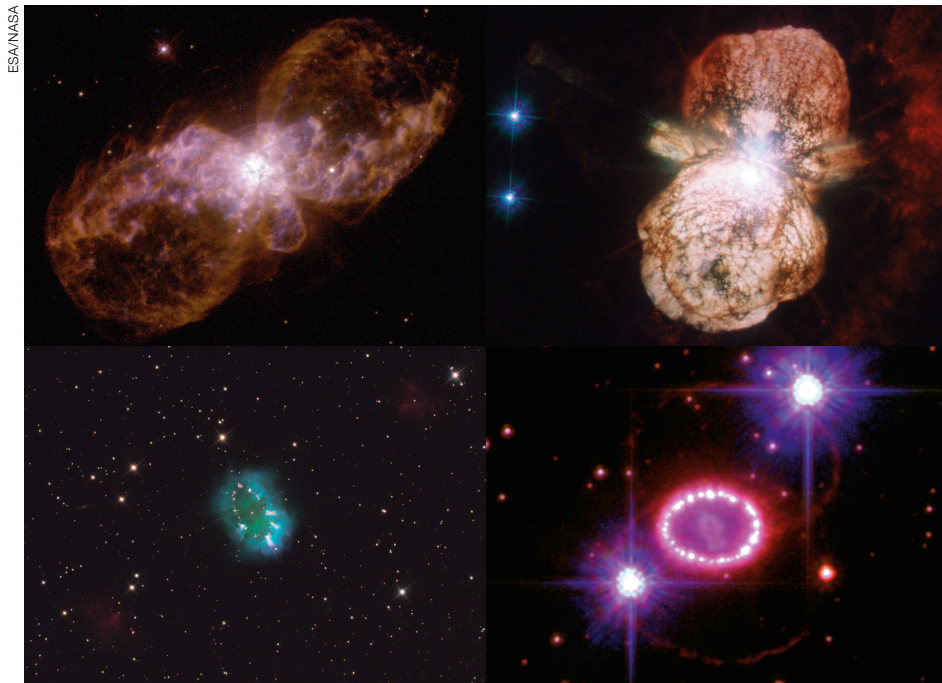
ESA/NASA

Figure 3. The striking similarities between the planetary nebula Hubble 5 (upper left) and Eta Carinae (upper right) on one hand, and the ring inside the Necklace Nebula (lower left) and around SN 1987A (lower right), on the other hand, potentially illustrate that similar phenomena are at play in solar-like and massive stars.

driving mechanism for the mass loss. Apart from AGB, supernovae also appear to be a major source of dust production. The Atacama Large Millimeter/submillimeter Array (ALMA), for example, has confirmed the presence and location of a vast amount of cold dust in SN 1987A, most likely produced in the ejecta, while the small amount of dust measured in the ring comes from the progenitor. Several talks covered various aspects of dust production: crystalline silicates around oxygen-rich AGB stars (Olivia Jones), metallicity effects in globular clusters and dwarf spheroidals (Eric Lagadec), in the Crab Nebula (Patrick Owen) and in a binary merger V1309 Sco (Christine Nicholls).

Astrosphere, astrosphere!

The next day, after an inspiring free afternoon where most participants went on a vineyard tour (Figure 4), Nick Cox devoted his presentation to astrospheres. When stars plough through space at supersonic speeds, the interaction between their stellar winds and the surrounding medium can give rise to spectacular bowshocks or pile-ups, collectively known as astrospheres. Although the underlying physics is equivalent, the sizes, shapes and properties of these bowshocks can vary drastically for different types of stars or different conditions of the ISM. Even binarity or internal stellar processes can be decisive in shaping the observed interaction regions. The scale of such astrospheres can vary between a couple of hundred astronomical units for G stars such as the Sun to several parsecs for young, hot stars. Betelgeuse is a very nice example as it shows several arcs in the direction of motion, due to the expelled wind that interacts with and sweeps up the surrounding ISM. Other examples are runaway OB stars, Mira variables or R Hya stars, but recent observations with Herschel have shown a whole new population of objects displaying signs of inter-

much emphasis is now given to the standing accretion shock instability. While it appears that although neutrino-driven explosions may explain supernovae with energy below 2×10^{51} ergs, hypernovae with higher energies seem to require a different, as yet unknown, mechanism.

Bernhard Müller and Bronson Messer presented further multi-dimensional explosion models of core-collapse supernovae, including the effect of general relativity, and the resulting astronomical signatures, such as the nucleosynthetic yields and gravitational waves. It was emphasised that only by comparing theory with observations will we see whether we understand the underlying physics. Takashi Moriya and Filomena Bufano presented observations of different flavours of Type II supernovae.

Letting the dust settle

On the third day Isabelle Cherchneff reviewed dust, which is ubiquitous in the Universe and impacts the physics and chemistry of many environments, such as the winds of evolved stars, the formation of planets in protostellar discs and the synthesis of complex organic molecules in molecular clouds. Large dust masses

have been inferred in primitive galaxies and are indicative of efficient production in the early Universe, despite the very low metallicity and short timescales involved. A wealth of observational data exists on this key component of the Universe, but the chemical nature of dust, its synthesis in stellar media and the dust yields produced by stars are still very poorly understood. Dust formation requires high gas temperatures and densities to persist for a long enough period of time, and the best loci seem to be the shocked circumstellar environments around evolved stars, i.e. AGB stars, supernova remnants, C-rich WR stars and RCrB stars. The main outcome of Cherchneff's talk was that no satisfactory model of dust formation in an evolved circumstellar environments currently exists, and the only way out may be to use a chemical kinetic approach.

Mikako Matsuura then provided a review of recent observational studies of dust in planetary nebulae and supernovae, and how they could impact the morphology, spectral appearance of nebulae and ambient interstellar media. Dust is not only produced in stars, but it can also play a crucial role in their further evolution, such as the case of AGB stars, where dust is considered to be the main
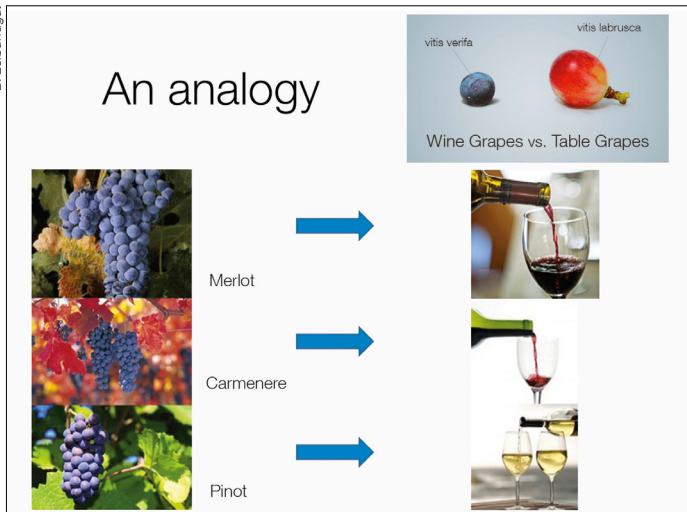
Figure 4. A perfect example of the blend between scientific and social activities. The vineyard tour on Wednesday afternoon provided a nice analogy to show how similar grapes produce rather different wines, in the same way that similar binary systems may explain the great diversity in Type Ia SNe.

action, allowing classification among those showing fermata, eye, ring or irregular shapes. A new branch of astrophysics is in the making here!

Moving to yet higher mass, Paul Crowther discussed evidence for and against the existence of very massive stars, i.e. stars more than 100 $M_\odot$ in young massive clusters. Such massive stars are thought to have existed as Population III stars when they exploded as pair supernovae, producing vast amounts (several solar masses) of nickel and other elements, and thereby playing an important role in the early chemical enrichment of galaxies. However, they also seem to belong to some young massive clusters, such as the Arches, R136, Trumpler 14 or NGC 3603. Resolution is key to finding such stars, as the literature contains several examples of claims for the existence of very massive stars that turned out to be unresolved clusters, such as R136a. Very massive stars appear to belong preferentially to binary systems, which is a bonus when deriving current masses without depending on models: an example is the eclipsing binary NGC 3603-A1, whose components of 116 ± 31 $M_\odot$ and 89 ± 16 $M_\odot$ orbit each other in four days. Eta Carinae is another well-known example of a binary containing a very massive star, with a current mass of 120 $M_\odot$, but a probable initial mass as high as 200 $M_\odot$. For some of the stars in R136, the initial mass lies in the range 165 to 320 $M_\odot$. Such stars will explode as highly luminous pair-instability

supernovae, leaving no remnant, and could explain some observations, such as SN 2007bi.

Galactic enrichment

Another important aspect by which stars contribute to their local environment is through their nucleosynthesis, and Francesca Matteucci discussed the chemical evolution of galaxies. All the basic ingredients needed to build galactic chemical models were presented, as well as the role of supernovae and their nucleosynthesis. Comparisons between model results and observations impose constraints on SN progenitors, stellar nucleosynthesis and galaxy formation processes. Alan Alves-Brito presented the different chemical enrichment timescales associated to the death of massive and low-mass stars in M22 and, ultimately, in the Galaxy. While Giovanni Carraro discussed the contribution to the integrated ultraviolet spectrum of the metal-rich old open cluster NGC 6791 from stars in late stages of stellar evolution: WDs, extreme horizontal branch stars and hot sub-dwarfs.

It was then time to leave the Galaxy and look at a broader view of the interplay between stars and galaxies in the Universe. Magda Arnaboldi presented the latest results on planetary nebula populations in external galaxies. Indeed, because of their bright emission in the [O III] 5007Å line, PNe are detected and

studied in galaxies out to 100 Mpc. Based on simple considerations, the peak flux of PNe should decrease with time, but this is contrary to the observations that the peak flux of PNe in galaxies is constant, and may, once again, point to the important role that binaries play in PN formation. Despite the fact that their formation is still far from understood, PNe can be used as important empirical tracers of galaxies and used as distance estimators. Warren Reid showed how PNe are now being used to map the outer kinematic structure of the Large Magellanic Cloud to refine the warps, velocity structures and system rotation uncovered in the inner regions.

Sundar Srinivasan discussed the computation of luminosities and dust injection rates for the entire mass-losing evolved stellar population in the Large Magellanic Cloud. Stacey Habergham described the use of the statistical distributions of the different subtypes of core-collapse supernovae to probe the host star formation properties. The results show: an excess of stripped-envelope SNe in the central regions of disturbed hosts; statistically different distributions of SNIb and SNIc in undisturbed hosts; different distributions of SNIc and SNIIn, both of which are thought to have the highest mass progenitor stars; and an interesting distribution of SNIIn across their host galaxies.

Paradigm shifts and angular momentum

On the last day of the conference, Bruno Leibundgut presented a review of Type Ia SNe as distance indicators. He stressed that it is time to give up some cherished paradigms. Perhaps the most important of which is that Type Ia SNe are not standard candles; in fact, they are not even "standardisable", even though it may be possible to normalise some of them to a common peak luminosity. Type Ia SNe present large variations in luminosity, light-curve shapes, colours, spectral evolution, and even polarimetry. This diversity is such that it is now important to mention which kind of Type Ia SNe is being referred to, as there are clearly several families. The second paradigm to abandon is that Type Ia SNe do not all come from Chandrasekhar-mass white dwarfs. The diversity of Type Ia's shows that

trying to find a single formation channel or explosion mechanism may be a utopian endeavour. However Type Ia SNe are still very good distance indicators and as such have led to the best determination of the Hubble constant, and have helped to confirm the existence of dark energy. Further progress in this area will require good data at $z > 1$, but mostly more infrared data at $z > 0.5$. It is nevertheless rather annoying that the origin of such important objects is still unknown.

The state of our current knowledge was summarised in the final talk of the conference by Noam Soker: "If WDs knew theory, they would not have exploded as SN Ia". Soker stressed that the main open questions in stellar evolution are related to angular momentum (AM) evolution, as AM is crucial both at the birth and at the death of stars. In this regard, the most important source of AM is either the contraction of a cloud/envelope — important during birth and core collapse SNe — or a binary companion (including brown dwarfs and planets). Binarity seemed to be a major ingredient to the many topics discussed during the workshop, and is perhaps the underlying fil rouge.

Most of the workshop talks are available on the meeting webpage[1].

Links

[1] Workshop web page: http://www.eso.org/sci/meetings/2013/dslg2013/program.html

ESO's Early Seeing Expedition to South Africa

Kristen Rohlfs[1]

[1] Institut für Astrophysik, Universität Bochum, Germany

Site-testing for a joint European observatory in the south began in the 1950s in South Africa, following the declaration of the intent to build a large optical telescope in the southern hemisphere. First hand reflections of one of the early site-testing teams working in South Africa, based at the Boyden Station, are described. Practical problems related to seeing measurement and site assessment are discussed.

The long-term result of the meeting of leading European astronomers with Walter Baade in Leiden in 1953 was the foundation of ESO in 1962. One of its immediate consequences, however, was the decision to send an expedition to South Africa with the aim of finding a suitable place for a large astronomical observatory. The foundation and early history of ESO have been described by Blaauw (1991) and in the more recent history in Madsen (2012). This article recalls an aspect only touched on in Blaauw's monograph (p. 23).

I joined the South African seeing expedition in November 1956 when I had just finished my Staatsexamen fur das Höhere Lehramt with a thesis on cosmology with Prof. Otto Heckmann at Hamburg as advisor. At that time the plans for the European Southern Observatory were still very informal, and nothing had been definitely decided yet. Not even the name of the enterprise was definite, and we were known at the time by the garage that serviced the expedition cars as "Joint European".

Observing conditions in South Africa

At that time very little was known about seeing and seeing conditions in South Africa, only that the number of clear nights in that country was much larger than in Europe and several observatories had been established there: the Cape Observatory at Cape Town; the Radcliffe Observatory with a 74-inch telescope at Pretoria; and the Boyden Observatory with a 60-inch telescope at Bloemfontein. The seeing expedition had the task of finding a fully satisfactory place for a modern observatory, but it was not clear what the meteorological conditions were that had to be fulfilled to meet the request.

The climate of South Africa is divided into two different regimes: in the southern part there is a Mediterranean-type climate with winter rain, and the more northern subtropical region has rain in the summer season. Therefore it was decided to split the expedition into two groups; one was to investigate the winter rain region, the other the summer rain region further north. Both regions have a large number of clear nights when compared to European conditions.

The group that worked in the south (under J. Dommanget) chose Oudtshoorn as their headquarters, while the other group (under H. Elsässer) selected Boyden Station near Bloemfontein. Starting from

Figure 1. Photograph of the Harvard Observatory's Boyden Station in South Africa in the 1950s during the time when ESO site-testing was taking place.

these locations sites were selected that looked promising for a closer inspection. For this the seeing quality and the zenith extinction were estimated several times per night for periods of about 14 days. After about one year, with more than 200 nights on duty and about 100 000 kilometres covered with the cars, a new crew was needed, and this was the situation when I joined the seeing expedition.

Site-testing instrumentation

In order to be able to investigate the astronomical quality of a site two different types of instruments were provided to the expedition. One was a very rugged, high quality 25-centimetre reflector on an azimuthal mount, quite similar to a Dobson mounting, that could be tracked manually and exceedingly smoothly so that a magnification of 700 times could be used on a routine basis. The seeing could then be judged by a method invented by Danjon, based on the visibility and quality of the diffraction rings of the telescopic stellar images. The other type of instrument was a small refractor on an equatorial mounting with a simple photoelectric photometer using an 1P21 photomultiplier. Because of the then

available electronic valve technique with photographic registration of the measurements, its use was exceedingly bothersome under field conditions. Experience in South Africa quickly showed that the difference in the extinction at different places is quite small if the sky is clear, and so extinction was no longer a strong criterion for site selection and extinction measurements could be dropped safely.

The seeing expeditions

During my stay in South Africa the seeing expedition consisted of Dr Walther Tripp from Göttingen, Father Bertiau SJ from Belgium and myself, and for a short time we were reinforced by a retired gentleman, whose name I unfortunately don't remember, who had been occupied during his active time by taking plates for the Franklin–Adams charts. We had our headquarters at the Boyden Observatory, which at that time had been closed down by Harvard Observatory and was rented by a consortium from the Hamburg Observatory, Sweden and Northern Ireland (see Figure 1).

At that time the southern group had boiled down their search to a single place —

Zeekoegat, just north of the Swartberg Mountains in the southern part of the Great Karroo — and therefore we dropped the Oudtshoorn headquarters and served Zeekoegat from Boyden station. In the northern region there were still several places to be investigated. We even decided to include another site in our investigation: a place on a mountain range close to Calvinia in the northwest part of the Cape Province. Atmospheric conditions similar to those at the Californian astronomical observatories could hopefully be expected in this area, caused by the cold Benguela current. Since the mountains were not accessible by car, we arranged an exploratory stay with the help of local people and the South African Air Force, who provided us with helicopter transport. W. Tripp and I stayed on the mountain for 14 days and made seeing estimates. While the seeing was reasonable, the weather was impaired by high ranging cirrostratus. Since the sky was clear at Boyden at the same time, we dropped Calvinia from the agenda.

It turned out to be fortunate that Boyden was a working observatory. At that time Jürgen Stock from the Hamburg Observatory was the local supervisor, and he was doing photoelectric photometry

with the 60-inch telescope, while we were doing our routine seeing estimates. Quite naturally we discussed our seeing problems with him and compared our seeing estimates with his estimates at the 60-inch at midnight tea. The results were confusing — sometimes they agreed and sometimes we obtained different results and so we decided to investigate this more closely. The 60-inch telescope had a rather thin mirror blank, and the mirror cell had three supporting pads whose pressure could be adjusted from the eyepiece so that the mirror shape could be adjusted manually. This was an art and a kind of active optics *avant le temps*. J. Stock was quite good at this and at the same time he obtained a good impression of the seeing. When he did this, he gave us notice so that we could do our seeing estimates at the same time.

The seeing measurements

Plotting the seeing estimates for our 10-inch telescopes against those of the 60-inch we obtained a generally positive correlation, but one with a peculiar scatter. When we found a medium value for the 10-inch seeing, the 60-inch showed mostly medium-quality seeing too. It could, however, just as well give bad seeing. The same was true if the 10-inch seeing was excellent. But we never found the situation that a bad or medium 10-inch seeing was accompanied by an excellent 60-inch seeing. In long discussions with J. Stock and the members of the seeing expedition, we arrived at a simple explanation of this result.

The air in front of the telescope is not uniform, but shows minute temperature fluctuations that result in similar variations of the index of refraction. If the linear scale of these variations is smaller than the telescope diameter, they will produce a loss in the sharpness of the stellar images, scales larger than the telescope diameter, on the other hand, will produce a lateral shift of the image, and when the fluctuating density field is moving, the stellar images will move too. Therefore, if we want to obtain good estimates for large-telescope seeing, we have to be able to measure both the small-telescope seeing and the image motion.

The problem in measuring the image motion is that it is exceedingly difficult to distinguish the part that is caused by the atmospheric disturbance from that caused by mechanical vibrations of the telescope. Either one needs a telescope with a very stable mounting and an exceedingly smooth drive, or one has to utilise a differential procedure, where two separate telescopes on a single mounting have common vibrations, so that the separation of their images is only affected by the atmospheric image motions. Quite naturally we discussed ways to make these measurements, but under expedition conditions it turned out not to be possible to provide an appropriate instrument.

Another problem connected with the seeing in South Africa could however be solved. According to astronomical folk-lore at Boyden Observatory, the seeing quite often deteriorates markedly after midnight, so that the observers could go to bed safely at convenient times. We had to do our regular seeing runs at midnight and at four o'clock irrespective of the prevailing seeing and so we noticed, as had other observers before, that the failing seeing is connected with falling temperatures. This occurred mainly in the winter months with quiet clear skies, when an inversion layer was forming in the air close to the ground. As soon as the telescope is covered by this cold air, the seeing deteriorates dramatically. We tested this by observing along the roads leading up to Boyden Kopje, rising by about 50 metres and then going to Naval Hill in Bloemfontein, rising about 100 metres. A hill with an elevation of more than 100 metres above its surroundings and the facility to drain the cold air downhill should therefore be a suitable place for an observatory. Just a few kilometres north of Bloemfontein we found a suitable *kopje* and we did some seeing observations from the top and found it quite suitable. Later on we heard that Walter Baade had already pointed out this very place as a possible site for an observatory some years earlier.

Aftermath

As 1957 drew to a close it was decided to end the seeing expedition to South Africa in its then-present form and so

we sat down to convert our experience into a report. At that time Xerox copy machines were not yet available, and it was not a trivial matter to produce several copies. We tried to do this with the help of a printing shop, but then their copy machine broke down, and therefore only very few copies were eventually made. I do not know who got them and I did not have one myself.

The seeing expedition to South Africa continued using a different setup. At two sites — Zeekoegat and at Klavervlei near Beaufort West at the northern border of the Great Karroo — semi-permanent small observatories with medium-sized telescopes were set up and used for regular astronomical programmes. By these means, longer-term experience with the seeing quality could be obtained.

The members of the first seeing expedition all returned to Europe. Father Bertiau returned to his congregation, Tripp became a personal assistant to Heckmann for some time, and after that he left astronomy for a consulting firm. I returned to Hamburg and helped Stock for some time as a student assistant and worked on my PhD thesis. After its completion I switched to radio astronomy and eventually became involved in the construction of the Effelsberg 100-metre telescope; I have never been concerned with ESO matters since. Unfortunately my photographs from the time of the seeing expedition have been lost in the course of several removals, as well as my notes and letters. So I have to rely on my memories. But because I am one of the very few of those active in the seeing expedition who is still alive, I thought it might be worthwhile to put my memories to print.

References

Blaauw, A. 1991, *ESO's Early History – The European Southern Observatory from Concept to Reality*, (Garching: ESO)
Koorts, W. 2012, MNASSA, 71, 248
Madsen, C. 2012, *The Jewel on the Mountaintop – The European Southern Observatory through Fifty Years*, (Weinheim: Wiley-VCH)

Staff at ESO

Zahed Wahhaj

I arrived at Santiago late in 2012 to join ESO as Faculty Astronomer with duties on Paranal. The SPHERE exoplanet-finding instrument was supposed to arrive at the observatory in late 2013, and I was to be one of three instrument scientists. I had spent the last six years in Hawaii, working on the Gemini NICI Planet-Finding Campaign, trying to directly image exoplanets with the 8-metre Gemini South Telescope. It was thrilling to know that I would get to work with one of the most powerful exoplanet imagers in the world, and that I was joining a vibrant research community at ESO, Santiago. Six months later, I find these expectations are not a bit untrue.

My journey to Chile is just as roundabout as my journey to exoplanets. Age zero to seven I spent in Iraq. The next 11 years I was incubating in my home country, Bangladesh. Then I decided to go to college in Philadelphia, followed by four years in Flagstaff, Arizona, then boomeranged off to Hawaii, finally arriving intact in Chile. In the beginning, I had decided not to be much of anything. Indeed, I had reportedly given up on life and attempted pneumonia a few days after birth. By age seven, I had found meaning in following my mom in prayer. Upon learning to read effectively, I thought my life until aged ten had been wasted, and that I would have a fruitful life in literature. Around age 13, I realised that all that fiction was depriving me of some essential truths. This was when I read a science populariser called *The Omega Point* and became obsessed with the end of the Universe. Also around this time, upon discovering some pictures of constellations in a library book, I decided to check if these were also "true" and climbed the water tank on our roof at night to compare with reality. It hit me then that some of the most interesting things about the Universe were not reaching me.

For the next few years I played with the interesting parts of physics, and then the next few years, the interesting parts of computer science. In college, I thought I should do both and that they would seamlessly combine into a double major. They did, but not seamlessly. In graduate

Zahed Wahhaj

school, I turned into a radical high-energy physics enthusiast. This enthusiasm cooled when I realised that the fourth-year enthusiasts had no conference money. In the third year of grad school, I thought back on the water-tank experience and decided that I should have received the message more directly. I went to talk to newly arrived University of Pennsylvania Professor Dave Koerner about the direct imaging of circumstellar matter, and whether he was finding something interesting there.

Dave had just obtained the first resolved images of a debris dust ring around the star HR 4796A using the Keck telescope. The images were obtained at mid-infrared wavelengths, where the thermal emission from the dust ring, formed from collisions between rocky bodies in the system's own exo-Kuiper Belt, was brighter than the star. In such debris disc systems any asymmetries in the dust distribution could be signatures of planets. I would do my PhD thesis on the measurement of the morphology of the dust discs in three young systems, β Pic, HR 4796A and 49 Ceti. This involved trying to match the images of the dust at wavelengths where it was radiating thermally and at shorter wavelengths were it was mainly reflecting stellar light. Dave had introduced me to Bayesian statistics, which I used to obtain probability distributions for the disc

properties. Bayesian statistics still has a great attraction for me, because it is essentially about asking a robot about its beliefs after being taught a few logical rules and then supplied with some observations.

Near the end of grad school and as a postdoc in Flagstaff, I worked with the Spitzer Cores to Disks Legacy team. We had been given 400 hours of the Spitzer Space Telescope observing time to study star formation through its disc and planet formation phases, by looking for dust at mid- and far-infrared wavelengths. My work was to figure out the evolutionary status of stars which showed signs of waning disc accretion, indicated by weak Hα emission. I found that these systems exhibited a wide variety of disc opacities but were generally transitioning towards the debris disc phase.

In 2006, I came to Hawaii to join the Gemini NICI Planet-Finding Campaign led by Mike Liu. We had a terrific instrument that was capable of detecting planets half a million times fainter than the star at 0.5-arcsecond projected separation. We imaged hundreds of stars. But bright massive planets are indeed very rare, and we discovered instead mainly brown dwarfs. The campaign was an immense amount of work, involving thousands of hours of data reduction, and careful cataloguing of hundreds of candidates, and follow-up imaging to look for common proper-motion companions. The campaign and pipeline design had also taken many man-years of labour. Our small ragtag team of planet hunters was transformed into a disciplined, hungry, small ragtag team of planet hunters. Currently, we are working on calculating the constraints on the exoplanet population from the campaign results, and dreaming about SPHERE and the Gemini Planet Imager (GPI), the next generation planet-finding instruments.

So with that history I came to join ESO, to support SPHERE's operation. With adaptive optics experts like Julien Girard and Dimitri Mawet behind the instrument scientist team, there's a fantastic excitement around direct imaging efforts at ESO. We have coalesced into a new Direct Imaging Group with PhD students,

ESO Fellows and faculty members interested in planet formation. Our meetings have been rich with ideas and we have already written a few proposals together. I hope for many more.

Observing duties on Paranal make a whole different world. We are telescope operators, engineers, astronomers, and living-support staff engaged in efficient, unrelenting and voluminous production of science. The work is physically hard for all of us up there, but this shared sacrifice, shared responsibility, and moments of shared celebration create perhaps an unusual sense of fellowship between us. We are different up on

Paranal from how we are when we are down in Santiago doing our research. I am sure the sharing of arduous and rewarding work and the rotation of supervision roles grew somewhat out of necessity. Although it is not as egalitarian as I am making it sound, I think that whatever camaraderie we experience up there comes from the supportive and unusually interwoven roles we play.

At the end of this piece, I feel obliged to look at the bigger picture. Even now, some of the most interesting things about the world are not reaching us. We may have the most technically advanced communication system in the history of our

existence, but it misinforms us to the point of self-destruction. As we have poured our labour into astronomy, I am sure that many of us have tried to work against climate destruction on our planet. We are just past midnight in the century, perhaps a fateful century for humankind. Whatever else I do, I am glad to be doing one of the things that proves that we were worth saving.

It is a cold May night in Santiago. I am going to call my wife now and tell her that I have finished writing. She joins ESO in November. It will be warm in our apartment then.

Fellows at ESO

Gabriel Brammer

Blame it on Hale-Bopp. I was a high-school student who enjoyed physics and mathematics when that comet made its trip through the inner Solar System, becoming easily visible to the naked eye on crisp spring nights in central Iowa. I was captivated by the comet and soon started taking out a small telescope that my parents had bought, exploring planets, nebulae and star clusters visible from only a short drive away from the city lights. I've been an observational astronomer ever since.

I am fortunate to have studied and worked in the field of astronomy at a time when travelling to remote observatories is still a critical component of research. To efficiently schedule observations at the most advanced, complex observatories in the world, such as the ESO Very Large Telescope, observations are increasingly carried out by professional observers, and the data are shipped electronically to research astronomers around the world. While the quality of the data is spectacular, part of the experience is lost: I feel a

Gabriel Brammer

visceral connection to the science of astronomy when I watch an enormous telescope track the night sky and I wait, perhaps for many hours, while it soaks up the light from a distant galaxy.

And this is to say nothing of the fact that observing often requires travelling to some of the most beautiful places on Earth. (If you meet an astronomer at a party and run out of things to say, we're

always happy to talk about airline frequent-flyer programmes.) My undergraduate and PhD research has taken me all over the world, from telescopes in Arizona to a total solar eclipse in Zambia. Now an ESO Fellow, I spend a week per month on a mountaintop in the Atacama Desert in northern Chile.

My own research, started during my PhD education at Yale University and

ESO/G. Brammer

Comet C/2011 W3 (Lovejoy) captured over Paranal in December 2011 while the laser guide star was operating from VLT UT4. One of Gabriel Brammer's photographs from the ESO Photo Ambassador programme.

Caroline Foster

continued now at ESO, is aimed at studying how galaxies form and evolve. Using telescopes such as the ESO VLT and the Hubble Space Telescope I search for, and then characterise, distant galaxy populations, from low-mass starburst galaxies to monster galaxies with masses already more than ten times the mass of the Milky Way only a few billion years after the Big Bang. By taking snapshots of these galaxy populations at different cosmic times, we can develop an understanding of the dominant physical processes that shape galaxies as we see them today.

Galaxies and cosmology involve scales of space and time that are difficult to comprehend, although these scales become slightly more accessible, and exciting, sitting at the telescope and recording the light from vibrating hydrogen and oxygen atoms many billions of light-years away.

Astronomy is an international discipline, and ESO stands out as an inspiring model of international collaboration. At ESO I have developed friendships and collaborations in Chile, Europe and many other countries around the world. I also appreciate the opportunity at ESO to communicate my excitement for astronomy with the general public, through media interviews, presentations to school groups, and sharing images of the VLT site through ESO's Photo Ambassador programme. Perhaps appropriately, those of my photos that have found the most enthusiastic reception have been of the

comets that recently graced the skies over Cerro Paranal.

Caroline Foster

I remember watching my dad building or taking things apart for hours as a child. I was always curious about how everything works. Growing up, I was not a particularly talented student; in fact I did not really like school at first. All that changed with my first physics class! I was (and still am) mesmerised at how elegantly mathematics describes our world! My first love was definitely for physics, astronomy came later.

Hence, I became a rather enthusiastic physics and mathematics undergraduate student at Bishops University in Sherbrooke, Canada. As a side project, my university opened a small observatory for public outreach. The small telescope (21 inches) was setup on the roof of my university. Volunteers were needed and I gladly helped out. I learned a great deal about the night sky and wondered about how it came to be.

When graduation came up, I realised that I still wanted to study physics. So I enrolled into a Masters degree at Bishops in astronomy… I had heard about immense regions of our Universe that were completely devoid of matter and was fascinated. I would write a thesis about "nothing"… or to be more technically correct, I would study cosmological voids!

I subsequently completed a PhD at Swinburne University in Melbourne, Australia, in observational extragalactic astronomy studying the assembly and chemical enrichment history of nearby galaxies. This gave me the privilege to use data from and observe at remote telescope facilities. Coming down from some observatory headquarters after my first-ever "professional" observing run I realised that I'd love to work at an observatory. I'd imagine myself watching sunsets above the clouds on a regular basis, getting accustomed to extremely dry and oxygen-deprived remote places and taking real photos that look like they must have been photoshopped!

In June 2011, I was thrilled to begin my position as an ESO Fellow in Chile. I have since been sharing my time between research in Santiago and support at Paranal as VIMOS instrument fellow and supporting night-time operations on UT3. Paranal feels like home, my colleagues are like family and the whole ESO experience has been very positive. It is with a pinch of sadness that I will leave Chile next month to start a new position at the Australian Astronomical Observatory. The skills learned and friendships created during my Fellowship will however always be with me.

ESO

European Organisation
for Astronomical
Research in the
Southern Hemisphere

ESO Fellowship Programme 2013/2014

The European Organisation for Astronomical Research in the Southern Hemisphere awards several postdoctoral fellowships each year. The goal of these fellowships is to offer outstanding early-career scientists the opportunity to further develop their independent research programmes in the exciting scientific environment of one of the world's foremost observatories.

ESO is the foremost intergovernmental astronomy organisation in Europe. Its approximately 110 staff astronomers, 40 Fellows and 50 PhD students conduct frontline research in fields ranging from exoplanets to cosmology, offering one of the most vibrant and stimulating scientific settings anywhere in the world.

Fellowships are available both at ESO's Headquarters in Garching near Munich, Germany, and at ESO's astronomy centre in Santiago, Chile.

The ESO Headquarters is situated in one of the most active research centres in Europe, boasting one of the highest concentrations of astronomers. ESO's offices are adjacent to the Max Planck Institutes for Astrophysics and for Extraterrestrial Physics and only a few kilometres away from the Observatory of Munich's Ludwig-Maximilian University. Additionally, ESO participates in the recently formed "Universe" Excellence Cluster at the Garching Campus, which brings together nearly 200 scientists to explore the origin and structure of the Universe. Consequently, ESO Fellows in Garching have many opportunities to interact and collaborate with astronomers at neighbouring institutes.

In Chile, Fellows have the opportunity to collaborate with the rapidly growing Chilean astronomical community as well as with astronomers at other international observatories located in Chile. The advent of the new ALMA building next to ESO's Santiago offices and the arrival of many astronomers and fellows working on the ALMA project have further enhanced the stimulating scientific environment available to ESO Chile Fellows.

The fellowships in Garching start with an initial contract of one year followed by a two-year extension (three years total). In addition to developing their independent research programmes, ESO Garching Fellows will be expected to engage in some functional work, for up to 25 % of their time, related to e.g. instrumentation, VLTI, ALMA, E-ELT, science operations support either in Garching or at one of ESO's observatories in Chile, or public outreach. This provides the Fellows with the opportunity to get involved with ESO projects or operations, and to gather valuable insights and experience not available in any other setting.

The fellowships in Chile are granted for one year initially, with annual extensions for three additional years (four years total). During the first three years, the Fellows are assigned to one of the science operations groups of Paranal, ALMA or APEX, where they will contribute to the operations at a level of 80 nights per year.

During the fourth year there is no functional work and several options are provided. The Fellow may be hosted by a Chilean institution where she/he will be eligible to apply for time on all telescopes in Chile via the Chilean observing time competition. Alternatively, the Fellow may choose to spend the fourth year either at ESO's astronomy centre in Santiago, or at the ESO Headquarters in Garching, or at any institute of astronomy/astrophysics in an ESO Member State.

The programme is open to applicants who will have achieved their PhD in astronomy, physics or a related discipline before 1 November 2014. Early-career scientists from all astrophysical fields are welcome to apply. Scientific excellence is the primary selection criterion for all fellowships.

We offer an attractive remuneration package including a competitive salary and allowances (tax-free), comprehensive social benefits, and we provide financial support for relocating families.

If you are interested in enhancing your early career through an ESO Fellowship, then please apply by completing the web application form available at: http://jobs.eso.org.

Please include the following documents in your application:
– a cover letter;
– a curriculum vitae with a list of publications;
– a proposed research plan (maximum of two pages);
– a brief outline of your technical/observational experience (maximum of one page);
– the names and contact details of three persons familiar with your scientific work and willing to provide a recommendation letter. Referees will be automatically invited to submit a recommendation letter. However, applicants are strongly advised to trigger these invitations (using the web application form) well in advance of the application deadline.

The closing date for applications is 15 October 2013. Review of the application documents, including the recommendation letters, will begin immediately. Incomplete or late applications will not be considered.

Candidates will be notified of the results of the selection process between December 2013 and February 2014. Fellowships will begin in the second half of 2014.

Further Information
For more information about the fellowship programme and ESO's astronomical research activities, please see: http://www.eso.org/sci/activities/FeSt-overview/ESOfellowship.html. For a list of current ESO staff and fellows, and their research interests please see: http://www.eso.org/sci/activities/personnel.html. Details of the Terms of Service for fellows including details of remuneration are available at: http://www.eso.org/public/employment/fellows.html.
For any additional questions please contact:
For Garching: Eric Emsellem, Tel. +49 89 320 06-914,
email: eemselle@eso.org.
For Chile: Claudio De Figueiredo Melo, Tel. +56 2 463 3032,
email: cmelo@eso.org.

Although recruitment preference will be given to nationals of ESO Member States (members are: Austria, Belgium, Brazil, the Czech Republic, Denmark, Finland, France, Germany, Italy, the Netherlands, Portugal, Spain, Sweden, Switzerland and United Kingdom) no nationality is in principle excluded.

The post is equally open to suitably qualified female and male applicants.

Fellows Past and Present

Since 2003 short self-penned profiles of ESO Fellows have been regularly featured in *The Messenger*, allowing young researchers to reflect upon their astronomical careers in a more informal context. All 90 profiles have now been collected into a booklet entitled "Fellows Past and Present".

This booklet is available for download at: http://www.eso.org/public/products/brochures/fellows/

Announcement of the ESO/NUVA/IAG Workshop

Challenges in UV Astronomy

7–11 October 2013, ESO Garching, Germany

The Network for Ultraviolet (UV) Astronomy (NUVA) organises interdisciplinary meetings every three years. At these meetings scientists and instrumentalists working in the UV can exchange information on the current status of the field. The third meeting of NUVA will come at a crucial time in UV astronomy. The ESA/NASA programmes that created the community are reaching completion and future missions, apart from the World Space Observatory (WSO-UV), are small scale, with some operating from balloons.

The advent of 10-metre-class telescopes and the projects for extremely large telescopes, such as the European Extremely Large Telescope, have opened up the possibility for efficient exploration from the ground of a fraction of the UV spectrum, which, even if it is small, is of extraordinary scientific interest. New UV instrumentation, such as CUBES — a joint ESO-Brazil high-resolution UV spectrograph — being planned for the VLT, will grant access to some prominent atomic and molecular transitions, the ozone jump, the Balmer jump, and the Universe at redshift ($z \sim 2$), connecting the recent history of the Universe with deep optical/infrared surveys.

The purpose of this ESO/NUVA/IAG workshop is to bring together the international community that is interested in UV astronomy to discuss the present and future of the field, and in particular to examine and broaden the scientific case for CUBES. Invited talks and reviews will cover topics on the UV astronomy of the Solar System, exoplanets, abundances of stars at various stages of evolution, resolved stellar populations in the Galaxy and beyond, the star formation history of the Universe, and the properties of the diffuse interstellar and intergalactic medium near and far. In addition, recent progress on UV detectors, coatings for the UV and molecular transitions in the UV will be reviewed.

More details can be found on the workshop web page: http://www.eso.org/sci/meetings/2013/UVAstro2013.html and more information is available from uvastro@eso.org

The registration deadline is 30 August 2013.

Announcement of the Joint ESO and Observatoire de Paris Workshop

Metal Production and Distribution in a Hierarchical Universe

21–25 October 2013, CNRS Observatoire de Paris Meudon, France

Metals trace the full evolution of the Universe: from primordial helium and lithium resulting from Big Bang nucleosynthesis to all heavier elements produced in stars and explosive events. Determining their relative abundances in different environments, and across cosmic time, reveals the underlying star formation history and gas exchange processes.

Recent progress in instrumentation and modelling now means that metal production and distribution can be used to test our ideas of galaxy evolution at many different hierarchical scales: from stellar clusters to clusters of galaxies. The hierarchical build-up of present-day structures at different redshifts can be followed, proceeding in parallel with the build-up of stellar and metal mass. These processes are interwoven: during most of cosmic history, metal production happens on stellar scales, but metal distribution is effective on spatial scales covering several orders of magnitude. Therefore simulations require exceptional computational power. Tracing metals across cosmic time needs an equivalent investment in observational facilities. The meeting will review the state of the art in all the different research areas.

Proceedings will be published in the *Supplement of the Memorie della Societá Astronomica Italiana* in April 2014. Further details are available at the conference website: http://rencontres2013.obspm.fr

The deadline for early registration, and abstract submission, is 31 August 2013.

Announcement of the

ALMA Community Days: Preparing for Cycle 2

19–20 November 2013, ESO Headquarters, Garching, Germany
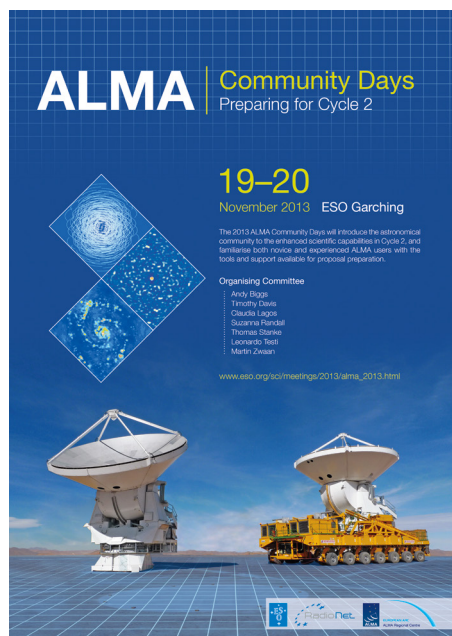
ALMA, the Atacama Large Millimeter/submillimeter Array, is currently carrying out Early Science Cycle 1 observations for the astronomical community. A global collaboration involving Europe, North America, East Asia and the host country Chile, ALMA is expected to be the leading observatory at millimetre and submillimetre wavelengths for decades to come. Early Science observations started in September 2011 with Cycle 0, and have already yielded data of unparalleled quality leading to spectacular scientific results. While the scientific capabilities offered in the current cycle are already greatly enhanced compared to the initial Cycle 0 capabilities, commissioning work is still ongoing and it is expected that further enhancements will be offered in the upcoming Cycle 2.

As for previous cycles, the ESO ALMA Regional Centre (ARC) will organise Community Days at ESO Headquarters in order to optimally prepare the European astronomical community for Cycle 2. The ESO ARC coordinates the network of nodes making up the European ALMA Regional Centre, which provides the interface between ALMA and the European scientific community. The Community Days will focus heavily on proposal preparation and include a series of presentations related to ALMA and Cycle 2, as well as hands-on tutorials for the ALMA Observing Tool and the simulators. These should enable novice and advanced users alike to create observing projects that make full use of the unique capabilities of ALMA in Cycle 2.

Further information can be found at: www.eso.org/sci/meetings/2013/alma_2013.html

Personnel Movements

Arrivals (1 April–30 June 2013)

Europe

Wang, Yue (CN)	Student

Chile

|	
Cox, Pierre (FR)	ALMA Director
Guzman, Lizette (MX)	Fellow
Hill, Tracey (AU)	ALMA Fellow
de Boer, Jozua (NL)	Student
Shultz, Matthew (CA)	Student

Departures (1 April–30 June 2013)

Europe

Bauvir, Bertrand (BE)	Software Engineer
Wesse, Yves (FR)	Senior Contract Officer
Pretorius, Magaretha (ZA)	Fellow
Cortese, Luca (IT)	Fellow
Westmoquette, Mark (GB)	Fellow
Spezzi, Loredana (IT)	Fellow
Zhao, Fei (CN)	Student
Lagerholm, Carina (SE)	Student

Chile

Bauerle, Mary (CL)	Executive Assistant
Sánchez-Janssen, Rubén (ES)	Fellow
Foster-Guanzon, Caroline (CA)	Fellow

Operating the Very Large Telescope
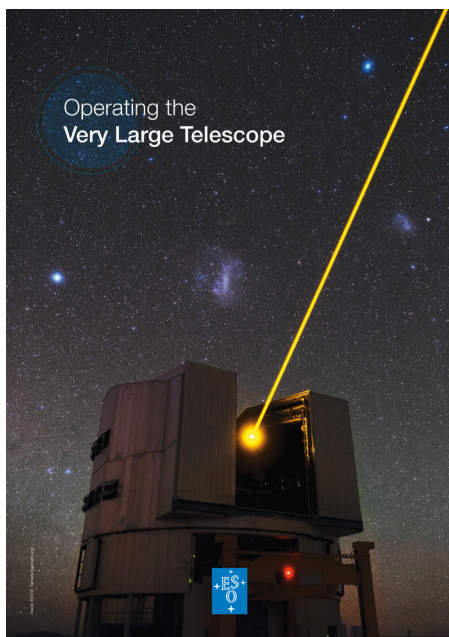
This edition of *The Messenger* comes with a brochure about the end-to-end science operations of the Very Large Telescope (VLT) at Paranal, Chile: how observing time on the VLT is allocated and scheduled; the two methods of observing — visitor and service; and how the data are collected, stored and shared.

This brochure also describes how the European Extremely Large Telescope (E-ELT) and the VLT will work together to tackle the future scientific challenges — and how ESO will help to make this a reality.

The brochure is also available as a PDF from: http://www.eso.org/public/products/brochures/operating_vlt_2013/

Contents

Front cover: An aerial view of the ALMA array taken in December 2012 looking eastwards. The ALMA Compact Array (ACA), which has been named after the Japanese astronomer Koh-ichiro Morita, member of the Japanese ALMA team and the designer of the ACA, is nearest to the camera. This image, and those shown on p. 7, were taken as part of the ORA Wings for Science project and more details can be found in Picture of the Week 29 April 2013.
Credit: Clem & Adri Bacri-Normier (wingsforscience.com)/ESO